Fall 12-18-2014

# Template-Assisted Fabrication of Ferromagnetic Nanomaterials

Jagnyaseni Tripathy

jtripath@uno.edu

Template-Assisted Fabrication of Ferromagnetic Nanomaterials

A Dissertation

Submitted to the Graduate Faculty of the
University of New Orleans
in partial fulfillment of the
requirements for the degree of

Doctor of Philosophy
in
Chemistry

by

Jagnyaseni Tripathy

B.S. Utkal University, 1999
M.S. Regional Engineering College, 2002

December 2014

ii

To My Family

wonderful friendship and for the time we spent together. Special thanks to Dr. Josepha for helping me with formatting this dissertation.

Successful completion of this research was also possible due to the companionship, encouragement and support of many friends. I cannot find words to express my gratitude to Dr. Hemant Chowdhary, Sheela Chowdhary, Dr. Hiranya Sahoo, Suchismita Sahoo, Marketa Jonasova, Robert Janous, Dr. Pranati Sahoo and Dr Dillip Panda for their help and support in all these years.

I would like to dedicate this research work to my family. The blessings of my family members kept me going and I thank them all for their continuous support and guidance in my progress throughout the course of my studies. Special thanks to my sister who came from India so that I could finish writing my dissertation. Last but not the least, I am thankful to my husband Padmanava for his understanding and support, and for being there for me in each step of this journey, guiding and encouraging me. Finally, I would like to thank my son Shriyansh. His ever smiling face was the ray of sunshine for me each day that kept me going.

# Table of Contents

## List of Figures

**List of Tables**

**Abstract**

Template assisted deposition was used to produce various nanomaterials including simple nanowires, nanorods, multi-segmented metal nanowires, core-shell nanowires, alloy and polymer wires and tubes. Anodized aluminum oxide (AAO) membranes were used as templates for the growth of the various structures using an electrochemical deposition method and also by wetting the porous templates. In the electrochemical deposition method, the pore size of the templates affects the rate of synthesis and the structures of the nanomaterials while in the wetting method, the viscosity and reaction time in the polymer solution influence the structures of the nanomaterials.

A conventional two-step anodization procedure was used to synthesize thick AAO templates with porous hexagonal channels at a constant applied voltage and temperature. A maximum thickness of over 180 µm oxide layer could be fabricated using mild anodization at 60 V and 80 V. Compared to conventional mild anodization, these conditions facilitated faster growth of oxide layers with regular pore arrangement.

Polyethylene glycol (PEG) containing ferromagnetic nanowires were synthesized using template assisted electrochemical deposition method. During the synthesis, simultaneous deposition of polymer and metal ions resulted nanowires coated with a uniform layer of PEG without interfering with the structure and magnetic properties of the nanowires.

PEG-coated Ni nanowires were embedded in polyethylene diacrylate (PEGDA) matrix after the removal of the AAO templates. Comparison of results with and without a magnetic field during embedding showed that the presence of magnetic field supported embedding of nanowire arrays in polymer.

Influence of using AAO templates with several pore diameters for the synthesis of bimetallic nanowires were studied by growing Ni-Fe and Ni-Co bi-metallic nanowires. At a constant applied current by using templates with a pore diameters of 60 nm alloy formed while with a pore diameter of 130 nm core-shell nanowires formed.

Polyvinylidene fluoride (PVDF) films and nanotubes were synthesized using a solution recrystallization method that favored the formation of piezoelectric β phase thin films. Variation in the concentration of polymer in the mixture solution allowed synthesis of different types of structures such as PVDF composites, nanorods and nanocrystals with tunable morphologies.

**Keywords:** One-dimensional structures, electrodeposition, porous alumina, ferromagnetic nanostructures, magnetic core-shell nanowires, alloys, polymer composite, stimuli-active, PEGDA, azobenzene, and PVDF.

**Chapter 1**

**Introduction**

**1.1 Nanotechnology**

Nanotechnology offers the ability to manufacture, observe and manipulate materials in the nanometer range (1 to 100 nm). These materials facilitate research and technological developments that can then lead to materials development, structures, and systems with novel properties and functions due to the materials size. These properties can sometimes be much improved compared with those exhibited by macromolecular sized materials of the same composition. Therefore, nanotechnology has potential applications that ranges from fundamental science to industrial use such as electronics,[1] optics,[2] catalysis,[3] energy and data storage,[4] sensors[5] as well as medicine.[6]

**1.2 Nanomaterials**

Nanomaterial fabrications often aim at making nanoscale structures in large quantities at potentially low cost. These materials can be classified as single-phase or multi-phase with crystal dimensions of a few nanometers. These crystals can act as building blocks in zero-dimensional (0D), one-dimensional (1D), two-dimensional (2D), and three-dimensional nanomaterials (3D). The 0D (nanoparticles, quantum dots, nanoclusters etc.) and 1D (nanowires, nanocables, nanotubes etc.) are two primary types of building blocks that have been extensively studied over the past decade both for fundamental research as well as technological applications.

A large number of methods have been developed for the synthesis of these materials. The technique to be used is determined by its economic viability, ease of the process and the purity of the final product. These include physical methods such as sputtering[7], pulse laser ablation[8] and lithography[9] or by using chemical methods, electrochemical deposition,[10] sol-gel[11] and chemical

vapor deposition.[12] Out of these two methods, the chemical methods are more commonly used due to their more easily controlled synthetic parameters and lower chance of contamination.

To investigate the properties of synthesized materials, specific techniques can be used to determine the various attributes including their surface morphology and composition profiles. For structural information, direct microscopy techniques such as field emission scanning electron microscopy (FESEM) and transmission electron microscopy (TEM) are used. FESEM gives morphology and topography of the specimens and TEM is used to characterize the morphological features, size, shape, and arrangement of atoms within nanomaterials. Additionally, energy dispersive X-ray spectroscopy (EDS), an accessory in modern electron microscopy, is used to infer the chemical composition of the materials. X-ray powder diffraction (XRD) patterns are used to analyze the crystal structure of the specimens and spectroscopic tools, including Fourier transform infra-red spectroscopy (FT-IR) and nuclear magnetic resonance (NMR) are used to investigate the non-molecular components.

**1.3 Template assisted deposition**

Nanomaterials show interesting properties owing to their size and shape. This is especially true in the 1D structures due to their shape anisotropy. With the recent developments in nanomaterials synthesis, many methods have been reported for the preparation of 1D materials such as those based on thermal decomposition,[13] physical vapor deposition,[14] vapor-liquid-solid deposition,[15] and template assisted deposition methods.[16] For the fabrication of uniformly arranged one-dimension structures, template assisted deposition is most preferred out of all these methods. The templates used can be soft or hard. Soft templates include surfactant and polymers based systems that can self-assemble and guide the growth of structures.[17] Hard templates provide a surface for the growth of materials, for example carbon nanotubes,[18] track-etched polymer films,[19]

2

and anodized aluminum oxide (AAO) films.[20] Using these templates, nanowires, nanorods, nanotubes and other structures can all be fabricated by various methods including sol-gel,[21] wet template assisted deposition,[22] electrochemical deposition,[23] and atomic layer deposition.[24]

Among the various template assisted deposition methods used to grow 1D structures, the electrochemical deposition method in hard templates is especially useful. This versatile technique readily allows for variations in composition, thickness, morphology as well as crystallographic structures. Additional advantages include faster growth, highly pure structures and it is fairly easy to control the length and diameter of the resulting nanostructures. Also, often the costs are less than other approaches. Figure 1.1 shows FESEM images of 1D structures prepared using hard template assisted deposition method grown in our lab.
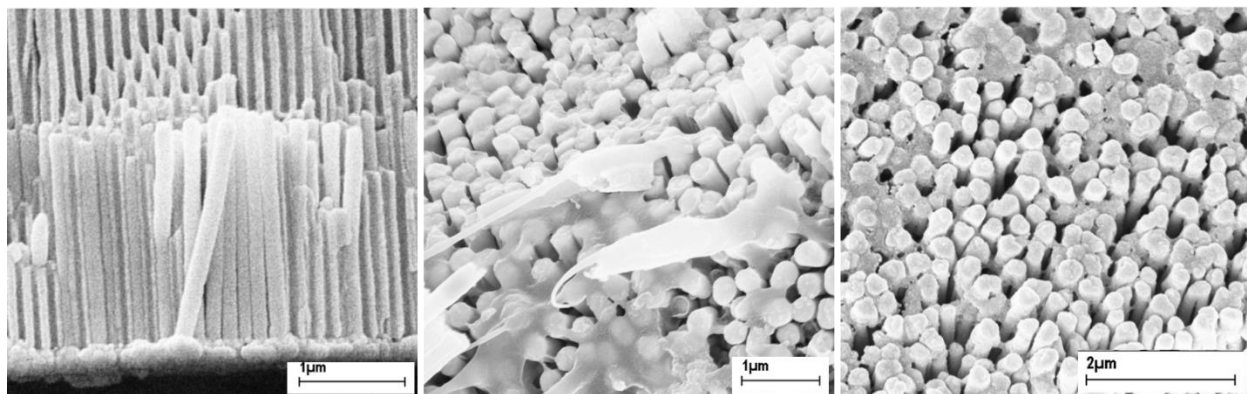


**Figure 1.1.** FESEM images of three different types of nanowires fabricated using AAO template assisted deposition method. (Nanowires shown are fabricated in this research).

### 1.3.1. Anodized Aluminum oxide

AAO membranes are extensively used in the template assisted electrochemical deposition method for the fabrication of 1D materials. Commercially available templates often have randomly distributed branched pore channels. However, by synthesizing templates in-house using a multi-step anodization process, hexagonally ordered parallel pore channels of uniform size and can be obtained as shown in Figure 1.2.
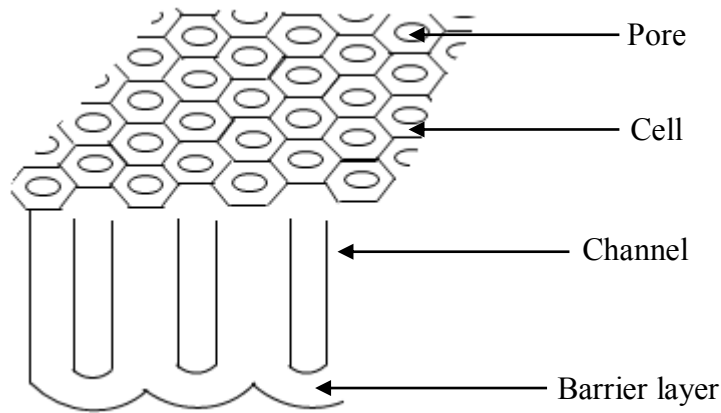


**Figure 1.2.** Schematic diagram of AAO template.

To grow templates with different pore diameters, the applied voltage and temperature are altered depending on the strength and concentration of the acids used.[24] For example, templates with a maximum pore diameter of 60 nm can be fabricated with 0.3M $H_2SO_4$ at 25 V and 10 ºC. Similarly, templates with a maximum pore diameter of 100 nm and 430 nm, using 0.3M $H_2C_2O_4$ (40 V and 17°C) and 0.3M $H_3PO_4$ (160 V and 5°C), respectively, can be synthesized. Further, by varying the acid and reactions conditions, the interpore distance of the fabricated templates can also be controlled.

Using a two-step anodization method, templates of uniform pore channels can be fabricated. High purity Al films (99.999% purity, 0.25 mm thickness, 1 cm X 2 cm) are used for anodization. Before the first step of anodization, Al films are degreased in acetone and annealed in an inert atmosphere at 450 ℃ for nearly 5 h. The surface of Al film are electropolished using 4:1 mixture of ethanol ($C_2H_5OH$) and perchloric acid ($HClO_4$). Further, anodization is conducted under constant cell potential using three types of aqueous acidic solutions, sulfuric, oxalic, and phosphoric acid as an electrolytic solution. The resultant oxide layer has broad size distribution randomly oriented pores due to uneven nucleation. These layer are removed by etching it using a mixture solution of 5wt% $H_3PO_4$ & 1.8% $H_2CrO_4$ at 80 °C. In order to obtain a better order and continuous pore channels, a second step of anodization is conducted under the same applied current and types of aqueous solution as the first step of anodization. The oxide layer formed are then removed from the Al film using electrochemical etching process at a temperature 5 ℃ higher than the synthesis temperature using 1.1 $C_2H_5OH$ and $HClO_4$. Figure 1.3 shows the FESEM images of AAO templates grown using the above parameters by a two-step anodization.
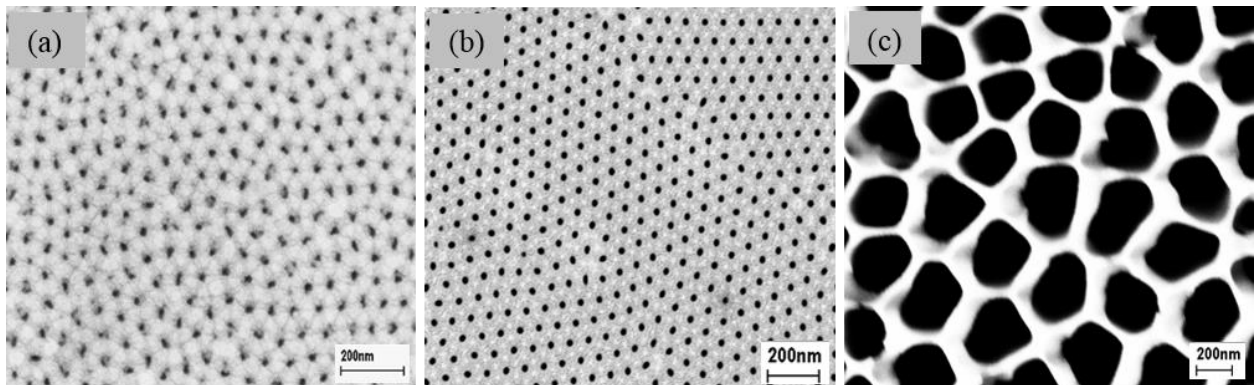


**Figure 1.3.** Shows the surface view of as synthesized template formed using (a) 0.3M $H_2SO_4$ at 25V and 10℃ (b) 0.3M $H_2C_2O_4$ at 40 V and 17℃ (c) 0.3M $H_3PO_4$ at 160 V and 5℃. (AAO templates shown in this figure are grown in this lab).

After the synthesis is complete, the pore diameter of each template can still be controlled by treating these templates with 5 wt% $H_3PO_4$ for specific time durations. For example, the size of pore channels of the templates formed above using oxalic can be modified into different sizes as given in Figure. 1.4
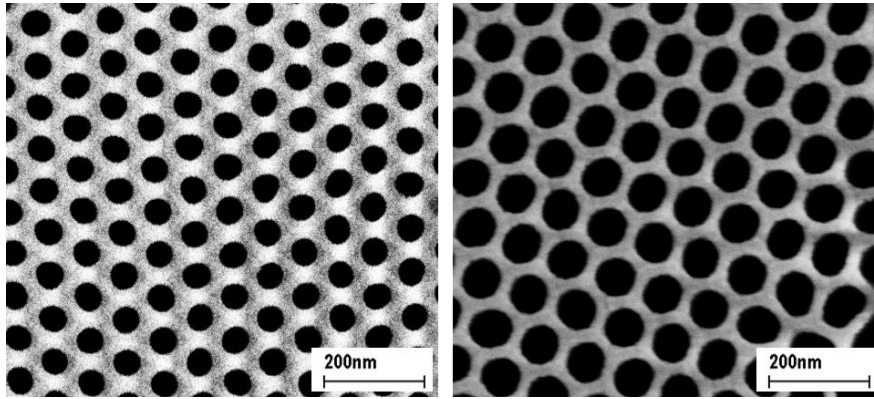


**Figure.1.4**. FESEM images of AAO templates synthesized using 0.3M $H_2C_2O_4$ immersed in 5wt% $H_3PO_4$ for (a) 30 min (b) 60 min. (Templates shown were grown in this lab by published methods.).

Similarly, the interpore distances of templates can also be changed using the same acid concentration and by altering the applied voltage using a three step anodization process. The conventional two step anodization using 0.3M oxalic acid at 40 V, 15°C for 2 h is known as mild anodization. When a third step of anodization is conducted on the same template at 100V, 2 °C for 2 h it is known as hard anodization. An increase in applied voltage enhances the reaction rate and as a result some channels terminate and their area is occupied by the nearby channels as shown in Figure 1.5c. Thus the pore to pore distance can be increased from 100 nm to nearly 260 nm. These self-organized aluminum templates with uniformly arranged hexagonal pore channels are used for the fabrication of orderly arranged materials. These can be use directly either by using the anodic

film with remaining aluminum substrate[25] or the resulting thin film after separating the aluminum base is used as template.[26]
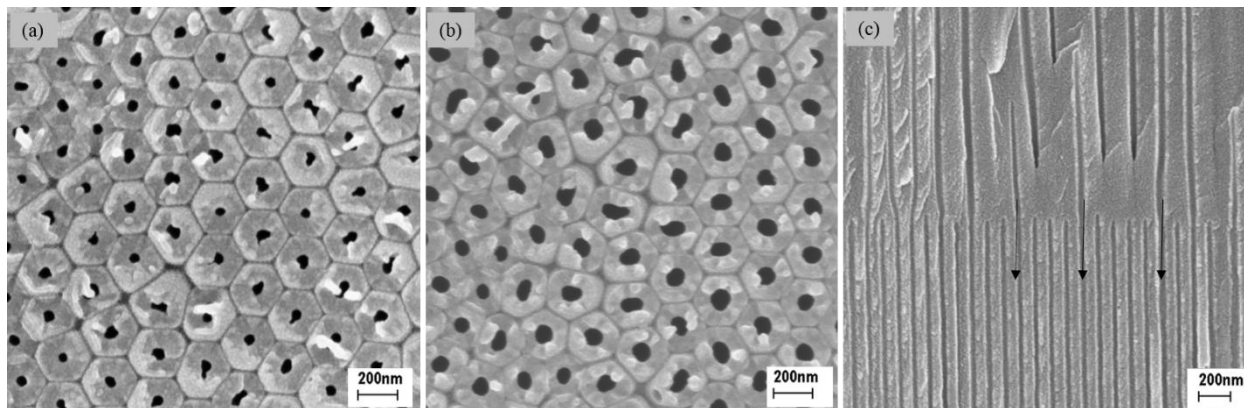


**Figure 1.5.** The surface view of templates synthesized using a three step mild-hard anodization process and after acid treatment with 5wt% $H_3PO_4$ for (a) 30 min, (b) 60 min and (c) cross-section images showing the continuous pore channel formed during the third step of anodization.

### 1.3.2. Electrochemical deposition

The electrodeposition of nanomaterials in AAO templates is conducted by removing the barrier layer and by sputter-coating a conductive metal layer on one side of the membrane. The AAO template with a metal coating on one side of the pore channel works as an electrode (cathode) in an electrolytic half-cell. Ag/ AgCl can then be used as reference electrode and a platinum wire used as counter electrode (anode). The cell arrangement is given in Figure 1.6.

Using sputtered AAO template as cathode, a variety of nanostructures with different morphologies can be fabricated. The deposition of materials is facilitated by applying a constant current at a specific voltage. In electrochemical deposition method, hydrated ions ($M (H_2O)_y^{n+}$) in

Pt wire as Counter electrode

Ag/ AgCl, Reference electrode

Sputtered AAO as working
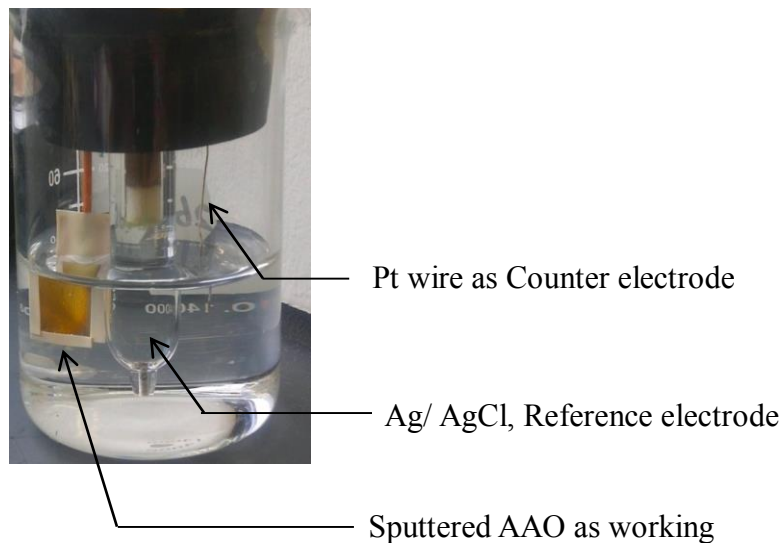
**Figure. 1.6.** Three-electrode system used for growing nanomaterials.

the electrolytes move towards the cathode under applied potential and adsorbed at the cathode. By the transfer of electrons from the external electron source, it produces metal ions, which further helps the growth of materials as following:[27]

$$M\ (H_2O)^{n+}\ (Solution) \longrightarrow M^{n+}\ (ads) \longrightarrow M$$
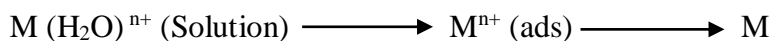
However, the final size distribution of the 1D materials during electrodeposition depends on the kinetics of the nucleation and growth of the metal. Presence of additives in the electrolyte can also influence the rate of deposition and crystal growth as these can be adsorbed at the cathode surface during synthesis. This adsorption can be physical, where van der Waals or electrostatic forces act between the surface and the adsorbate without sharing or transforming electrons, or it may be chemical adsorption (covalent bond, ionic bond). Thus, an additive can change the number of available growth sites on a surface. As a result, the kinetics of electrodeposition changes and in some studies, this leads to different shapes of materials.[27d]

Electrochemical deposition offers specific advantages of growing nanomaterials with controlled crystalline structures of uniform length.[28] Therefore, in recent years, many groups have used template assisted electrodeposition methods to grow different types of 1D structures.[29] For example, Salem *et al.*[30] used a pulsed electrochemical deposition method to grow Ni-Fe nanowires. By changing the applied potential during the fabrication from the same electrolyte they were able to fabricate two types of alloy nanowires with different concentrations of Ni and Fe. Furthermore, Lee *et al.*[31] modified the surface of AAO template with silver nanoparticles and subsequently sputtered a thin layer of metal on to the bottom of the pores. This helped in the fabrication of nanotubes, nanorods, and multi-segmented nanowire arrays at different applied potentials.

### 1.3.2. Magnetic nanowires

1D materials synthesized by the template assisted deposition method include nanorods, nanowires, nanodots or nanotubes of metals,[32] metal oxides,[32b, 33] polymers,[34] and semiconductors.[35] These materials can be used in many fields because of their ordered arrangement and their unique directional properties. By controlling the structure and aspect ratio of these materials their properties can be modified as required. Various properties are accessible including electrical, optical, and magnetic properties.

Magnetic materials synthesized using AAO templates are an important class of 1D materials, especially the ferromagnetic materials synthesized using AAO templates allows fabrication of uniform arrays of nanowires with controlled aspect ratio. Different magnetic materials have different interactions of atomic magnetic moments. Out of diamagnetic, paramagnetic, ferromagnetic and antiferromagnetic materials, ferromagnetic materials are mostly used because of their spontaneous magnetization properties and unique magnetic ordering

temperatures. The shape anisotropy and uniform arrangement of ferromagnetic nanowires with controlled aspect ratio have the desirable magnetic properties which makes them ideal candidates for use as sensors,[36] magnetic recording media[37] and high density magnetic storage devices[38]. For high quality sensors, media and storage devices, nanowires should have specific aspect ratio and suitable separation among them. Separation among nanowires is needed to avoid the interwire interaction and magnetic dipole coupling. These factors significantly affect the magnetic properties of these nanowires in terms of coercivity and squareness. These two values can be calculated from the magnetic hysteresis loop which is a plot of the variation of magnetization (M) as response to applied magnetic field (H) (Figure 1.7).
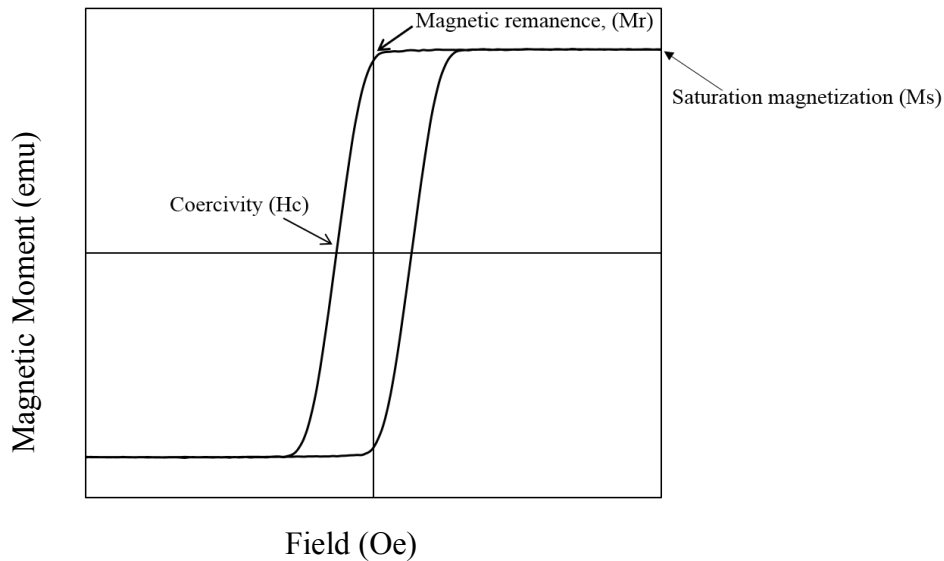


**Figure 1.7.** Magnetic hysteresis loop of ferromagnetic nanowires.

Prior to the application of magnetic field, the magnetic domains in each material are randomly oriented, therefore the net magnetization is zero. After application of magnetic field, the polarization increases slowly due to the growth of favorably oriented domains along the direction of the energetically favorable direction of spontaneous magnetization. When all the domains are

10

aligned in the direction of the magnetic field, maximum value of magnetization is reached, which is known as saturation magnetization (Ms), after which no further increase in polarization occurs. Thus, the degree of magnetic domain orientation increases with increase in the applied external magnetic field strength but not linearly (Figure 1.7). After saturation magnetization, a reverse magnetic field is applied to achieve saturation polarization in the negative direction. When the field is reduced, a hysteresis effect is produced. The remaining residual magnetic susceptibility at zero applied field is called magnetic remanence ($M_r$). The retained $M_r$ indicates that the material remains magnetized even in the absence of external applied field. The reverse field required to decrease the magnetization to zero is known as coercive field ($H_c$). The ratio of $M_r$ and $M_s$ ($M_r/M_s$) is used for determining the squareness of a magnetic hysteresis (M-H).
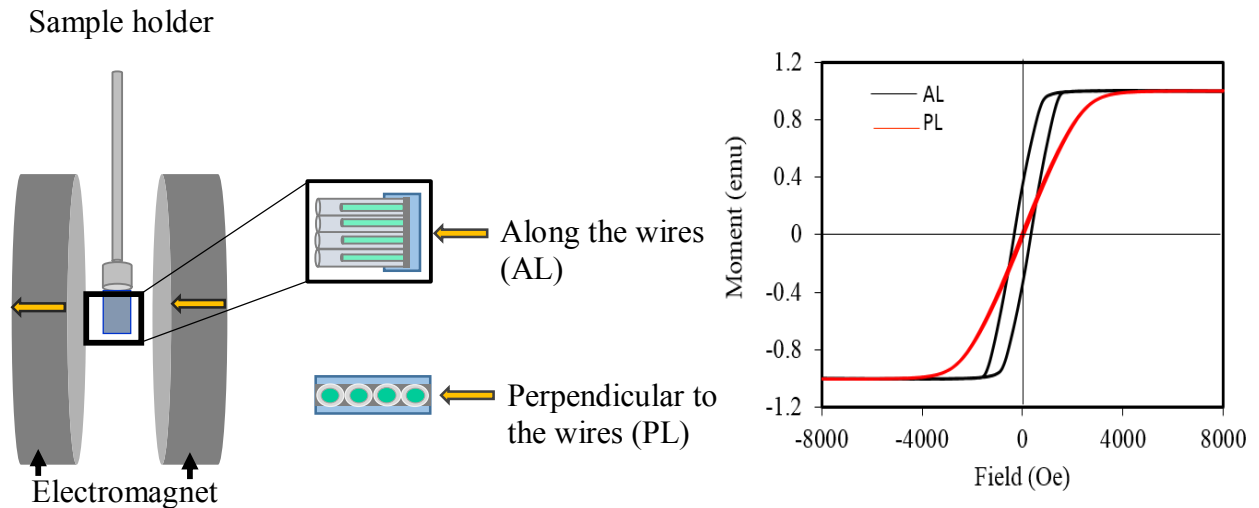


**Figure 1.8.** Variations in magnetic properties with a change in orientation of nanowires using vibrating sample magnetometer (VSM).

Coercive field is usually used to differentiate between soft and hard magnetic materials. Magnetic materials with low coercivity are called soft and those with high coercivity are called

hard magnetic materials. Depending on the angular variation in nanowires orientation with applied magnetic field, the value of coercivity changes as given in Figure 1.8. Current research efforts are therefore directed towards altering synthesis route to decrease the dipolar coupling between the nanowires to increase the magnitude of total magnetization.

Chen et al.[39] reported a special fabrication strategy for nanowires. In brief, Ni-Cu-Ni multi-segmented nanodisk and nanorods were fabricated using electrochemical deposition method using polycarbonate templates. Magnetic crystalline anisotropy of Ni is smaller compared to Fe and Co, therefore its magnetic response is dominated by shape and aspect ratio of each Ni segments. As a result, with increase in segment length, the dipole-dipole interaction between Ni segments decreased favoring an increase in coercivity and saturation field.
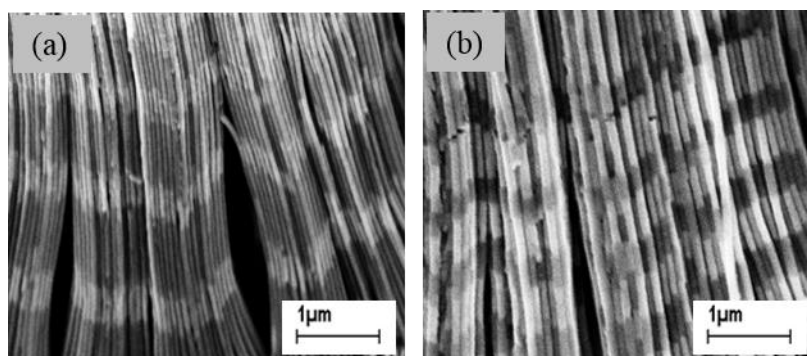


**Figure 1.9**. FESEM images of (a) Ni-Au and (b) Au-Ni multi-segmented nanowires (synthesized in this lab).

Using this strategy, Ni-Au segmented nanowires were synthesized using AAO template by electrochemical deposition method (Figure 1.8). These nanowires show higher coercivity compared to only Ni nanowires of same dimensions. Further, magnetostatic interactions between ferromagnetic nanowires can also be reduced using templates with higher interwire distance that

leads to remarkable coercivity and squareness[40] and can be modified to a great extent by altering the structure of magnetic materials by synthesizing core-shell and alloy nanowires.[41]

**1.4. Stimulus-active polymers**

In the year 1827, Swedish chemist J. J. Berzelius devised the term polymer.[42] A polymer is a substance that is composed of many smaller units known as monomers which joined together by chemical bonds to form macromolecules. In some polymers, the monomers can be different from the constitutional repetitive units (CRU) that are combined together to form the polymer. The method to grow polymers is known as polymerization. These polymers can have different composition and arrangement of their CRUs. Based on which, these polymers are classified as homopolymer, copolymers and grafted polymers.[42]

There are two types of polymers, natural polymers and synthetic polymers. Natural polymer are available in nature whereas synthetic polymers are artificially synthesized in the laboratory. Properties of polymers vary depending on their composition. Some of the polymers such as rubber, nylon, polystyrene are resistant to chemicals, and some others such as polyvinylchloride, polychlorotrifluoroethylene are thermal and heat resistant.[43] Polymers such as azobenzene and polyvinylidene fluoride are stimuli–responsive.[44]

The configuration, dimension and physical properties of the stimuli–responsive polymers can be controlled by applying appropriate external stimuli. Under the influence of stimulants such as temperature,[45] pH,[46] light,[47] electric fields,[48] and solvent / water,[49] the shape and size of stimuli-active polymers can change. Some stimuli-responsive polymers can come back to their original form after the removal of the applied external stimulants, these are known as smart polymers. Stimuli-active/responsive smart gels were first reported in 1982 by Prof. Toyoichi Tanak.[50] Variety

smart responsive polymers are reviewed by He et al. such as thermal, light and moisture responsive polymers, which can be used to manufacture different textiles and its future possible applications.[51] This includes molecular rearrangement based thermochromic spirolactone which consists of three components: a dye precursor, a color developer and a non-polar solvent. Molecular rearrangement of spirolactone leads to a reversible thermochromic effect that forms a die which can be used in textiles as thermochromic paints.

With development in technology, smart polymers are also used in fabrication of different types of polymer composites including magneto-active polymers, electroactive polymers and composites etc.[52] Ferroelectric polyvinylidene fluoride (PVDF) is an example of smart polymer that have an important influence on nanotechnology due its piezoelectric nature.[53] PVDF in β phase can mechanically deform by the application of an applied electric field. In absence of electric field the charge distribution within the polymer is symmetric so the net dipole moment is zero. However when an external field is applied the charges are displaced and they are no longer symmetric. There will be a variation in its planar dimensions. As a result it can behave as ferroelectric polymer. Piraux et al. has used track etched PVDF polymer template to grow Ni nanowires and have demonstrated the magnetoelectric effect resulted from the mechanical coupling between magnetostastic and piezoelectric effect phase.[44b] Similarly, polyethylene diacrylate (PEGDA) is a solvent active polymer swell in volumes due to solvent uptake and after the removal of solvent it can come back to its original shape. Polyethylene Diacrylate (PEGDA) is another smart solvent and pH responsive polymer that changes its size depending on the concentration of different solvent used to polymerize it.[54] The swelling cause by the absorption of water molecule forms specific hydrates through hydrogen bonds. The oxygen atom of PEG and the hydrogen atom of water are the reason of formation of hydrogen bonds and these bonds are nonresistance to

14

temperature. Therefore, it breaks when the temperature is increased while hydrophobic interaction is enhanced. Azobenzene-polyacrylate has been studied in this research which a light active polymer that switch its configuration in contact with light irradiation. The longer trans-azobenzene can be change into shorter cis-azobenzene and vice-versa due the presence of the N=N in the azobenzene molecule.

In this research, we have developed a two-step anodization method using which nearly 160 μm thick AAO templates can be fabricated under mild anodization reaction conditions. The pore channels are uniform in size and are discussed in Chapter 2. These thick templates are helpful in fabrication of micron size nanowires. In addition to thicker AAO template several different templates were synthesized that were used to grow 1D nanowires of various structures. For example, using template assisted electrochemical deposition method we have fabricated polymer coated ferromagnetic nanowires where polymer and metal and metal oxide of one dimensional structures can be formed with uniform controlled length and diameter. Chapter 3 will cover synthesis and characterization of polyethylene glycol (PEG) coated Fe, Ni, Co nanowire arrays. Chapter 4 will cover the synthesis of stimuli active polymers including Azobenzene-polyacrylate, polyethylene glycol diacrylate (PEGDA) and their use in embedding the nanowires after the removal of AAO template. NiFe and NiCo nanowires were synthesized using electrodeposition method is major focus of Chapter 5. There the focus is to study the effect of pore size on growth of these nanowires. The result showed formation of structurally different nanowires from the same electrolytes by using different pore diameter of AAO templates at a constant applied current. This variation in structure further helps changing their magnetic properties. Fabrication of PVDF films, tubes and composites will discussed in Chapter 6.

## 1.5. References

1. Li, Y.; Wu, Y.; Ong, B. S., Facile Synthesis of Silver Nanoparticles Useful for Fabrication of High-Conductivity Elements for Printed Electronics. *Journal of the American Chemical Society* **2005,** *127* (10), 3266-3267.
2. Chen, J.; Saeki, F.; Wiley, B. J.; Cang, H.; Cobb, M. J.; Li, Z.-Y.; Au, L.; Zhang, H.; Kimmey, M. B.; Li; Xia, Y., Gold Nanocages: Bioconjugation and Their Potential Use as Optical Imaging Contrast Agents. *Nano Letters* **2005,** *5* (3), 473-477.
3. Watt, J.; Cheong, S.; Toney, M. F.; Ingham, B.; Cookson, J.; Bishop, P. T.; Tilley, R. D., Ultrafast Growth of Highly Branched Palladium Nanostructures for Catalysis. *ACS Nano* **2009,** *4* (1), 396-402.
4. Lou, X. W.; Wang, Y.; Yuan, C.; Lee, J. Y.; Archer, L. A., Template-Free Synthesis of SnO2 Hollow Nanostructures with High Lithium Storage Capacity. *Advanced Materials* **2006,** *18* (17), 2325-2329.
5. Comini, E., Metal oxide nano-crystals for gas sensing. *Analytica Chimica Acta* **2006,** *568* (1–2), 28-40.
6. Jeon, I. T.; Cho, M. K.; Cho, J. W.; An, B. H.; Wu, J. H.; Kringel, R.; Choi, D. S.; Kim, Y. K., Ni-Au core-shell nanowires: synthesis, microstructures, biofunctionalization, and the toxicological effects on pancreatic cancer cells. *Journal of Materials Chemistry* **2011,** *21* (32), 12089-12095.
7. (a) Song, H.; Kim, Y. J., Characterization of luminescent properties of ZnO : Er thin films prepared by rf magnetron sputtering. *Journal of the European Ceramic Society* **2007,** *27* (13-15), 3745-3748; (b) Yun, E.-J.; Jung, J. W.; Lee, B. C.; Jung, M., Characterization of the properties of high-energy electron irradiated Al-doped ZnO thin films prepared by rf magnetron sputtering using Ar plasma. *Surface & Coatings Technology* **2011,** *205* (21-22), 5130-5134.
8. (a) Chen, Z. W.; Lai, J. K. L.; Shek, C. H., Insights into microstructural evolution from nanocrystalline SnO2 thin films prepared by pulsed laser deposition. *Physical Review B* **2004,** *70* (16); (b) Sasaki, T.; Liang, C.; Nichols, W. T.; Shimizu, Y.; Koshizaki, N., Fabrication of oxide base nanostructures using pulsed laser ablation in aqueous solutions. *Applied Physics a-Materials Science & Processing* **2004,** *79* (4-6), 1489-1492.
9. (a) Hicks, E. M.; Zou, S. L.; Schatz, G. C.; Spears, K. G.; Van Duyne, R. P.; Gunnarsson, L.; Rindzevicius, T.; Kasemo, B.; Kall, M., Controlling plasmon line shapes through diffractive coupling in linear arrays of cylindrical nanoparticles fabricated by electron beam lithography. *Nano Letters* **2005,** *5* (6), 1065-1070; (b) Ra, Y.-W.; Choi, K.-S.; Kim, J.-H.; Hahn, Y.-B.; Im, Y.-H., Fabrication of ZnO nanowires using nanoscale spacer lithography for gas sensors. *Small* **2008,** *4* (8), 1105-1109.
10. Yin, Z.; Wu, S.; Zhou, X.; Huang, X.; Zhang, Q.; Boey, F.; Zhang, H., Electrochemical Deposition of ZnO Nanorods on Transparent Reduced Graphene Oxide Electrodes for Hybrid Solar Cells. *Small* **2010,** *6* (2), 307-312.
11. Mackenzie, J. D.; Bescher, E. P., Chemical Routes in the Synthesis of Nanomaterials Using the Sol–Gel Process. *Accounts of Chemical Research* **2007,** *40* (9), 810-818.
12. Che, G.; Lakshmi, B. B.; Martin, C. R.; Fisher, E. R.; Ruoff, R. S., Chemical vapor deposition based synthesis of carbon nanotubes and nanofibers using a template method. *Chemistry of Materials* **1998,** *10* (1), 260-267.

13. Puntes, V. F.; Krishnan, K. M.; Alivisatos, A. P., Colloidal nanocrystal shape and size control: The case of cobalt. *Science* **2001,** *291* (5511), 2115-2117.

14. Xiang, B.; Wang, P.; Zhang, X.; Dayeh, S. A.; Aplin, D. P. R.; Soci, C.; Yu, D.; Wang, D., Rational synthesis of p-type zinc oxide nanowire arrays using simple chemical vapor deposition. *Nano Letters* **2007,** *7* (2), 323-328.

15. (a) Wu, Y. Y.; Yang, P. D., Direct observation of vapor-liquid-solid nanowire growth. *Journal of the American Chemical Society* **2001,** *123* (13), 3165-3166; (b) Li, S. Y.; Lin, P.; Lee, C. Y.; Tseng, T. Y., Field emission and photofluorescent characteristics of zinc oxide nanowires synthesized by a metal catalyzed vapor-liquid-solid process. *Journal of Applied Physics* **2004,** *95* (7), 3711-3716.

16. (a) Cao, G.; Liu, D., Template-based synthesis of nanorod, nanowire, and nanotube arrays. *Advances in Colloid and Interface Science* **2008,** *136* (1-2), 45-64; (b) Han, Y. J.; Kim, J. M.; Stucky, G. D., Preparation of noble metal nanowires using hexagonal mesoporous silica SBA-15. *Chemistry of Materials* **2000,** *12* (8), 2068-2069.

17. Stein, A.; Rudisill, S. G.; Petkovich, N. D., Perspective on the Influence of Interactions Between Hard and Soft Templates and Precursors on Morphology of Hierarchically Structured Porous Materials. *Chemistry of Materials* **2013,** *26* (1), 259-276.

18. Ajayan, P. M.; Stephan, O.; Redlich, P.; Colliex, C., Carbon nanotubes as removable templates for metal oxide nanocomposites and nanostructures. *Nature* **1995,** *375* (6532), 564-567.

19. Schönenberger, C.; van der Zande, B. M. I.; Fokkink, L. G. J.; Henny, M.; Schmid, C.; Krüger, M.; Bachtold, A.; Huber, R.; Birk, H.; Staufer, U., Template Synthesis of Nanowires in Porous Polycarbonate Membranes: Electrochemistry and Morphology. *The Journal of Physical Chemistry B* **1997,** *101* (28), 5497-5505.

20. (a) Zeng, Z.; Huang, X.; Yin, Z.; Li, H.; Chen, Y.; Li, H.; Zhang, Q.; Ma, J.; Boey, F.; Zhang, H., Fabrication of Graphene Nanomesh by Using an Anodic Aluminum Oxide Membrane as a Template. *Advanced Materials* **2012,** *24* (30), 4138-4142; (b) Sander, M. S.; Gronsky, R.; Sands, T.; Stacy, A. M., Structure of Bismuth Telluride Nanowire Arrays Fabricated by Electrodeposition into Porous Anodic Alumina Templates. *Chemistry of Materials* **2002,** *15* (1), 335-339.

21. (a) Ji, G.; Tang, S.; Xu, B.; Gu, B.; Du, Y., Synthesis of CoFe2O4 nanowire arrays by sol–gel template method. *Chemical Physics Letters* **2003,** *379* (5–6), 484-489; (b) Kovtyukhova, N. I.; Mallouk, T. E.; Mayer, T. S., Templated surface sol-gel synthesis of SiO2 nanotubes and SiO2-insulated metal nanowires. *Advanced Materials* **2003,** *15* (10), 780-+.

22. Jana, N. R.; Gearheart, L.; Murphy, C. J., Wet Chemical Synthesis of High Aspect Ratio Cylindrical Gold Nanorods. *The Journal of Physical Chemistry B* **2001,** *105* (19), 4065-4067.

23. (a) Huczko, A., Template-based synthesis of nanomaterials. *Appl Phys A* **2000,** *70* (4), 365-376; (b) Sun, X.-Y.; Xu, F.-Q.; Li, Z.-M.; Zhang, W.-H., Cyclic voltammetry for the fabrication of high dense silver nanowire arrays with the assistance of AAO template. *Materials Chemistry and Physics* **2005,** *90* (1), 69-72.

24. Nielsch, K.; Bachmann, J.; Daub, M.; Jing, J.; Knez, M.; Gösele, U.; Barth, S.; Mathur, S.; Escrig, J.; Altbir, D., Ferromagnetic nanostructures by atomic layer deposition: from thin films towards core-shell nanotubes. *ECS Transactions* **2007,** *11* (7), 139-148.

25. Zhang, Z.; Lai, C.; Xu, N.; Ren, S.; Ma, B.; Zhang, Z.; Jin, Q., Novel nanostructured metallic nanorod arrays with multibranched root tails. *Nanotechnology* **2007,** *18* (9).

26. Pan, H.; Liu, B.; Yi, J.; Poh, C.; Lim, S.; Ding, J.; Feng, Y.; Huan, C. H. A.; Lin, J., Growth of Single-Crystalline Ni and Co Nanowires via Electrochemical Deposition and Their Magnetic Properties. *The Journal of Physical Chemistry B* **2005,** *109* (8), 3094-3098.

27. (a) Salem, M. S.; Sergelius, P.; Zierold, R.; Moreno, J. M. M.; Goerlitz, D.; Nielsch, K., Magnetic characterization of nickel-rich NiFe nanowires grown by pulsed electrodeposition. *Journal of Materials Chemistry* **2012,** *22* (17), 8549-8557; (b) Zhu, W.; Wang, G.; Hong, X.; Shen, X., One-Step Fabrication of Ni/TiO2 Core/Shell Nanorod Arrays in Anodic Aluminum Oxide Membranes. *Journal of Physical Chemistry C* **2009,** *113* (14), 5450-5454; (c) Tan, M.; Chen, X., Growth Mechanism of Single Crystal Nanowires of fcc Metals (Ag, Cu, Ni) and hcp Metal (Co) Electrodeposited. *Journal of the Electrochemical Society* **2012,** *159* (1), K15-K20; (d) Chowdhury, T.; Casey, D. P.; Rohan, J. F., Additive influence on Cu nanotube electrodeposition in anodised aluminium oxide templates. *Electrochemistry Communications* **2009,** *11* (6), 1203-1206.

28. Graham, L. M.; Cho, S.; Kim, S. K.; Noked, M.; Lee, S. B., Role of boric acid in nickel nanotube electrodeposition: a surface-directed growth mechanism. *Chemical Communications* **2014,** *50* (5), 527-529.

29. (a) Huang, C.; Hao, Y., The fabrication of short metallic nanotubes by templated electrodeposition. *Nanotechnology* **2009,** *20* (44); (b) Downey, P. R.; Flatau, A. B.; McGary, P. D.; Stadler, B. J. H., Effect of magnetic field on the mechanical properties of magnetostrictive iron-gallium nanowires. *Journal of Applied Physics* **2008,** *103* (7).

30. Salem, M. S.; Sergelius, P.; Zierold, R.; Montero Moreno, J. M.; Gorlitz, D.; Nielsch, K., Magnetic characterization of nickel-rich NiFe nanowires grown by pulsed electrodeposition. *Journal of Materials Chemistry* **2012,** *22* (17), 8549-8557.

31. Lee, W.; Scholz, R.; Niesch, K.; Gosele, U., A template-based electrochemical method for the synthesis of multisegmented metallic nanotubes. *Angewandte Chemie-International Edition* **2005,** *44* (37), 6050-6054.

32. (a) Pirota, K. R.; Béron, F.; Zanchet, D.; Rocha, T. C. R.; Navas, D.; Torrejón, J.; Vazquez, M.; Knobel, M., Magnetic and structural properties of fcc/hcp bi-crystalline multilayer Co nanowire arrays prepared by controlled electroplating. *Journal of Applied Physics* **2011,** *109* (8), -; (b) Zheng, M. J.; Li, G. H.; Zhang, X. Y.; Huang, S. Y.; Lei, Y.; Zhang, L. D., Fabrication and structural characterization of large-scale uniform SnO2 nanowire array embedded in anodic alumina membrane. *Chemistry of Materials* **2001,** *13* (11), 3859-3861; (c) Kamalakar, M. V.; Raychaudhuri, A. K., A novel method of synthesis of dense arrays of aligned single crystalline copper nanotubes using electrodeposition in the presence of a rotating electric field. *Advanced Materials* **2008,** *20* (1), 149-+.

33. Zheng, M. J.; Zhang, L. D.; Li, G. H.; Shen, W. Z., Fabrication and optical properties of large-scale uniform zinc oxide nanowire arrays by one-step electrochemical deposition technique. *Chemical Physics Letters* **2002,** *363* (1-2), 123-128.

34. Malinauskas, A.; Malinauskiene, J.; Ramanavicius, A., Conducting polymer-based nanostructurized materials: electrochemical aspects. *Nanotechnology* **2005,** *16* (10), R51-R62.

35. Xu, D. S.; Chen, D. P.; Xu, Y. J.; Shi, X. S.; Guo, G. L.; Gui, L. L.; Tang, Y. Q., Preparation of II-VI group semiconductor nanowire arrays by dc electrochemical deposition in porous aluminum oxide templates. *Pure and Applied Chemistry* **2000,** *72* (1-2), 127-135.

36. McGary, P. D.; Tan, L.; Zou, J.; Stadler, B. J. H.; Downey, P. R.; Flatau, A. B., Magnetic nanowires for acoustic sensors (invited). *Journal of Applied Physics* **2006,** *99* (8), -.

37. Gavrila, H., Patterned magnetic recording media. *Journal of Optoelectronics and Advanced Materials* **2008,** *10* (4), 757-767.

38. Xu, C.-L.; Li, H.; Zhao, G.-Y.; Li, H.-L., Electrodeposition of ferromagnetic nanowire arrays on AAO/Ti/Si substrate for ultrahigh-density magnetic storage devices. *Materials Letters* **2006,** *60* (19), 2335-2338.

39. Chen, M.; Chien, C. L.; Searson, P. C., Potential modulated multilayer deposition of multisegment Cu/Ni nanowires with tunable magnetic properties. *Chemistry of Materials* **2006,** *18* (6), 1595-1601.

40. Lim, J.-H.; Rotaru, A.; Min, S.-G.; Malkinski, L.; Wiley, J. B., Synthesis of mild-hard AAO templates for studying magnetic interactions between metal nanowires. *Journal of Materials Chemistry* **2010,** *20* (41), 9246-9252.

41. (a) Chan, K. T.; Doran, C.; Shipton, E. G.; Fullerton, E. E., Core-Shell Structured Nanowire Spin Valves. *Ieee Transactions on Magnetics* **2010,** *46* (6), 2209-2211; (b) Wang, C. Z.; Meng, G. W.; Fang, Q. Q.; Peng, X. S.; Wang, Y. W.; Fang, Q.; Zhang, L. D., Structure and magnetic property of Ni-Cu alloy nanowires electrodeposited into the pores of anodic alumina membranes. *Journal of Physics D-Applied Physics* **2002,** *35* (8), 738-741.

42. Campbell, I. M., *Introduction to Synthestic polymer*. Oxrofr Science Publications.

43. http://plastics.americanchemistry.com/Education-Resources/Plastics-101/The-Basics-Polymer-Definition-and-Properties.html.

44. (a) Meng, H.; Hu, J., A Brief Review of Stimulus-active Polymers Responsive to Thermal, Light, Magnetic, Electric, and Water/Solvent Stimuli. *Journal of Intelligent Material Systems and Structures* **2010,** *21* (9), 859-885; (b) Piraux, L.; Hamoir, G.; Lee, M.-W.; Ferain, E.; Jonas, A. M.; Huynen, I.; De La Torre Medina, J., Template Approach for Novel Magnetic-Ferroelectric Nanocomposites. *Applied Physics Express* **2011,** *4* (11).

45. (a) Crespy, D.; Rossi, R. N., Temperature-responsive polymers with LCST in the physiological range and their applications in textiles. *Polymer International* **2007,** *56* (12), 1461-1468; (b) Aoki, T.; Kawashima, M.; Katono, H.; Sanui, K.; Ogata, N.; Okano, T.; Sakurai, Y., temperature-responsive interpenetrating polymer networks constructed with poly(acrylic acid) and poly(n,n-dimethylacrylamide). *Macromolecules* **1994,** *27* (4), 947-952.

46. (a) Schmaljohann, D., Thermo- and pH-responsive polymers in drug delivery. *Advanced Drug Delivery Reviews* **2006,** *58* (15), 1655-1670; (b) Dai, S.; Ravi, P.; Tam, K. C., pH-Responsive polymers: synthesis, properties and applications. *Soft Matter* **2008,** *4* (3), 435-449.

47. (a) Ikeda, Y. Z. a. T., *Smart Light-Responsive Materials: Azobenzene-Containing Polymers and Liquid crystals*. Wiley and Sons; (b) Jochum, F. D.; zur Borg, L.; Roth, P. J.; Theato, P., Thermo- and Light-Responsive Polymers Containing Photoswitchable Azobenzene End Groups. *Macromolecules* **2009,** *42* (20), 7854-7862.

48. Ma, W. H.; Cross, L. E., Tunable electric-field-induced piezoelectricity in high strain relaxor ferroelectric P(VDF-TrFE) copolymer. *Journal of Physics-Condensed Matter* **2005,** *17* (6), 1011-1018.

49. Bennett, M. D.; Leo, D. J., Ionic liquids as stable solvents for ionic polymer transducers. *Sensors and Actuators A: Physical* **2004,** *115* (1), 79-90.

50. Tanaka, T.; Nishio, I.; Sun, S. T.; Uenonishio, S., COLLAPSE OF GELS IN AN ELECTRIC-FIELD. *Science* **1982,** *218* (4571), 467-469.

51. Hu, J.; Meng, H.; Li, G.; Ibekwe, S. I., A review of stimuli-responsive polymers for smart textile applications. *Smart Materials and Structures* **2012,** *21* (5).

52. Chen, J.-K.; Chang, C.-J., Fabrications and Applications of Stimulus-Responsive Polymer Films and Patterns on Surfaces: A Review. *Materials* **2014,** *7* (2), 805-875.

53. (a) Hadimani, R. L.; Bayramol, D. V.; Sion, N.; Shah, T.; Qian, L.; Shi, S.; Siores, E., Continuous production of piezoelectric PVDF fibre for e-textile applications. *Smart Materials and Structures* **2013,** *22* (7); (b) Chang, C.; Tran, V. H.; Wang, J.; Fuh, Y.-K.; Lin, L., Direct-Write Piezoelectric Polymeric Nanogenerator with High Energy Conversion Efficiency. *Nano Letters* **2010,** *10* (2), 726-731; (c) Persano, L.; Dagdeviren, C.; Su, Y.; Zhang, Y.; Girardo, S.; Pisignano, D.; Huang, Y.; Rogers, J. A., High performance piezoelectric devices based on aligned arrays of nanofibers of poly(vinylidenefluoride-co-trifluoroethylene). *Nature Communications* **2013,** *4*.

54. Sipics, J.; Libera, M. In *Poly(acrylic acid) modified PEG hydrogels*, Bioengineering Conference, 2005. Proceedings of the IEEE 31st Annual Northeast, 2-3 April 2005; 2005; pp 204-205.

**Chapter 2**

**Fabrication of Thick Porous Anodized Aluminum Oxide Templates**

**2.1 Introduction**

Hexagonally ordered anodized aluminum oxide (AAO) membranes have been widely used as templates in nanotechnology. Due to their characteristic continuous, highly ordered pore structures, they have been utilized extensively in the fabrication of nanomaterials leading to various applications including those in magnetic materials,[1] energy storage,[2-3] biosensors,[4] and separation filters.[5] The properties of the resulting membranes can vary widely depending on the length and diameter of the pores within the AAO template.

While standard mild anodization (MA) methods typically produce AAO membranes about 50 - 60 microns thick, there is an interest in creating thicker membranes for the production of arrays with nanowires of higher aspect ratios. This interest arises from a desire to probe fundamental properties[6] as well as to better integrate resulting structures (e.g. nanowires) into functional materials. Thicker AAO templates can be used to fabricate long continuous ordered parallel metal, semiconducting, piezoelectric and polymer nanowires and nanotube arrays that offer better performance in metal electrode touch panels,[7-8] printed inks and displays,[8] large-area flexible sensor platforms,[9] phase-change memory,[10] and nanostructure-enhanced photovoltaics.[11] For the fabrication of thick AAO templates, hard anodization (HA) methods have been reported.[12-13] However, the increased oxidation rate that occurs during HA produces a large amount of heat, which requires extensive cooling to avoid inadvertently "burning" the oxide layer. A more recently reported approach for the fabrication of thick ($\leq 135$ µm) aluminum oxide films used high acid concentrations (up to 1M) and higher temperatures (up to 20 °C) that resulted in a higher rate of growth than seen in conventional MA; using various concentrations of oxalic acid at different

temperatures and voltages, researchers were also able to increase the average sizes of ordered pore regions.[14]

Herein, we have systematically investigated the oxide layer growth rate in the presence of oxalic acid (0.3M) with applied voltages of 60 V and 80 V. Under strict conditions, ordered AAO layers greater than 135 μm thick were successfully fabricated. By optimizing the temperature and applied voltage conditions, we were able to increase the thickness of hexagonally arranged continuous pore channels.  Details on the optimized synthesis of thick templates (> 180 μm) are presented along with evidence for their effectiveness in the growth of long nanowires.


**2.2 Experimental**

A high purity Al (from Sigma Aldrich 99.999 %, 0.5 mm thick with 1.5 x 2.5 cm$^2$) piece was degreased in acetone and then annealed in argon atmosphere at 450 °C for 5 h. It was then electropolished using a solution containing 1:4 ratio of perchloric acid ($HClO_4$) and ethanol ($C_2H_5OH$) at 25 V and 10 °C. (***Caution:*** The combination of perchloric acid and alcohols is a known explosion hazard—extreme caution should be exercised, even when the sample is cooled.) AAO templates were fabricated using a three electrode system in which two carbon electrodes were used as counter electrodes. The first step of anodization was conducted at 15 °C under constant voltage of 40 V with rigorous stirring of 0.3M oxalic acid at for 12 h. The oxide layer was then completely etched away from the Al film using a mixture of 1.8 wt% chromic acid and 5 wt% phosphoric acid at 80 °C for 6 h. Subsequently, a second step of anodization was carried out in 0.3 M oxalic acid solution for the growth of pores.

During the second step of anodization, thick AAO templates were produced in 0.3M oxalic acid. Fabrications were conducted under two constant voltages, 60 V or 80 V. The most favorable

22

reaction conditions for the synthesis of thicker and ordered porous oxide layers was determined by conducting the anodization over a range of temperature at a constant voltage: temperatures of 7, 10, and 12 °C were applied at a constant voltage of 60 V and temperatures of 2, 7, 10 and 12 °C were applied at a constant voltage of 80 V. The oxide layers formed during each reaction were detached electrochemically by applying 1:1 mixture of perchloric acid and ethanol at 7 °C with an applied voltage of 10 V more than the synthesis voltage. Next, 5 wt% phosphoric acid was used for several hours to completely remove the barrier layers. During anodization, the reactions were maintained at constant temperature and constant voltage using an MGW Lauda RM-6 closed cycle chiller and Kepco power supply (KLP-300-8), respectively. Ni nanowires were grown in these AAO templates using a template assisted electrodeposition method.[15]

Thicknesses and surface views of AAO templates and fabricated Ni nanowires were observed with a LEO 1530 VP field-emission scanning electron microscope (FESEM). Magnetic properties of Ni nanowire arrays were measured at room temperature using a vibrating sample magnetometer (VSM), Lakeshore 7300 Series. X-ray diffraction (XRD) analysis was carried out using a Philips X-pert PW 3040 MPD X-ray powder diffractometer with a CuKα X-ray source.

**2.3. Results**

Initial studies focused on the synthesis of membranes at 60 V under various times and temperatures. Reactions were successfully completed at 10 °C and 12 °C for synthesis times varying from 7 to 21 h (Table 2.1). While reactions carried out at 7 °C were rapid and produced thick films, the quality of the films was poor and indicated that under these conditions low temperatures did not support ordered pore formation. Figure 2.1a shows the membrane produced by this process where the pore structure is irregular in growth pattern and dimensions.

**Table 2.1.** *Reaction conditions and thicknesses of AAO formed at 60 V.*

| Voltage (V) | 60 | 60 | 60 | 60 |
|---|---|---|---|---|
| Temperature (°C) | 7 | 10 | 10 | 12 |
| Thickness (µm)* | 195(1) | 100(2) | 188(3) | 167(3) |
| Duration (h) | 7 | 10 | 21 | 21 |
| Rate (µm/h) | 27.8 | 10.0 | 8.9 | 7.9 |

*based on 3-5 different samples made under these conditions.

In subsequent experiments the temperature was increased slightly to 10 °C; this small change resulted in much higher quality membranes. Experiments carried out for 7 h and 10 h produced highly ordered arrays of 89 µm and 100 µm thicknesses, respectively, with very regular pore structures (Figure 2.1b). When anodization times for both 10 and 12 °C were increased to 21 h, thicker membranes could be realized but the pores were found to be wide and multilayered (Figures 2.1c and 2.1d).
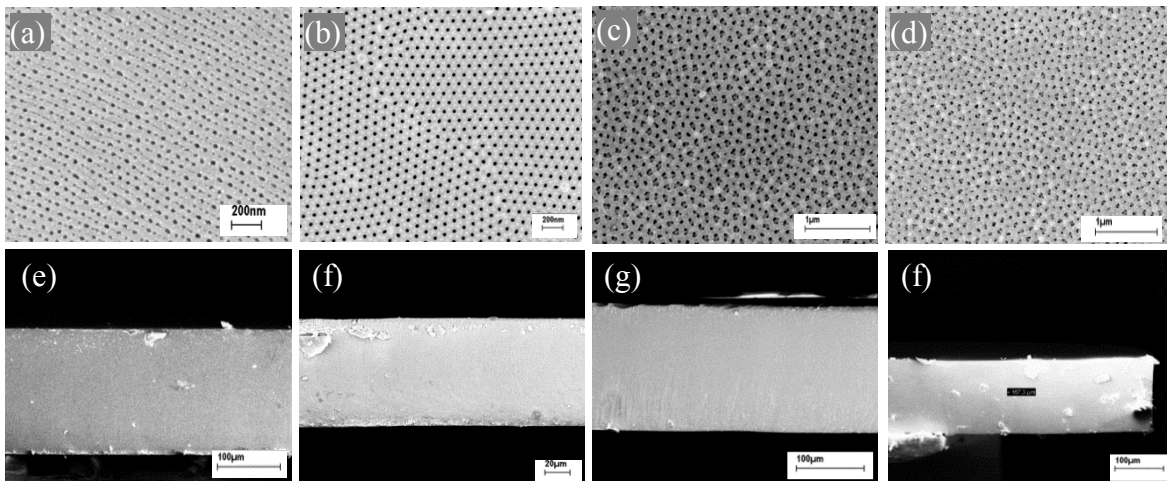


**Figure 2.1.** Top and cross-sectional view of AAO synthesized at (a & e) 60 V, 7 °C, 7 h, (b & f) 60 V, 10 °C, 10 h (c & g) 60 V, 10 °C, 21 h (d & h) 60 V, 12 °C, 21 h.

These imperfections could be readily removed by carrying out a simple pore widening treatment with 5 wt% $H_3PO_4$. Figures 2.2a and 2.2b show the top images of the resulting pore structures for the acid treatment of the 60 V/10 °C and 60 V/12 °C sample. Figures 2.2c and 2.2d show the top and bottom views of AAO template formed at 60 V/12 °C. The pore diameter of the channels was nearly 100 nm. In both of these cases, the top and bottom pore diameters were nearly the same after $H_3PO_4$ treatment.
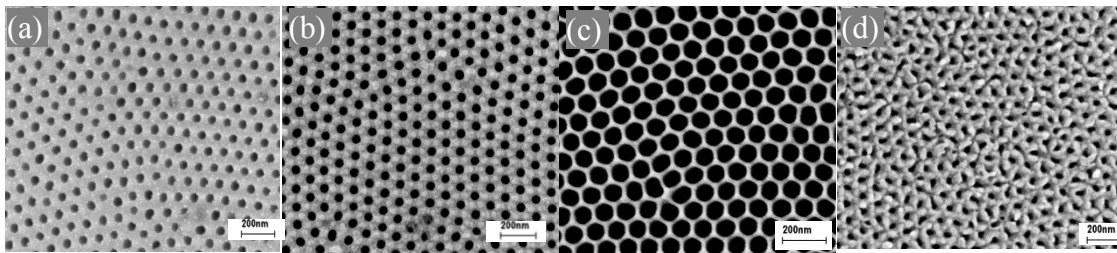


**Figure 2.2**. (a, b) Top surface of the AAO template formed at 60 V for 21 h at 10 °C and 12 °C after 1h of acid treatment, respectively. (c, d) Top view and bottom view of oxide layer formed at 60 V, 12 °C for 21 h after complete acid treatment with pore diameter nearly 100 nm and the inter-pore distance 100 nm.

**Table 2.2.** *Reaction conditions and thickness of AAO formed at 80 V.*

| Voltage (V) | 80 | 80 | 80 | 80 | 80 | 80 | 80 | 80 |
|---|---|---|---|---|---|---|---|---|
| Temperature (°C) | 2 | 2 | 7 | 7 | 10 | 10 | 10 | 10 |
| Thickness (µm)* | 156(1) | 100(4) | 120(2) | 108(2) | 79(1) | 140(4) | 124(2) | 188(1) |
| Duration (h) | 7 | 10 | 7 | 10 | 3 | 7 | 10 | 16 |
| Rate (µm/h) | 22.2 | 10.0 | 17.1 | 10.8 | 26.3 | 20.0 | 12.4 | 11.7 |

*based on 3-5 different samples made under these conditions.

Similar anodization studies were carried out at 80 V (Table 2.2) at different temperatures. This increase in voltage directly affects the rate of porous oxide layer formation such that the AAO growth is much faster. AAO films formed at 80 V and 12 °C however exhibited brown color (burning) after a few minutes. Three lower temperatures 2 °C, 7 °C and 10 °C were then examined to determine the best conditions for this voltage. Initially, the synthesis was conducted at 7 °C for 7 h keeping the reaction conditions the same as what they were at 60 V. The resulting fabricated templates were 120 µm thick with ordered pore structures. Subsequently, when the reaction was conducted for 10 h, the thickness of oxide layer decreased to 108 µm. Compared to the oxide layer formed at 60 V and 7 °C for 10 h, these oxide layers formed with more ordered pore channels. When the synthesis was conducted at 2 °C for 7 h and 10 h time periods the thicknesses of hexagonally ordered porous AAO templates were 156 µm and 100 µm, respectively.

The next set of anodizations was conducted at 80 V and 10 °C for 21 h. These conditions were not successful. The anodizations resulted in very large pores such that acid treatment to remove the barrier layer was not possible without dissolving the pore structure itself. Further
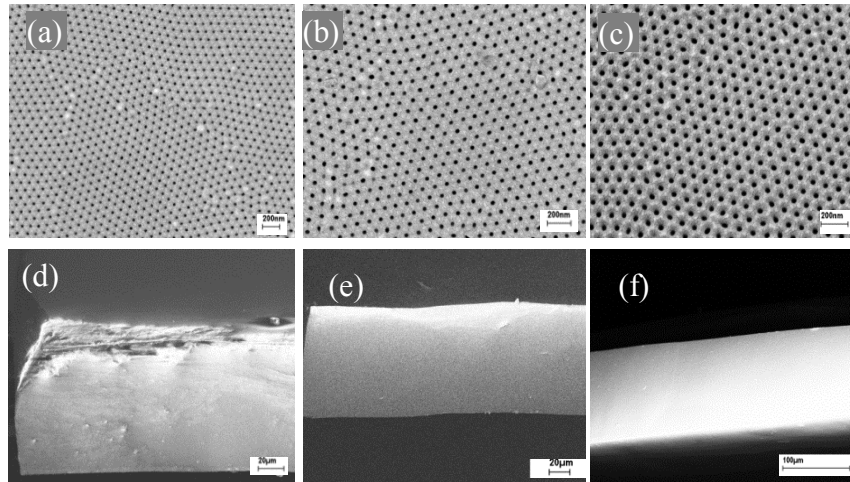


**Figure 2.3.** Top and cross-sectional view of AAO template formed at 80 V (a,d) 2 °C 10 h, (b,f) 7 °C 10 h, (c, g) 10 °C 10 h.

26

analysis was carried out at 80 V and 10 °C at shorter reaction times of 3 h, 7 h, 10 h, and 16 h. The thickness of AAO templates was found to be 79, 140, 124 and 188 µm, respectively; the thickest resulting AAO template was 188 µm with a continuous ordered porous oxide layer. It is important to note that although the pore size increased with increasing temperature, the inter-pore distance remained the same. Typical pores sizes were 24 nm, 30 nm and 34 nm for 2 °C, 7 °C and 10 °C, respectively. The surface and cross-sectional FESEM images of AAO templates synthesized at 80 V for 10 h with different temperatures are given in Figure 2.3. In both syntheses (60 V and 80 V) domain sizes were affected by the applied temperature which is a parameter that supports self-ordering and orderly arranged porous channel were formed with increase in temperature.
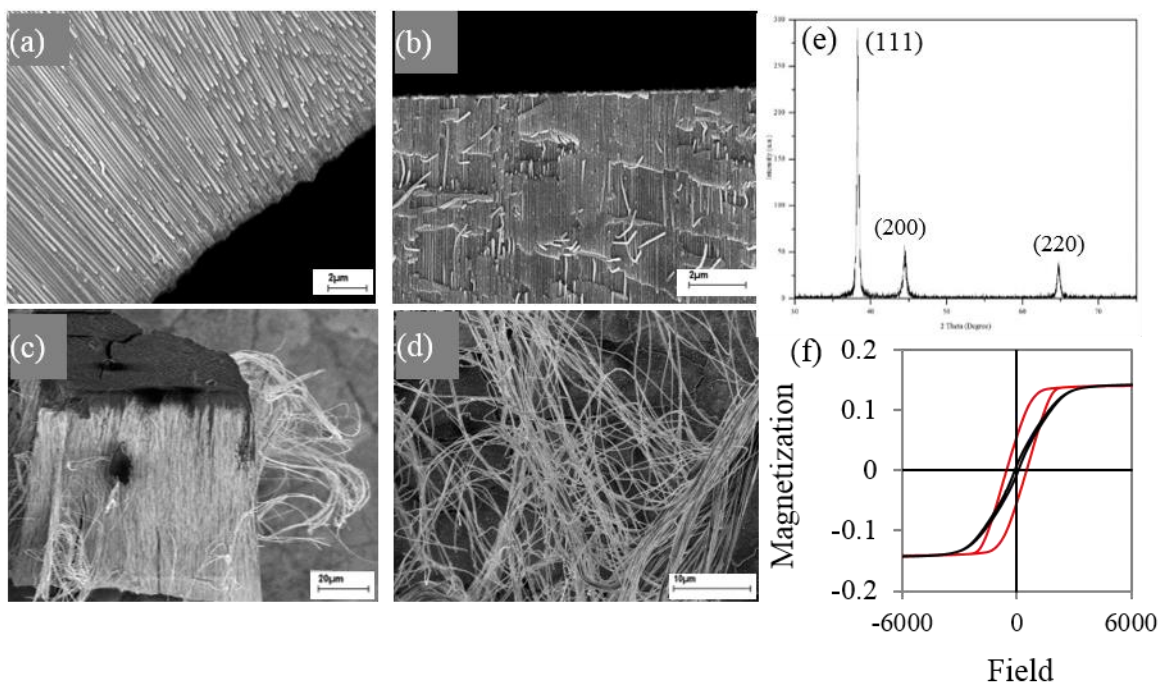


**Figure 2.4.** (a) Cross-sectional top surface view of AAO template formed at 60 V and 12 °C with Ni nanowires, (b) Cross-sectional bottom surface view of Ni nanowires within the same AAO template, (c) (d) Cross-sectional view of Ni nanowires without AAO (e) XRD result of Ni nanowire showing fcc crystal structure and (f) Hysteresis plots of Ni nanowire arrays with coercivity, Hc of 527 Oe and squareness of Mr/Ms of 0.38.

27

To demonstrate the utility of these thicker membranes, nickel nanowires were grown along the length of the templates. Following a pore widening step, the 167 μm thick membrane, formed at 60 V, 12 °C for 21 h, was used to grow Ni nanowires by electrodeposition. FESEM images of the wires are shown in Figure 2.4. XRD data on Figure 2.4e Showed wires with fcc crystal structure. Figure 2.4f shows the magnetic data for 100 nm pore diameter Ni nanowire arrays with ~160 μm length. These nanowires showed coercivity of 527 Oe and squareness of 0.38.

### .2.4 Discussion

Herein we report a method for the fabrication of more than 100 μm thick hexagonal-shaped aluminum oxide membranes. Different thicknesses of the oxide layer could be obtained at a constant voltage by varying the temperature and reaction time. Both the applied voltage and the temperature influence the ionic current. It is therefore important that these parameters are kept constant during the fabrication process.

Ono et al. studied the self-ordering behavior of AAO templates at different reaction conditions using several types of acids and various applied voltages.[16] It was shown that a specific combination of voltage, temperature and synthesis time is critical for growing homogeneous oxide films. In our study, when anodization was conducted at 60 V and 7 °C, homogenous pore arrangement was not obtained although thick AAO layers were formed. This indicated that the applied temperature was too low during the synthesis for the formation of the oxide layer. Hence, it was adjusted to 10 °C or 12 °C. As a result, continuous pore channels with 188 μm and 167 μm thick oxide layers were successfully fabricated.

Anodization conducted at 80 V led to a faster rate of oxide layer formation than that of anodization at 60 V. This higher voltage led to a variation in ionic current usually associated with

hard anodization processes.[17] After 3 h of synthesis, the thickness of the AAO template was about 79 μm and reached 140 μm at 7 h. However, further reaction to 10 h showed a reproducible decrease in thickness to 124 μm. Interestingly, upon further treatment the thickness of AAO template again increased. When measured at 16 h, the thickness of the porous oxide layer was 188 μm. Further studies showed that this is related to the ionic current of the system; Figure 2.5 shows the variation in ionic current over time. A steady drop in the current is seen up to about 10 h. This corrects itself, leveling off after longer reaction times.
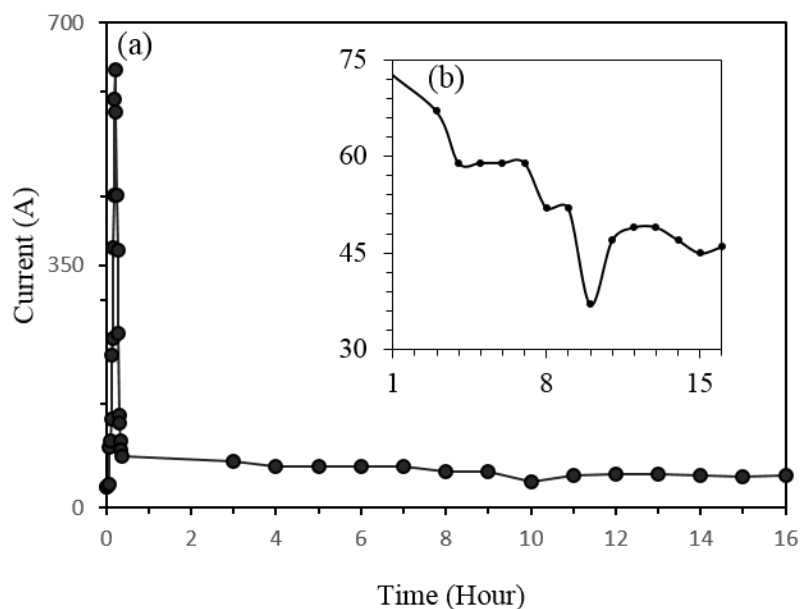


**Figure 2.5.** (a) Change in current vs time plot for anodization at 80 V, 10 °C. (b) Showing the magnified plot of current with time.

In order to explain the behavior in growth variation of thick templates at 80 V and different temperature, a better understanding of the pore formation is required. During anodization (Figure 2.6), the Al film acts as the anode and the carbon electrode behaves as the cathode.
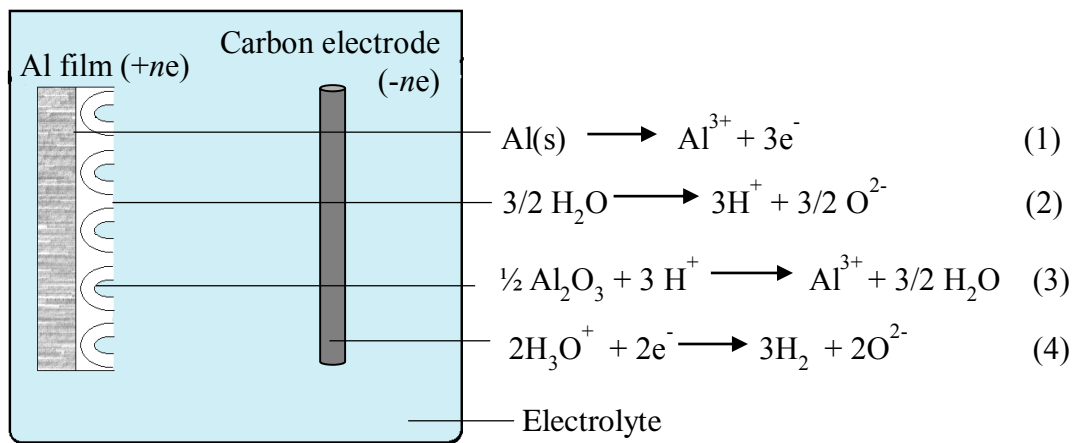
**Figure 2.6**. Schematic diagram for fabrication of AAO template.

The aluminum oxidizes producing $Al^{3+}$ ions at the metal/ metal oxide interface.[18]

$$Al(s) \quad \rightarrow \quad Al^{3+} + 3\ e^{-} \tag{1}$$

Due to reaction of water at the oxide/electrolyte interface, oxide ions form and migrate to the metal/ oxide interface to form the oxide, $Al_2O_3$.

$$3/2\ H_2O\ (\ell) \quad \rightarrow \quad 3\ H^{+}\ (aq) + 3/2\ O^{2-}\ (oxide)$$

$$2Al + 3O^{2-} \quad \rightarrow \quad Al_2O_3 + 6e^{-}$$
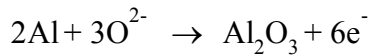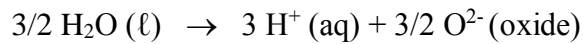
In presence of acidic media some of the $Al_2O_3$ dissolves and releases $Al^{3+}$ ions into the solute

$$\tfrac{1}{2}\ Al_2O_3 + 3H^{+}\ (aq) \quad \rightarrow \quad Al^{3+}\ (aq) + 3/2\ H_2O\ (\ell) \tag{3}$$
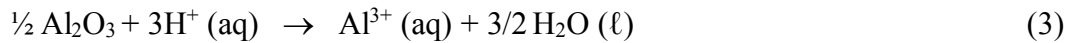
At the carbon electrode (cathode), hydronium ions dissociate and generate $H_2$ gas.

$$2H_3O^{+} + 2e^{-} \quad \rightarrow \quad 3H_2 + 2O^{2-} \tag{4}$$

The relative rates of these growth and dissolution processes play an important role in anodization of Al film. Should the oxidation rate (ionic current) drop below a certain level, the dissolution step dominates and the membranes become thinner; once the oxidation rate increases, then growth is reestablished in the membranes. The variation in growth rate is associated with local diffusion rate into and out of the pore structures. Experiments show that increasing the stirring rate results in an increase in the ionic current.

In our study, with an increase in applied voltage (from 60V to 80V), the rate of synthesis was faster and growth rate became less stable. This can be seen in the current vs. time plot (Figure 2.5). Additionally, we observed a slight variation in pH of about 0.4, initially increasing from ~1.5 to ~1.9 before reaching a steady state after about 2 hrs. This could be correlated to the large change in the ionic current during the early stages of anodization. A comparison of the oxide layer growth rate with ionic current and pH demonstrated that the rate of reaction was faster during the initial stage of film growth (nearly up to 3 h), hence, a higher rate of field-assisted hydrogen ion attack on the oxide layer occurred. As a result the oxide layer thickness increased together with an increase of the pH of the solution.

After 7 h of the synthesis we found a decrease in current and increase pH while the thickness of oxide layer was 140 μm. As described by Lee et al., the formation of a thick oxide layer with deep pore prohibits the migration of ionic species through the inner oxide layer at metal/ oxide interface.[12] As ionic current is mainly related to movement of ions ($O^{2-}$, $OH^-$, $Al^{3+}$) through the oxide layer, with an increase in oxide layer thickness, ionic current decreases. This slows down the growth of $Al_2O_3$ due to a surpression of the reactions given in equations 5 and 6.

$$2Al + 6OH^- \rightarrow Al_2O_3 + 3H_2O + 6e^- \tag{5}$$

$$2Al + 3O^{2-} \rightarrow Al_2O_3 + 6e^- \tag{6}$$
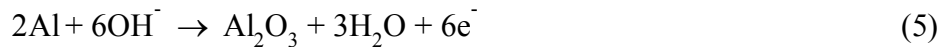
At the oxide/electrolyte interface, $Al^{3+}$ is released into the electrolyte.[19] This maintains a constant $Al^{3+}$ ion concentration in the electrolyte that suppresses pore widening during the anodization process.[20] However, the presence of $H_3O^+$ ion can increase dissolution (eq. 3). As a result, the oxide layer thickness decreased at 10 h of synthesis. This change in thickness further accelerated the oxide containing ion entering the oxide layer, which resumed anodization by increasing the ionic current. Anodization conducted in all other conditions except 80 V and 10 °C did not produce

31

thick templates due the absence of adequate electrolyte concentration and appropriate temperature and voltage.

After the synthesis of templates, polycrystalline Ni nanowires were fabricated using thick templates. As shown in Figure 2.4, nanowires are realized that have uniform length and regular interwire distances. The variation in their magnetic behavior along the wires (parallel to the field) and orthogonal to the wires (perpendicular to the field) are consistent with the formation of continuous pore channels.

## 2.5 Conclusions

Thick AAO templates with ordered pore channels were synthesized by a two-step anodization process. A maximum thickness of over 180 μm oxide layer could be achieved using mild anodization with 60 V and 80 V. Compared to conventional mild anodization, these conditions facilitated faster growth of oxide layers with regular pore arrangement. Ni nanowire arrays readily grow within these membranes demonstrating their utility for producing magnetic nanowires grown successfully using electrochemical AAO template assisted deposition have large coercivity and higher squareness.

## 2.6 References

1. Whitney, T. M.; Searson, P. C.; Jiang, J. S.; Chien, C. L., Fabrication and magnetic properties of arrays of metallic nanowires. *Science* **1993**, 261 (5126), 1316-1319.
2. Che, G.; Lakshmi, B. B.; Fisher, E.R.; Martin, C. R., Carbon Nanotubule Membranes for Electrochemical Energy Storage and Production. *Nature* **1998**, 393, 346-349.
3. Chen, D.; Zhao, W.; Russell, T. P., P3HT nanopillars for organic photovoltaic devices nanoimprinted by AAO templates. *ACS nano* **2012**, 6(2), 1479-1485.
4. Matsumoto, F.; Nishio, K.; Masuda, H. Flow-Through-Type DNA Array Based on Ideally Ordered Anodic Porous Alumina Substrate. *Advanced Materials* **2004**, 7, H27.

5.   Kasi, A. K.; Kasi, J. K.; Ashraf, M. W.; Tayyaba, S.; Afzulpurkar, N.; Tuantranont, A., Two layered novel Anodic Aluminum Oxide nanoporous membrane. In *Mechanical and Electronics Engineering (ICMEE),* 2010 2nd International Conference on (Vol. 2, pp. V2-11). IEEE.

6.   Chang, Y.; Ling, Z.; Liu, Y.; Hu, X.; Li, Y., A simple method for fabrication of highly ordered porous [small alpha]-alumina ceramic membranes. *Journal of Materials Chemistry* **2012**, 22 (15), 7445-7448.

7.   Lee, J.; Lee, P.; Lee, H. B.; Hong, S.; Lee, I.; Yeo, J.; Ko, S. H., Room-Temperature Nanosoldering of a Very Long Metal Nanowire Network by Conducting-Polymer-Assisted Joining for a Flexible Touch-Panel Application. *Advanced Functional Materials* **2013**, 23(34), 4171-4176.

8.   SeobáLee, S.; & HwanáKo, S., Very long Ag nanowire synthesis and its application in a highly transparent, conductive and flexible metal electrode touch panel. *Nanoscale* **2012**, *4*(20), 6408-6414.

9.   Yi, J.; Lee, J. M.; Park, W. I., Vertically aligned ZnO nanorods and graphene hybrid architectures for high-sensitive flexible gas sensors. *Sensors and Actuators B: Chemical* **2011**, 155 (1), 264-269.

10. Xiong, F.; Bae, H.; Dai, Y.; Liao, A.;Behnam,A.; Carrion, E.A.; Hong,S.; Ielmini,D.; Pop,E., Self-Aligned Nanotube–Nanowire Phase Change Memory. *Nano Letters* **2013**, 13 (2), 464-469

11. Xu,C.;Shin, P.; Cao, L.; Gao, D., Preferential growth of long ZnO nanowire array and its application in dye-sensitized solar cells. *The Journal of Physical Chemistry C* **2009**, 114(1), 125-129

12. Lee, W.; Ji, R.; Gösele, U.; Nielsch, K. Fast fabrication of long-range ordered porous alumina membranes by hard anodization. *Nature materials* **2006**, 5(9), 741-747

13. Schwirn, K.; Lee, W.; Hillebrand, R.; Steinhart, M.; Nielsch, K.; Gösele, U., Self-ordered anodic aluminum oxide formed by H2SO4 hard anodization. *ACS nano* **2008**, 2(2), 302-310

14. Cheng, C.; Ngan, A. H., Fast fabrication of self-ordered anodic porous alumina on oriented aluminum grains by high acid concentration and high temperature anodization. *Nanotechnology* **2013**, 24 (21), 215602.

15. Qin, J.; Nogués, J.; Mikhaylova, M.; Roig, A.; Muñoz, J. S.; Muhammed, M., Differences in the Magnetic Properties of Co, Fe, and Ni 250−300 nm Wide Nanowires Electrodeposited in Amorphous Anodized Alumina Templates. *Chemistry of Materials* **2005**, *17* (7), 1829-1834.

16. Ono, S.; Saito, M.; Ishiguro, M.; Asoh, H., Controlling factor of self-ordering of anodic porous alumina. *Journal of The Electrochemical Society* 2004, 151(8), B473-B478

17. Noh, K.; Brammer, K. S.; Kim, H.; Jung, S. Y.; Seong, T. Y.; Jin, S., Highly self-assembled nanotubular aluminum oxide by hard anodization. *Journal of Materials Research* **2011**, 26(02), 186-193.

18. Gong, D.; Grimes, C. A.; Varghese, O. K.; Hu, W.; Singh, R. S.; Chen, Z.; Dickey, E. C., Titanium oxide nanotube arrays prepared by anodic oxidation. *Journal of Materials Research* **2001**, 16(12), 3331-3334.

19. Li, F. Y.; Zhang, L.; Metzger, R. M., On the growth of highly ordered pores in anodized aluminum oxide. *Chemistry of Materials* **1998**, 10 (9), 2470-2480.

20. Zhao, S.; Chan, K.; Yelon, A.; Veres, T. Novel structure of AAO film fabricated by constant current anodization. *Advanced Materials* **2007**, 19(19), 3004-3007.

**Chapter 3**

**Electrochemically Synthesized Polyethylene Glycol Coated Ferromagnetic Nanowire Arrays**

**3.1. Introduction**

Nanostructured magnetic materials have been intensively studied in the past few decades owing to their potential applications in various fields including sensors,[1] data storage, catalysis,[3] drug and gene delivery,[4] and magnetic imaging.[5] A number of studies have been carried out on the synthesis of one-dimensional (1D) nanostructured materials such as nanowires, nanotubes, and nanorods. Synthesis of such materials can be accomplished by a variety of ways.[6] One common method is template assisted electrodeposition where nanowires are grown within anodized aluminum oxide (AAO) templates. The length and diameter of these template-grown structures can easily be controlled by varying the time of synthesis, applied current, and size of pore diameters of the AAO membranes. In addition, by coating the outer layers of the nanowires with metals,[7] oxides,[8] semiconductors,[9] or by encapsulating polymers inside nanotubes,[10] the physical and chemical properties of the nanowires can be altered.

Interest in these 1D structures arises from unique properties related to their large shape anisotropy. There can be some advantage in the use of wires versus nanoparticles in biomedical applications, such as drug delivery [11] due to their elongated shape and in these types of biomedical applications, the surface can be modified using polymers or oxide materials in order to prevent toxicity caused by internalization. Further, in the case of magnetic nanowires, high coercivities can be realized increasing their response to external magnetic fields, important for directing magnetically active species to target sites in the body.[11a]

PEG is a biocompatible, biodegradable, protein resistant, nontoxic material that has been utilized in a variety of biomedical applications.[12] Syntheses of nanomaterials involving PEG have

been studied by a number of groups. The outer polymer can interact with therapeutic proteins hence these nanowires may have potential use in various biotechnological and bio-medical applications.[13] Anwar *et al.* have used a PEG assisted co-precipitation method to grow morphologically varied nanoparticles of $Mn_{0.5}Ni_{0.5}Fe_2O_4$.[14]Topkaya *et al.* used the same method for the synthesis of PEG coated $CoFe_2O_4$ nanoparticles; the magnetic nanoparticles were found to show room temperature saturation and coercive field values close to bulk $CoFe_2O_4$.[15]Muraliganth et al. have synthesized carbon-coated single-crystalline $Fe_3O_4$ nanowires using a microwave hydrothermal method with PEG-400; in this case the PEG served as a soft porous template that allowed the growth of nanowires.[16] Herein we report a new approach to the synthesis of metal nanowires in the presence of PEG. This results in a series of PEG-coated magnetic nanowires. The PEG is found to impact the growth rate of some of the wires, but magnetically, the quality of the wires is retained with improved structural stability.

## 3.2. Experimental

*Synthesis of Anodized Aluminum Oxide (AAO) templates.* A two-step anodization process was used to fabricate AAO templates with pore diameters less than 100 nm and a three-step anodization was used to grow templates with diameters greater than 100 nm pore diameter. *Two-Step Anodization*: A high purity Al (Sigma Aldrich, 99.999 %, 1 cm x 2.5 cm x 0.25mm) film was degreased in acetone and annealed in an argon atmosphere at 450 °C for 5 h. Subsequently, the film was electropolished using a solution containing perchloric acid and ethanol (1:4 volume ratio) at 25 V. Anodization was carried out using 0.3M oxalic acid at 40 V at 17 °C for approximately 12 h. The oxide layer was completely etched at 80 °C in a solution mixture of chromic acid (1.8 wt.%) and phosphoric acid (5wt.%) so that the remaining Al surface (with a hemispherical pattern) would help in the further growth of uniform pores. A second step of anodization was carried out

for 3 h, using similar reaction conditions as the first step of anodization, to grow uniformly arranged continuous pore channels. *Three-Step anodization:* Templates with 130 nm pore diameter were fabricated in which an additional third step of anodization was conducted at 100 V, 5 °C for 2 h. This higher applied voltage assisted with an increase in the interpore distances.[17]  Finally, oxide sections were removed from the Al film by an electrochemical etching process and the required sized pores were obtained by treating these templates with phosphoric acid (5 wt%).

*Synthesis of Polymer containing Ferromagnetic Nanowires.*  For template assisted electrochemical deposition, one side of the AAO template was sputtered with a silver metal layer and used as the working electrode. Ag/AgCl was used as the reference electrode, and a platinum wire was used as the counter electrode. A VMP2 potentiostat (Princeton Applied Research Inc.) was used to grow wires at an applied current of -0.25 mA for ~4.5 h. Various deposition solutions were prepared by changing the concentration of PEG (Mw1500) and the metal salts (Table 3.1). Several different PEG-metal NWs were grown using the above procedures. When needed, the AAO template was removed by treating the samples with 0.1M NaOH solution overnight and then gently rinsing the NW sample with distilled water and acetone.

**Table 3.1.** Deposition solutions used to grow PEG-magnetic nanowires.

| Type of Nanowires | $H_3BO_3$ | Polyethylene glycol | Metal Salt | Current (mA) |
|---|---|---|---|---|
| PEG-Ni-1[a] | 0.02M | 0.02M | 0.05M | -0.25 |
| PEG-Ni-2[a] | 0.02M | 0.02M | 0.05M | -0.50 |
| PEG-Ni-3[a] | 0.02M | 0.02M | 0.1M | -0.25 |
| PEG-Ni-4[a] | 0.02M | 0.04M | 0.05M | -0.25 |
| PEG-Fe[b] | 0.02M | 0.02M | 0.05M | -0.25 |
| PEG-Co[c] | 0.02M | 0.02M | 0.05M | -0.25 |

Metal salt: [a]$NiSO_4 \cdot 6H_2O$, [b]$FeSO_4 \cdot 7H_2O$, [c]$CoSO_4 \cdot 7H_2O$.

*Characterization.* The surface morphology and structure of the NWs were characterized using a LEO 130 VP field emission scanning electron microscope (FESEM) and a JEOL EM 2010 transmission electron microscope (TEM). For TEM analysis, AAO containing NWs were placed in 0.1M NaOH solution for overnight to dissolve the template and then carefully rinsed with distilled water and acetone. TEM samples were prepared by evaporating a drop of an ethanol nanowire solution on a TEM grid; samples were analyzed at an accelerating voltage of 200 kV. To measure the crystallinity and phase purity of the NWs, X-ray powder diffraction (XRD) analysis was performed using a Philips X-pert PW 3040 MPD diffractometer with a CuKα X-ray source. Finally, the magnetic behavior of the wires were studied at room temperature using a vibrating sample magnetometer (VSM, Lake Shore 7300 series).

### 3.3. Results

Figure 3.1 shows cross-sectional views of a series of PEG-coated magnetic nanowires grown in alumina templates by electrodeposition. Templates with an average diameter of either 60 nm or 130 nm (Figure 3.1a and 3.1b) were used to grow Fe, Co, and Ni containing wires. Polymer coated Ni nanowire arrays were fabricated using the composition PEG-Ni-1 given in Table 3.1 at a constant current of -0.25 mA in both 60 nm and 130 nm AAO templates. The FESEM images of these wires within the templates are given in Figure 3.1c and 3.1d. The smaller pore diameters led to a decrease in the length of nanowires, opposite to what is typical for wire growth in such membranes.
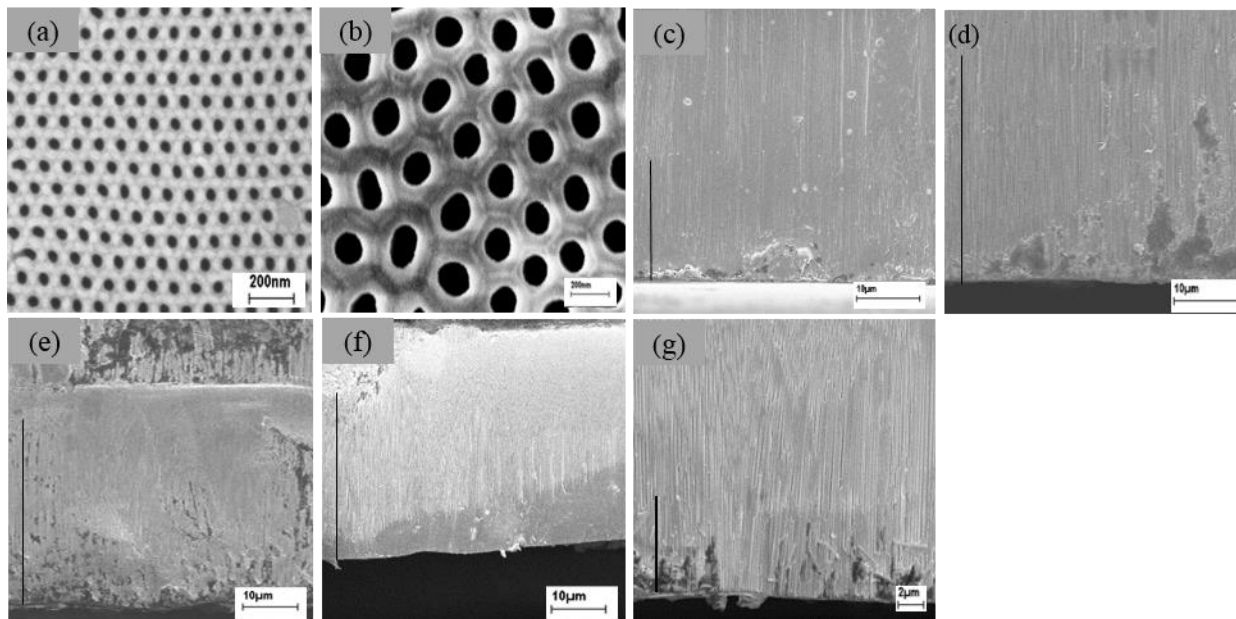
**Figure 3.1.** FESEM images. Top view of AAO templates used for the fabrication of ferromagnetic polymer composite nanowires (a) 60 nm (b) 130 nm. Cross-sectional view of the nanowires within AAO templates (c) PEG-Ni-1-60 nm NWs fabricated using 60 nm diameter AAO (length = 14μm), (d) PEG-Ni-1-130 nm NWs fabricated using 130 nm diameter AAO (length = 35 μm), (e) PEG-Ni-2-130 nm, NWs length = 33 μm (increase in current to -0.5 mA), (f) PEG-Ni-3-130 nm, length = 30 μm, (increase in concentration of $NiSO_4 \cdot 6H_2O$), (g) PEG-Ni-4-130 nm, length = 7 μm, (increase in PEG concentration).

Further studies of wire growth then focused on 130 nm templates. In order to analyze the growth rate of wires in the presence of polymer, the synthetic approach was varied by changing the applied current and the concentrations of metal salt and polymer. When the applied current is doubled (PEG-Ni-2), the increase does not have much effect on the growth rate (Figure 3.1e). Doubling the Ni concentration (PEG-Ni-3) also did not show a significant change in the nanowire

growth rate (Figure 3.1f). In the case of the polymer component, however, there was a change – an increase in PEG concentration significantly decreased the growth rate and wires grown under these conditions were typically a quarter the size of the other wires.
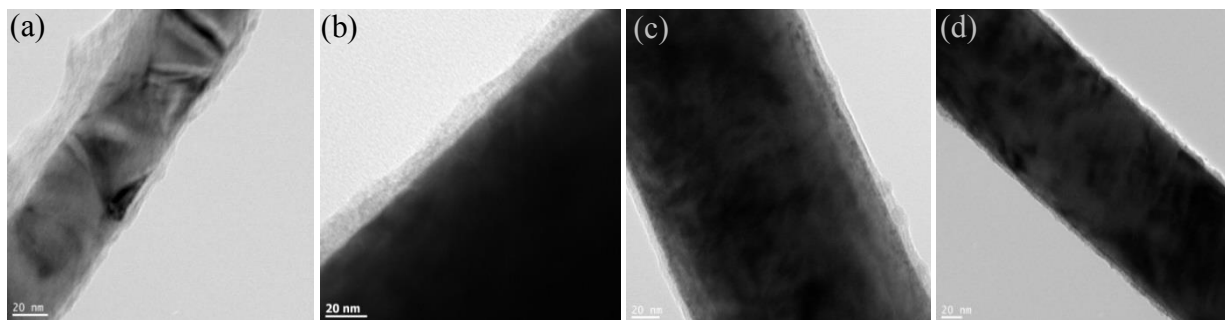


**Figure 3.2.** TEM images of polymer-coated Ni, Fe, Co, nanowires a) PEG-Ni-1-60 nm, b) PEG-Ni-1-130 nm, c) PEG-Fe-130 nm, and d) PEG-Co-130 nm.
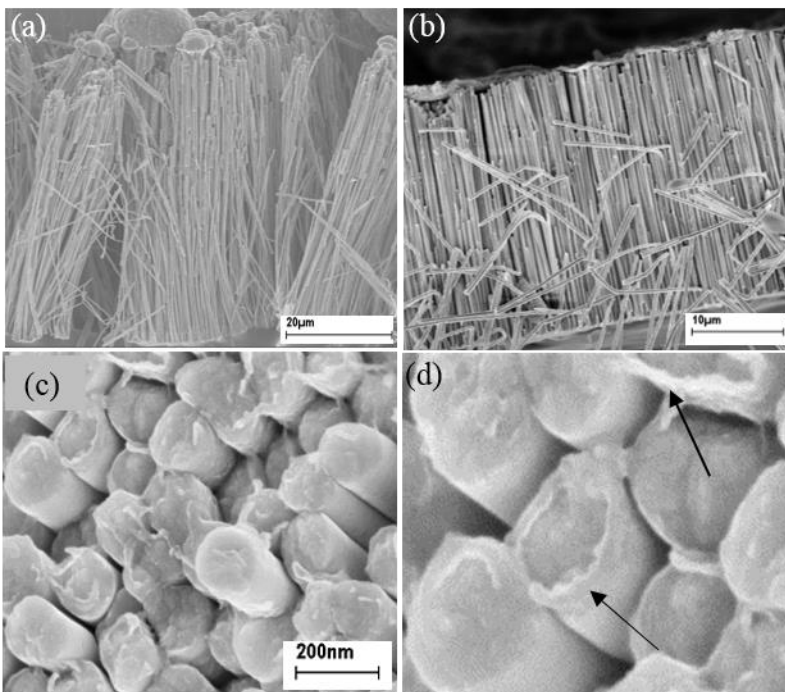


**Figure 3.3.** FESEM images of nanowires without AAO template. (a) Uncoated Ni nanowires, (b) PEG coated Ni nanowires, (c) top view of PEG coated nanowires, and (d) higher magnification images of c showing polymer coating on tip of nanowire as highlighted by arrows.

TEM (Figure 3.2) and FESEM images (Figure 3.3) of polymer coated Ni, Fe and Co nanowires were collected after the removal of template with 0.1M NaOH solution. Figure 3.2 shows the thin polymer coating on the wires typically ranging from about 5-20 nm in thickness and extending along the full length of the wires. This behavior was observed in both the 60 nm and 130 nm diameter wires. Figure 3.3 shows a series of micrographs of nickel wires. Figure 3.3a and 3.3b compare cross-sectional images of nanowire arrays with and without polymer coating, respectively. It is seen that the uncoated wires have a greater tendency to bunch together and those wires on the periphery are seen to break off all along the length of the wires. In contrast, the polymer coated wires show less evidence of bunching and instead of breaking, exhibit a greater tendency to bend before breaking. Higher magnification images (Figures 3.3c and 3.3d) of the tops of the nickel wires show further evidence for the polymer coating.
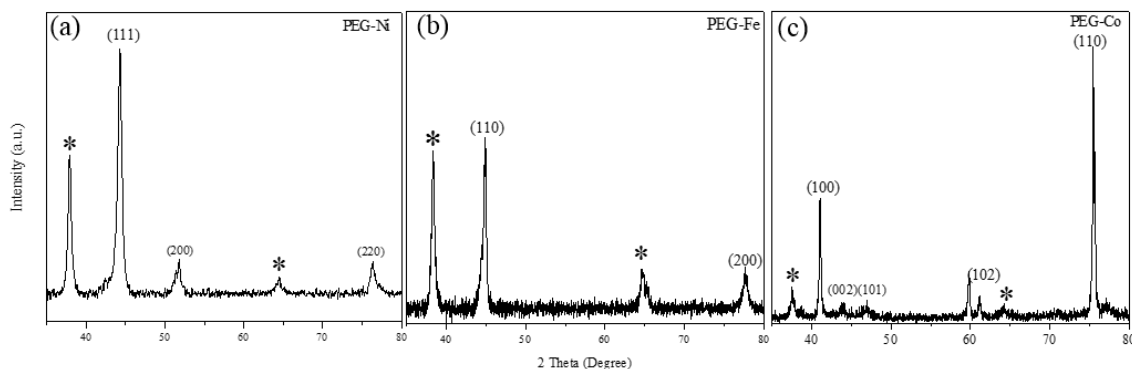


**Figure 3.4.** XRD patterns of metal wire arrays of (a) FCC Ni (PEG-Ni-1-130 nm) (b) BCC Fe (PEG-Fe-130 nm), and (c) HCP Co (PEG-Co-130 nm). Indices are shown above select reflections for each sample. Peaks with (*) are from sputtered gold on templates.

All of the nanowires synthesized in this study are polycrystalline. From the XRD patterns of the nanowires after template removal (Figure 3.4), the Ni, Fe and Co nanowires are found to

grow in the typical FCC, BCC, and HCP crystal structures, respectively.  There is no indication that the polymer affected the growth of the crystalline materials.

Magnetic properties of the various nanowires were measured while embedded in AAO templates. Hysteresis loops for polymer coated Ni, Fe, and Co and nanowires are presented in Figure 3.5. Data include along the wires axis (solid line, 0 degrees) and perpendicular to the wires axis (dotted line, 90 degrees) with the corresponding coercivity ($H_c$) values given in Table 3.2. For all these systems, the hysteresis loop exhibits a higher coercivity when the applied field is parallel to the wires than when the field is perpendicular, which is a typical characteristic of such wires. Furthermore, magnetic data shows no effect of polymer on the magnetic properties of nanowire arrays. Table 3.2 contains coercivity values for uncoated Ni 60 nm and 130 nm nanowires, Ni-60 nm and Ni-130 nm, respectively.
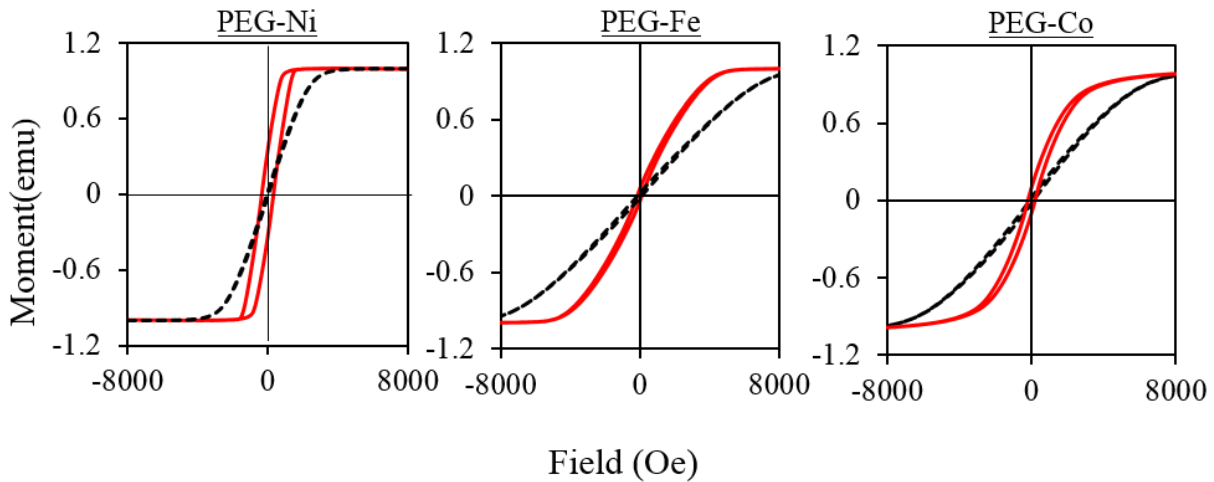


**Figure 3.5.** Hysteresis loops of PEG-magnetic nanowires along the wires (solid lines) and perpendicular to the wires (dotted lines) at room temperature.

**Table 3.2.** Coercivity ($H_c$) values of PEG coated Ni nanowire samples along the wires (0 deg) and perpendicular to the wires (90 deg) of magnetic plane. Uncoated Ni nanowires are shown for comparison.

| Sample | $H_c$ (Oe, 0 deg) | $H_c$ (Oe, 90 deg) |
|---|---|---|
| Ni-60[a] nm | 907 | 90 |
| Ni-130[a] nm | 323 | 91 |
| PEG-Ni-1-60 nm | 914 | 98 |
| PEG-Ni-1-130 nm | 363 | 82 |
| PEG-Ni-2-130 nm | 323 | 76 |
| PEG-Ni-3-130 nm | 314 | 123 |
| PEG-Ni-4-130 nm | 293 | 95 |

[a]Nickel nanowire samples not coated with PEG.

## 3.4. Discussion

This work shows that it is possible to fabricate PEG coated nanowires by simultaneous deposition of metal and polymer. To understand the growth mechanism, synthesis parameters including the concentrations of the salts and the polymer, the current density, and the pore diameter of AAO were varied. All the nanowires were fabricated at -0.25 mA except PEG-Ni-2, which was fabricated at -0.5 mA. An outer polymer layer formed in each synthesis, irrespective of fabrication conditions. By monitoring the growth of nanowires using deposition solutions with and without PEG it was found that the presence of polymer in the electrolyte decreases the rate of synthesis of

nanowires. While preparing zinc oxide nanowires from a mixture of zinc acetate and sodium hydroxide using lower molecular weight PEG (400), Li *et al.* found that the kinetics of colloid growth decrease due to polymer adsorption the on colloid surface such that it restricts growth direction.[18] Also Stojilkovic *et al.* showed that the conductivity of a solution decreases with an increase in polymer concentration due to decreased ionic mobility.[19] The cross-sectional FESEM images show (Figure 3.1) not much variation in the length of nanowires that were synthesized under different reaction conditions (Table 3.1 - samples PEG-Ni-1, 2 and 3) using 130 nm AAO templates. There was a difference however in 130 nm versus 60 nm; under the same conditions of deposition the growth rate decreased with the decrease in template pore diameter, the opposite of what usually occurs in nanowire growth. Typically under these reaction conditions, the 60 nm diameter wire would be about twice the length of the 130 nm template, but in the presence of the polymer, the 60 nm wire is about 2.5 times smaller. It would appear that the presence of PEG in the 60 nm pore serves to limit diffusion of metal ions which in turn suppresses the growth of the nanowires. A similar effect can be seen in the 130 nm diameter wires when the concentration of the PEG is doubled; the increase in polymer concentration used in the PEG-Ni-4 sample decreases the growth rate of the 130 nm nanowires by about 5 times.

While the addition of the polymer does affect the growth of the wires, the wires themselves still retained their structural and physical properties. XRD data (Figure 3.4) shows the three metals in crystal structures typical in direct electrodeposition, Ni (FCC), Co (HCP), and Fe (BCC), and hysteresis data (Figure 3.5 and Table 3.2) show the expected results for high aspect nanowires, [20] where the there is an orientation dependence that varies with aspect ratio.

The simultaneous growth of both nanowires and their polymer coating appears to occur readily with the AAO porous membranes. One can then speculate on a possible mechanism for

this process. During electrochemical deposition, the nanowire grew as a result of reduction of metal ions ($M^{2+}$) on the cathode surface.[21] This process has been well detailed in the literature [22] and is thought to proceed by the following four steps (Equations 1-4). Initially, the electrolyte was prepared by adding inorganic salt in water. As a result, dissociation of water and formation of metal hydroxide ion can take place as given in equation 1 and 2. Hydrated metal ions present in the solution are adsorbed on the conductive metal surfaces at cathode in the presence of an applied field. These hydrated metal ions are then neutralized by accepting electrons. The neutral metal atom adsorbs on the cathode surface and further diffuses to the surface site where it unites with metal ions and results in the subsequent growth of the metal nanowires. These four steps are described by the following equations:

$$H_2O \quad \rightarrow \quad H^+ + OH^- \tag{1}$$

$$M^{2+} + OH^- \quad \rightarrow \quad M(OH)^+ \tag{2}$$

$$M(OH)^+ \quad \rightarrow \quad M(OH)^+_{(ads)} \tag{3}$$

$$M(OH)^+_{(ads)} + 2\,e^- \quad \rightarrow \quad M^0 + OH^- \tag{4}$$
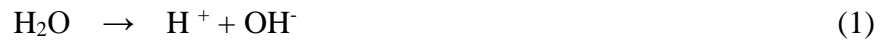
PEG contains continuous chain structure, $-O-CH_2-CH_2-O-$, with hydrophobic $-CH_2-CH_2-$ and hydrophilic $-O-$ components. The electron-rich $-O-$ atoms interact with metal cations through coordination bonds. As a coordination polymer, PEG is known to adsorb metal cations.[23] This property of PEG makes the compound useful in the synthesis of a variety of nanomaterials. For example, metal oxide nanowires were synthesized by Jiang *et al.* by combining ethylene glycol in with metal salts.[24] They found that this water-soluble polymer forms a helical-like structure when dissolved in water (Figure 3.6) and coordinates to metal cations, like nickel. When the polymer grows sufficiently long, it aggregates into bundles and, after calcination, leads to amorphous metal oxide nanowires.
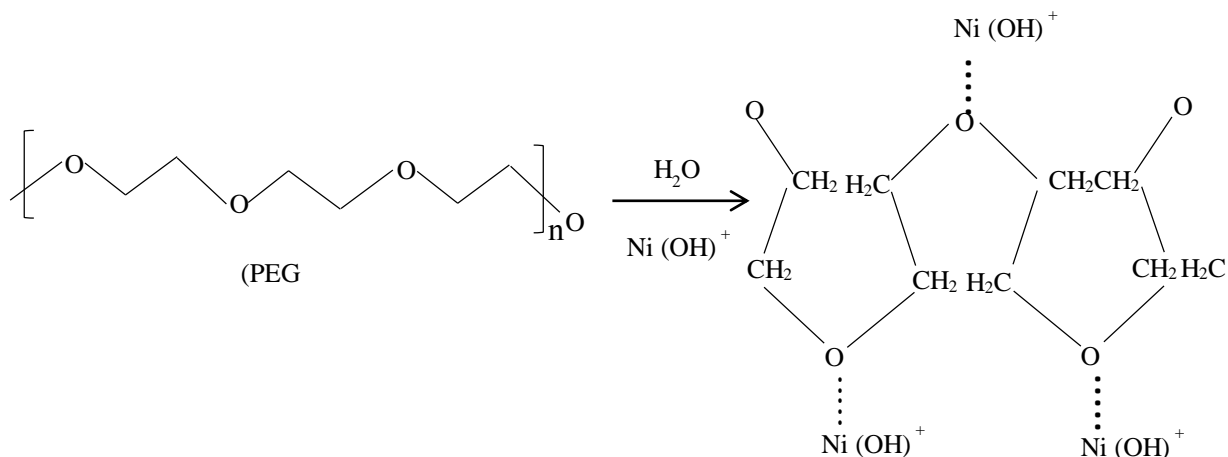
**Figure 3.6.** Coordination of metal hydroxide ion to polyethylene glycol.

In this study, the deposition solutions contained PEG along with boric acid and the corresponding ferromagnetic salts. In the presence of an applied current the polymer moves with the metal ions toward the template pore channels, which act as a cathode. As reported before by Shankar *et al.* the pore walls of the AAO templates are positively charged due to the presence of complex anion $Al(H_2O)_4(OH)_2^+$ on the surface of anodic films. These species help the metal



$\overset{\curlywedge}{\underset{|}{M}} (OH)^+$ represents the polymer adsorbed metal hydroxide ions.
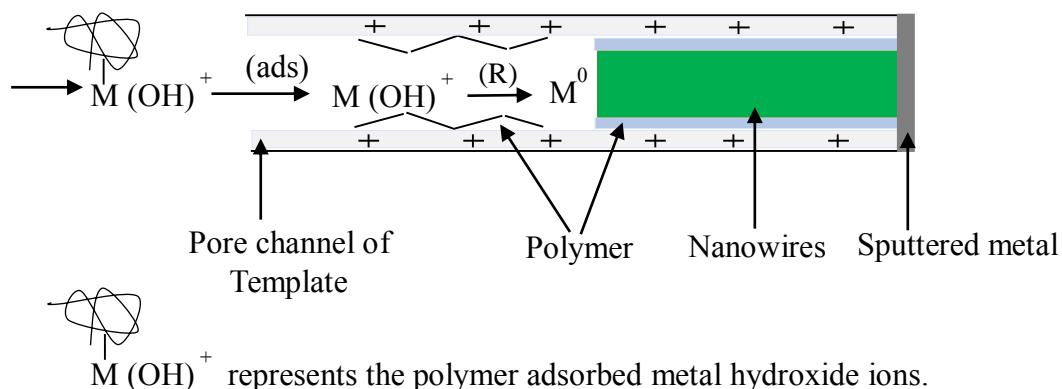
**Figure 3.7.** Schematic illustrations of PEG-NW formation inside the pore wall of template.

cations to move to the center of the pore while the polymer moves to the pore wall (Figure 3.7) and gets adsorbed onto the inner pore wall of the AAO template.[25] As a result of nucleation and crystallization during deposition, nanowires were synthesized within the pore channels with PEG as an outer supporting layer because of simultaneous deposition of metal ions and the polymer.

## 3.5. Conclusions

Polymer coated nanowires were fabricated at room temperature by simultaneous deposition of metal ions and polymer during template assisted electrochemical deposition. A systematic study of nanowire fabrication was carried out by varying the synthesis parameters. A growth mechanism is proposed in which the AAO template acted as the adsorption site during the simultaneous growth of polymer and metal nanowires. It was found that the polymer did not have any influence on the crystallinity and magnetic behavior of the nanowire arrays. The polymer, however played an important role in the rate of synthesis as an increase in polymer concentration decreases the wire growth rate.

### Acknowledgments

## 3.6. References

1. Anguelouch, A.; Reich, D. H.; Chien, C. L.; Tondra, M., Detection of ferromagnetic nanowires using GMR sensors. *Ieee Transactions on Magnetics* **2004,** *40* (4), 2997-2999.
2. Wang, Z. K.; Kuok, M. H.; Ng, S. C.; Lockwood, D. J.; Cottam, M. G.; Nielsch, K.; Wehrspohn, R. B.; Gösele, U., Spin-Wave Quantization in Ferromagnetic Nickel Nanowires. *Physical Review Letters* **2002,** *89* (2), 027201.
3. Ding, L. X.; Wang, A. L.; Li, G. R.; Liu, Z. Q.; Zhao, W. X.; Su, C. Y.; Tong, Y. X., Porous Pt-Ni-P Composite Nanotube Arrays: Highly Electroactive and Durable Catalysts for Methanol Electrooxidation. *Journal of the American Chemical Society* **2012,** *134* (13), 5730-5733.

4. Salem, A. K.; Searson, P. C.; Leong, K. W., Multifunctional nanorods for gene delivery. *Nature Materials* **2003,** *2* (10), 668-671.

5. Harisinghani, M. G.; Weissleder, R., Sensitive, noninvasive detection of lymph node metastases. *Plos Medicine* **2004,** *1* (3), 202-209.

6. (a) Hu, X.; Yu, J. C., High-Yield Synthesis of Nickel and Nickel Phosphide Nanowires via Microwave-Assisted Processes. *Chemistry of Materials* **2008,** *20* (21), 6743-6749; (b) Xu, D.; Liu, Z.; Liang, J.; Qian, Y., Solvothermal Synthesis of CdS Nanowires in a Mixed Solvent of Ethylenediamine and Dodecanethiol. *The Journal of Physical Chemistry B* **2005,** *109* (30), 14344-14349; (c) Wang, D.; Dai, H., Low-Temperature Synthesis of Single-Crystal Germanium Nanowires by Chemical Vapor Deposition. *Angewandte Chemie* **2002,** *114* (24), 4977-4980; (d) Miao, Z.; Xu, D.; Ouyang, J.; Guo, G.; Zhao, X.; Tang, Y., Electrochemically Induced Sol−Gel Preparation of Single-Crystalline TiO2 Nanowires. *Nano Letters* **2002,** *2* (7), 717-720.

7. (a) Shi, D. W.; Chen, J. Y.; Riaz, S.; Zhou, W. P.; Han, X. F., Controlled nanostructuring of multiphase core-shell nanowires by a template-assisted electrodeposition approach. *Nanotechnology* **2012,** *23* (30); (b) Jeon, I. T.; Cho, M. K.; Cho, J. W.; An, B. H.; Wu, J. H.; Kringel, R.; Choi, D. S.; Kim, Y. K., Ni-Au core-shell nanowires: synthesis, microstructures, biofunctionalization, and the toxicological effects on pancreatic cancer cells. *Journal of Materials Chemistry* **2011,** *21* (32), 12089-12095.

8. Zhang, D. H.; Liu, Z. Q.; Han, S.; Li, C.; Lei, B.; Stewart, M. P.; Tour, J. M.; Zhou, C. W., Magnetite (Fe3O4) core-shell nanowires: Synthesis and magnetoresistance. *Nano Letters* **2004,** *4* (11), 2151-2155.

9. (a) Pimpinella, R. E.; Zhang, D.; McCartney, M. R.; Smith, D. J.; Krycka, K. L.; Kirby, B. J.; O'Dowd, B. J.; Sonderhouse, L.; Leiner, J.; Liu, X.; Dobrowolska, M.; Furdyna, J. K., Magnetic properties of GaAs/Fe core/shell nanowires. *Journal of Applied Physics* **2013,** *113* (17); (b) Tivakornsasithorn, K.; Pimpinella, R. E.; Nguyen, V.; Liu, X.; Dobrowolska, M.; Furdyna, J. K., Magnetic anisotropy of GaAs/Fe/Au core-shell nanowires grown by MBE. *Journal of Vacuum Science & Technology B* **2012,** *30* (2).

10. Park, D. H.; Lee, Y. B.; Cho, M. Y.; Kim, B. H.; Lee, S. H.; Hong, Y. K.; Joo, J.; Cheong, H. C.; Lee, S. R., Fabrication and magnetic characteristics of hybrid double walled nanotube of ferromagnetic nickel encapsulated conducting polypyrrole. *Applied Physics Letters* **2007,** *90* (9).

11. (a) Hultgren, A.; Tanase, M.; Chen, C. S.; Meyer, G. J.; Reich, D. H., Cell manipulation using magnetic nanowires. *Journal of Applied Physics* **2003,** *93* (10), 7554-7556; (b) Hultgren, A.; Tanase, M.; Chen, C. S.; Reich, D. H., High-yield cell separations using magnetic nanowires. *Ieee Transactions on Magnetics* **2004,** *40* (4), 2988-2990.

12. Inada, Y.; Furukawa, M.; Sasaki, H.; Kodera, Y.; Hiroto, M.; Nishimura, H.; Matsushima, A., biomedical and biotechnological applications of peg-modified and pm-modified proteins. *Trends in Biotechnology* **1995,** *13* (3), 86-91.

13. (a) Arakawa, T.; Timasheff, S. N., Mechanism of polyethylene glycol interaction with proteins. *Biochemistry* **1985,** *24* (24), 6756-6762; (b) Wu, J.; Zhao, C.; Lin, W.; Hu, R.; Wang, Q.; Chen, H.; Li, L.; Chen, S.; Zheng, J., Binding characteristics between polyethylene glycol (PEG) and proteins in aqueous solution. *Journal of Materials Chemistry B* **2014,** *2* (20), 2983-2992.

14. Anwar, H.; Maqsood, A.; Pervaiz, E., Structural, Magnetic, and Dielectric Properties of PEG Assisted Synthesis of Mn0.5Ni0.5Fe2O4 Nanoferrites. *Journal of Superconductivity and Novel Magnetism* **2013,** *26* (9), 2955-2960.

15. Topkaya, R.; Kurtan, U.; Baykal, A.; Sozeri, H.; Toprak, M. S., Polymer Assisted Co-precipitation Synthesis and Characterization of Polyethylene Glycol (PEG)/CoFe2O4 Nanocomposite. *Journal of Inorganic and Organometallic Polymers and Materials* **2013,** *23* (3), 592-598.

16. Muraliganth, T.; Vadivel Murugan, A.; Manthiram, A., Facile synthesis of carbon-decorated single-crystalline Fe3O4nanowires and their application as high performance anode in lithium ion batteries. *Chemical Communications* **2009,** (47), 7360-7362.

17. Chen, S.; Ling, Z.; Hu, X.; Li, Y., Controlled growth of branched channels by a factor of 1/root n anodizing voltage? *Journal of Materials Chemistry* **2009,** *19* (32), 5717-5719.

18. Li, Z.; Xiong, Y.; Xie, Y., Selected-Control Synthesis of ZnO Nanowires and Nanorods via a PEG-Assisted Route. *Inorganic Chemistry* **2003,** *42* (24), 8105-8109.

19. Stojilkovic, K. S.; Berezhkovskii, A. M.; Zitserman, V. Y.; Bezrukov, S. M., Conductivity and microviscosity of electrolyte solutions containing polyethylene glycols. *Journal of Chemical Physics* **2003,** *119* (13), 6973-6978.

20. Qin, J.; Nogues, J.; Mikhaylova, M.; Roig, A.; Munoz, J. S.; Muhammed, M., Differences in the magnetic properties of Co, Fe, and Ni 250-300 nm wide nanowires electrodeposited in amorphous anodized alumina templates. *Chemistry of Materials* **2005,** *17* (7), 1829-1834.

21. (a) Tan, M.; Chen, X. Q., Growth Mechanism of Single Crystal Nanowires of fcc Metals (Ag, Cu, Ni) and hcp Metal (Co) Electrodeposited. *Journal of the Electrochemical Society* **2012,** *159* (1), K15-K20; (b) Cao, H.; Wang, L.; Qiu, Y.; Wu, Q.; Wang, G.; Zhang, L.; Liu, X., Generation and growth mechanism of metal (Fe, Co, Ni) nanotube arrays. *Chemphyschem* **2006,** *7* (7), 1500-1504.

22. Tan, M.; Chen, X., Growth Mechanism of Single Crystal Nanowires of fcc Metals (Ag, Cu, Ni) and hcp Metal (Co) Electrodeposited. *Journal of the Electrochemical Society* **2012,** *159* (1), K15-K20.

23. Comini, E., Metal oxide nano-crystals for gas sensing. *Analytica Chimica Acta* **2006,** *568* (1–2), 28-40.

24. Jiang, X. C.; Wang, Y. L.; Herricks, T.; Xia, Y. N., Ethylene glycol-mediated synthesis of metal oxide nanowires. *Journal of Materials Chemistry* **2004,** *14* (4), 695-703.

25. Shankar, K. S.; Raychaudhuri, A. K., Growth of an ordered array of oriented manganite nanowires in alumina templates. *Nanotechnology* **2004,** *15* (9), 1312-1316.

**Chapter 4**

**Synthesis and Characterization of Polymer-Embedded Ferromagnetic Nanowire Arrays**

**4.1. Introduction**

When solids are characterized at the nanometer scale many interesting properties emerge which can sometimes be completely different from the bulk sized material. In terms of magnetic properties, slight variations in the characteristics of materials such as size, shape, anisotropy, chemical deposition, spatial assembly etc. can strongly affect the magnetic behavior. In the case of nanostructured materials these characteristics can lead to a number of novel properties with potential applications in different interdisciplinary research fields ranging from biomedicine[1] to energy and data storage.[2] An ideal ultrahigh density recording medium, for example, is a nanostructure with magnetically isolated small grains. The development of magnetic recording media is impacted by the super-paramagnetic limit, the size limit where thermal effects disrupt data storage. Ferromagnetic nanowires have been suggested as a way of improving properties.[3] Different methods have been used for synthesizing nanowires such as sol-gel method,[4] hydrothermal method,[5] template method,[6] etc. Under appropriate conditions these methods allow for tight control over the size and shape of nanoscaled materials. The template method of preparing a variety of micro- and nano-materials has been especially effective. Metallic nanowires are fabricated by electrodeposition in nanoporous membranes. Commercially available anodized aluminum oxide (AAO) and track-etched polycarbonate (PC) membranes can be used. AAO membrane can also be synthesized in-house with a multistep anodization procedure resulting in templates with desired pore sizes of uniform diameters.[7] Due to the controlled aspect ratio

49

synthesis and shape anisotropy magnetic nanowires have wide applications such as magnetic data storage,[8] microwave devices,[9] and spin-transfer torque devices.[10]

A drawback of the template assisted electrodeposition method is that the wires often agglomerate together forming tee-pee like structures after the removal of the template. This can be controlled by fabricating composites and embedding the nanowire arrays within a matrix that can tune the nanowire surface without disturbing the orientation of the wires.  In recent studies, different types of materials have been synthesized as composite nanowires that can be used in biology as a nano-label in biological assays,[11] electronics,[12] solar cells,[13] and magnetic applications.[14] The main focus of the research presented herein was to study the variation in magnetic properties of the nanowire arrays after removing the template and embedding the wires within a polymer matrix. For the fabrication of polymer embedded ferromagnetic nanowires, polymer coated nanowires were synthesized and embedded within two different stimuli-active polymers, polyethylene glycol diacrylate (PEGDA) and azobenzene-polyacrylate. These two polymer are solvent active. The swelling ratio of PEGDA depends on the concentration of solvents used to synthesize it whereas the change in length of azobenzene-polyacrylate in presence of UV light depends on the thickness of the film and the amount of photo initiator used during polymerization.[15]

## 4.2. Experimental

Polyethylene glycol (PEG) coated Ni nanowires were fabricated using electrochemical deposition method where simultaneous deposition of PEG and metal nanowires occurred (Given in Chapter 3). After the removal of AAO templates, azobenzene-polyacrylate and PEGDA polymers were used to embed nanowires. The steps of synthesis are discussed below.

*1) Fabrication of PEG-Ni nanowires:*

Polyethylene glycol coated Ni nanowires were fabricated from solution containing 0.05M NiSO$_4$·6H$_2$O (98% Alfa-Aesar), 0.02M Polyethylene Glycol (PEG-M$_w$1500, Alfa-Aesar) and (0.02M) H$_3$BO$_3$ (99.8% EM Science) at -0.25 mA applied current. Gold sputtered AAO template served as working electrode with platinum wire as counter electrode and Ag/AgCl as reference electrode. A set of three different pore diameter 60 nm, 80 nm, 130 nm of PEG-Ni nanowires were fabricated and the variations in magnetic properties of polymer embedded polyethylene glycol (PEG) containing Ni nanowires (PEG-Ni) were measured.

*2) Polymerization*

Two different polymers, PEGDA and azobenzene-polyacrylate, were used to embed with PEG coated nanowires after removing the AAO template. Out of these two polymers, PEGDA was polymerized in the presence of UV light and azobenzene-polyacrylate was polymerized an inert atmosphere in presence of heat. Further, embedding nanowires within a polymer matrix in the presence or absence of magnetic field and its effect on nanowire orientation was also studied during PEGDA polymerization.

*(a) Polyethylene glycol diacrylate (PEGDA)*

The synthesis of this polymer was from PEG 575 DA (Aldrich), Type I water (Millipore MilliQ), and Darocur 1173 photo initiator (Ciba). These polymeric materials are well known to absorb polar solvents and swell, and thus have been used in many biomedical applications.[16] To study the swelling ratio of PEGDA, four different percent ratio 2%, 4%, 6%, and 8% of PEG 575 DA were taken in Millipore water with 0.1% photo initiator. The solution mixtures were then exposed to UV light for polymerization. For the varying amounts of PEGDA units used, the texture

of each of the polymers were different after polymerization. 2% PEGDA was gelatinous whereas 8% PEGDA was solid. Subsequently, weight was measured before and after evaporating the solvent from the polymer using an oven at 70 °C overnight. Subtraction of the weights per the total weight provides the swelling ratio. Figure 4.1 shows a change in size of 6% PEGDA after and before drying the synthesized polymer. This composition was later used to embed nanowire arrays.
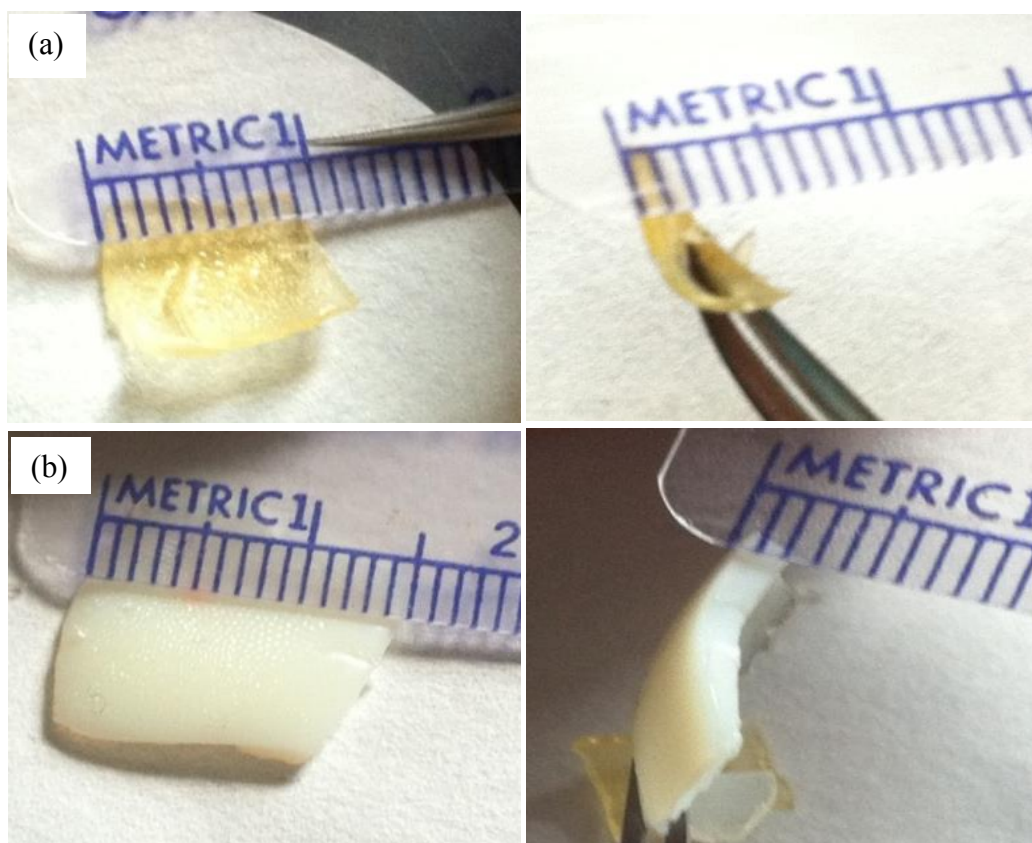


**Figure 4.1.** Surface and cross-section of (a) dry and (b) hydrated piece of piece of polymer, respectively.

*(b) Azobenzene-polyacrylate:*

Azobenzene-polyacrylate polymers were fabricated following the method given by Zhang et al.[17] Briefly, the crosslinkers and monomers were first synthesized as given below. For this

synthesis, 4-ethoxyaniline, phenol, 6-chloro-1-hexanol and acryloyl chloride, 4-aminophenol were purchased from Alfa Aesar and tetrabutylammoniumbromide, 2, 2´-azobisisobutyronitrile (AIBN) were purchased from Sigma-Aldrich.

*(i) Synthesis of Crosslinker.* Crosslinkers were synthesized following the three-step procedure given below.

a) 4-amino phenol (0.150M) was dissolved in 82 ml of 1:1 mixture solution of water and concentrated HCl in a round bottom flask. The solution was kept in iced-water bath and stirred vigorously at all times. Next, 0.166 M of sodium nitrite was added slowly in 35 ml of water. This solution was then added drop by drop to the mixture of solvents containing 0.155M of phenol dissolved in 7.5M of sodium hydroxide. 12M HCl was then added to adjust the pH of this solution to 1. After continuously stirring for 2 h a precipitate was formed. The precipitate was filtered using a sintered glass filter. After filtration, distilled water was used to wash the precipitate on the filter to bring the pH of the filtrate to 7. Finally, the precipitate was recrystallized using acetone and then by water. The solution was dissolved in acetone and characterized using ¹H-NMR. The ¹H-NMR spectra confirmed the formation of 4, 4´-Dihydroxyazobenzene (6.93 (d, 4H, Ar-H), 7.78 (d, 4H, Ar-H), 8.96 (s, 2H, Ar-OH)).

b) In an inert atmosphere of dry nitrogen, 14.15 mmol of 4, 4´-Dihydroxyazobenzene, 70.75 mmol of potassium carbonate and tetrabutylammoniumbromide (5% amount to 4, 4´-dihydroxyazobenzene) was dissolved in 30 ml of anhydrous dimethylformamide (DMF) in a round bottom flask on a magnetic stirrer. Next, 31.13 mmol of 6-chloro-1-hexanol was added slowly and heated at 90 °C for 48 h on an oil bath. After completely cooling the solvent mixture to room temperature, 100 ml of 12 M HCl was added. The resulting precipitate was washed with distilled water until pH 7 was achieved followed by recrystallization with acetone and water. The solution

was dissolved in acetone and characterized using $^1$H-NMR. The $^1$H-NMR spectra showed at 7.88 (d, 4H, Ar-H), 7.09 (d, 4H, Ar-H), 4.11 (t, 4H), 3.56 (q, 4H), 3.44 (t, 2H), 2.80 (t, 4H), 1.82 (quin, 4H), 1.59-1.43 (m, 12H) for 4, 4´-Bis (6-hydroxyhexyloxy) azobenzene.

c) In an inert atmosphere, 4.919 mmol of 4, 4´–bis (6-hydroxyhexyloxy) azobenzene was dissolved in 30 ml of tetrahydrofuran (THF) and 11.8 mmol of triethylamine on a magnetic stirrer. 11.8 mmol of acryloyl chloride added drop-by-drop to this solution and the solution was stirred for 2 h. The precipitate formed was filtered and washed with THF. From the filtered solvent THF was evaporated and the product was recrystallized with acetone. The solution was dissolved in acetone and characterized using $^1$H-NMR. The $^1$H-NMR spectra at 7.86 (d, 4H), 7.8 (d, 4H), 6.34 (dd, 2H), 6.14 (q, 2H), 5.87 (dd, 2H), 4.14 (m, 8H), 1.43-1.33 (m, 16H) showed the presence of crosslinker 4, 4´–bis (6-acryloyloxyhexyloxy) azobenzene.

*(ii)Monomer synthesis*: Like the crosslinkers, monomers were synthesized following the three-step procedure given below.

a) First, monomer 4-ethoxy-4´-(6-acryloyloxyhexyloxy) azobenzene was synthesized using the same method as for the synthesis of the cross linker described above but using 0.155 mmol of 4-ethoxyaniline instead of 4-amino phenol. The solution was dissolved in acetone and characterized using $^1$H-NMR. The $^1$H-NMR spectra showed 9.01(s, 1H), 7.82 (dd, 4H), 7.05 (dd, 4H), 4.15 (q, 2H), 1.41(t, 3H) for confirming the presence of 4-Ethoxy-4´-hydroxyazobenzene.

b) 4-Ethoxy-4´-(6-hydroxyhexyloxy) azobenzene was produced from 4-Ethoxy-4´-hydroxyazobenzene using the same method as for crosslinker in a dry nitrogen atmosphere but with a different amount of reagents. 22.75 mmol of 4-ethoxy-4´-hydroxyazobenzene was mixed with 45.50 mmol of potassium carbonate and tetrabutylammoniumbromide (5% amount to 4, 4´–

bis (6-acryloyloxyhexyloxy) azobenzene) dissolved in 20ml of DMF. The mixture solvent was heated at 90 °C for 48 h after adding 24 mmol of 6-chloro-1-hexanol drop-by-drop. 100 ml of 6M HCl was added after cooling it down to room temperature. The precipitate was filtered using a sintered glass filter. After filtration, distilled water was used to wash the precipitate on the filter to bring the pH of the filtrate to 7. The precipitate was vacuum dried and recrystallized using acetone. The solution was dissolved in acetone and characterized using $^1$H-NMR. The $^1$H-NMR spectra at 7.86 (d, 4H), 7.10 (d, 4H), 6.34 (dd, 2H), 6.15 (q, 2H), 5.87 (dd, 2H), 4.14 (m, 8H), 1.43-1.33 (m, 16H) showed the presence of 4-Ethoxy-4´-(6-hydroxyhexyloxy) azobenzene.

c) Finally, 4-Ethoxy-4´- (6-acryloyloxyhexyloxy) azobenzene was prepared using the same method as the last step for the synthesis of the crosslinker but 3.928 mmol of 4-ethoxy-4´-(6-hydroxyhexyloxy) azobenzene was dissolved in 30 ml of THF and 4.714 mmol of triethylamine was added by vigorously stirring the solution. Then 4.714 mmol of acryl chloride was added drop-by-drop. After the reaction continued overnight, the precipitate was filtered and then washed by THF. After distillation of THF the product was vacuum-dried. The solution was dissolved in acetone and characterized using $^1$H-NMR. The $^1$H-NMR spectra at 7.86 (d, 4H), 7.08 (dd, 4H), 6.34 (d, 1H), 6.15 (q, 1H), 6.87(d, 1H), 4.19-4.10 (m, 6H), 1.43-1.33 (m, 11H) showed the presence of 4-Ethoxy-4´- (6-acryloyloxyhexyloxy) azobenzene.

*3) Embedding PEG-Ni nanowires in PEGDA Polymer*

After studying the polymer swelling behavior, nanowire arrays were embedded in the 6% PEGDA polymer. The samples were attached to copper tape and the templates were removed using 0.1 M NaOH. After washing the sample with water and then with ethanol, a few drops of PEGDA (Average Mw 575) solution were introduced into the wire array and exposed to UV light in the presence of a vertically applied magnetic field. This external applied magnetic field helped

nanowires to orient along the growth direction. Simultaneous polymerization supported embedding of polymer in nanowire arrays. To evaporate the solvent, the sample was heated in an oven overnight. The schematic diagram of this method is given in Figure 4.2 and 4.3.



Nanowire arrays within template     Nanowire arrays on Cu tape     Nanowire arrays without template on Cu tape
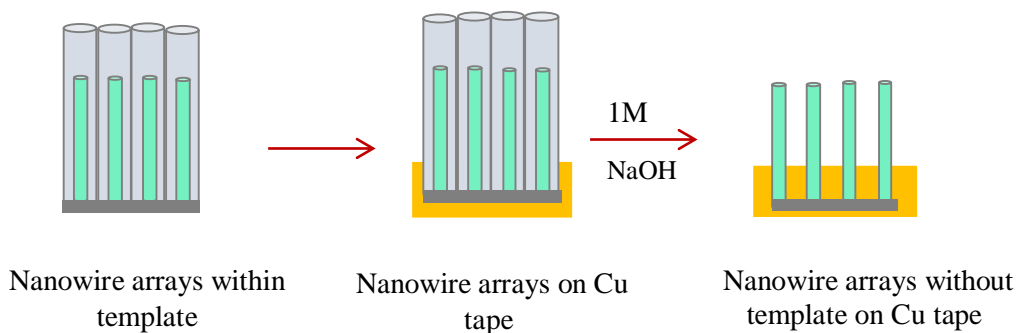
**Figure 4.2** Schematic diagram of steps used before embedding wires in PEGDA.
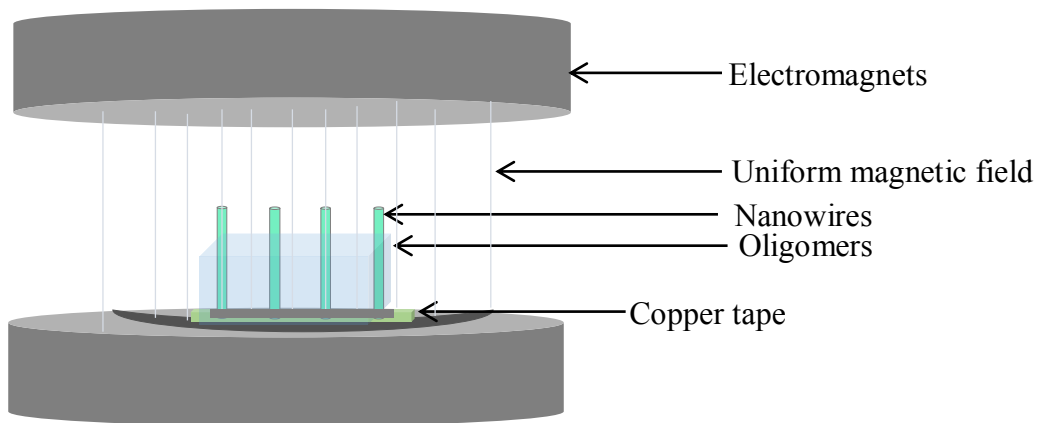


**Figure 4.3.** Illustration of embedding polymer using UV light with simultaneous application of magnetic field.

*4) Embedding PEG-Ni nanowires with azobenzene-polyacrylate*

To embed PEG-Ni nanowires with azobenzene-polyacrylate, a mixture of oligomer, crosslinker and azobisisobutyronitrile initiator (AIBN) with a weight ratio of 9:1:0.1, in 1 ml of toluene was placed on a round bottom flask and heated to 90 °C after three freeze-thaw cycles. Ni nanowires without AAO templates were then inserted directly to the melted solution and the reaction was continued overnight.

**Characterization**

To investigate the shape and size of synthesized nanowire arrays, field-emission scanning electron microscopy (FESEM, LEO 130VP) and transmission electron microscopy (TEM, JEOL EM 2010) were used. The TEM was operated at accelerated voltage of 200 keV. The composition of nanowires were measured by spot energy dispersive X-ray (EDS) analysis using an EDAX GENESIS equipped with JSM 5410 electron microscope. These fabricated PEG-Ni nanowire arrays were placed in 1M NaOH solution to dissolve the AAO template and then washed with distilled water. After the sample is completely dried at room temperature, the crystal structures of these nanowires were analyzed using a Philips X-pert PW 3040 MPD X-ray powder diffractometer. The magnetic hysteresis loops were measured by a vibrating sample magnetometer (VSM).

**4.3. Results**

PEG-coated nanowires were fabricated from AAO templates with pore diameters of 60 nm, 80 nm and 130 nm. The AAO templates with 60 nm and 80 nm pore diameter had an interpore distance of 100 nm whereas the AAO template with pore diameter of 130 nm had an interpore distance of 240 nm. After the removal of template, the wires with less interpore distance (e.g. 100 nm) were less vertically stable and tended to disorder more compared to the nanowires with higher

interpore distance (e.g. 240 nm). FESEM and TEM images after dissolving the template are given in Figure 4.4 for the larger 130 nm wires. Figure 4.4.a shows the magnified FESEM image of the top surface of these nanowire arrays with a polymer coating and Figure 4.4.b shows the resulting nanowires contained a thin outer polymer layer after the removal of the template.
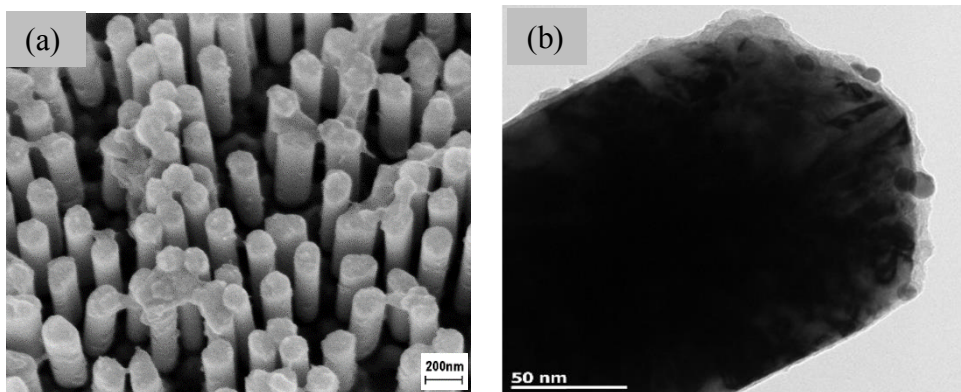


**Figure 4.4** (a) Surface view FESEM image of the 130 nm PEG-Ni nanowire arrays wires (b) TEM image of polymer coated nanowires.
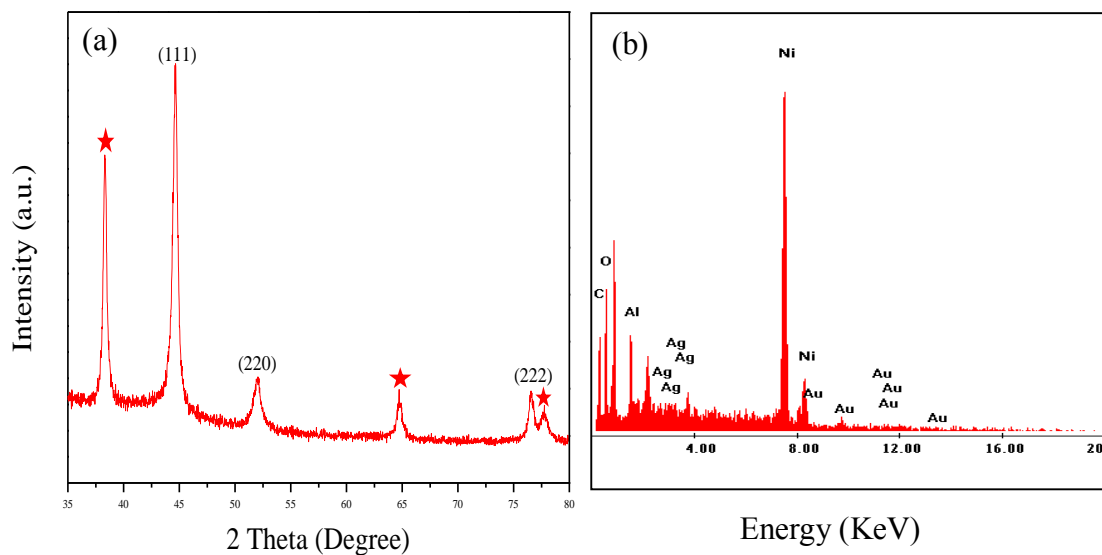


**Figure 4.5.** (a) XRD patterns for PEG-coated Ni nanowires. The (*) in XRD pattern is from the sputtered silver layer. (b) EDS spectrum showing the composition of the nanowire arrays.

The XRD patterns and EDS spectra for the nanowires were further analyzed after dissolving the AAO (Figure 4.5). The XRD patterns shows that these nanowires have an FCC crystal structure. The extra peaks are from the sputtered gold that was used for the fabrication of nanowires. EDS spectroscopy further confirmed the presence of Ni and the polymer. The extra peaks in this case are for the sputtered silver that was used during EDS analysis.

After the removal of AAO templates, 60 nm and 80 nm diameter nanowire arrays with 5 µm length and 130 nm diameter nanowire arrays with 11 µm length were embedded in PEGDA using the method as shown in Figures 4.2 and 4.3. The magnetic properties of these polymer embedded nanowires were measured in each step of the syntheses to study changes in magnetism as a response to variations in the synthesis method. As given in Figure 4.6 the magnetic properties of template assisted nanowires changes with and without template due to the change in orientation of nanowires.
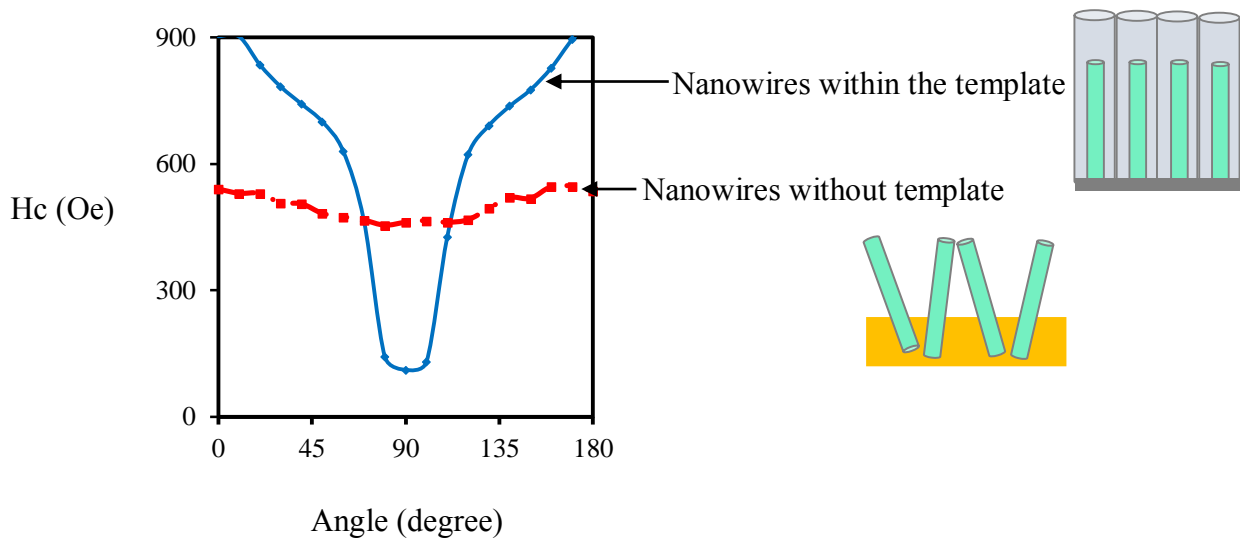


**Figure 4.6** Variations in magnetic properties with and without template.

Wires within the template are oriented, thus there is a transition in magnetization with angle (corresponds to the blue line in Figure 4.6). After the removal of template wires are disoriented

59

and some cases connected with each other. Therefore, change in magnetization is negligible (the red line in Figure 4.6). However, in some cases embedding nanowires after the removal of templates could help in changing the disorientation of nanowires. Figures 4.8 show the angular dependence of coercivity of polymer embedded nanowires. The magnetic properties of nanowires with AAO are shown in blue, those without are shown in red, after embedding with polymer and drying are shown in green, and after swelling the polymer are show in black. In Fig. 4.8e, purple corresponds to drying the sample second time and green dotted line corresponds to swelling the sample second time. This result showed wires with high aspect ratio are disoriented after the removal of the templates, which could not be improved further by embedding in PEGDA in the presence of applied magnetic field. However, after dissolving the template, polymer embedded nanowires with 130 nm pore diameter and 5 µm length (Figure 4.7d) showed a better response relative to the other nanowires of same length and different pore diameter Figure 4.7a (60 nm) and Figure 4.7b (80 nm) or same pore diameter with different length Figure 4.7c (130 nm diameter with 11µm) . Therefore, 5 µm length and 130 nm PEG-Ni nanowires were further embedded with azobenzene-polyacrylate to verify changes in its magnetic properties due to the use of azobenzene-polyacrylate in place of PEGDA (Figure 4.8f). It was found that this synthesis with azobenzene-polyacrylate resulted in disordered nanowires in the absence of magnetic field.
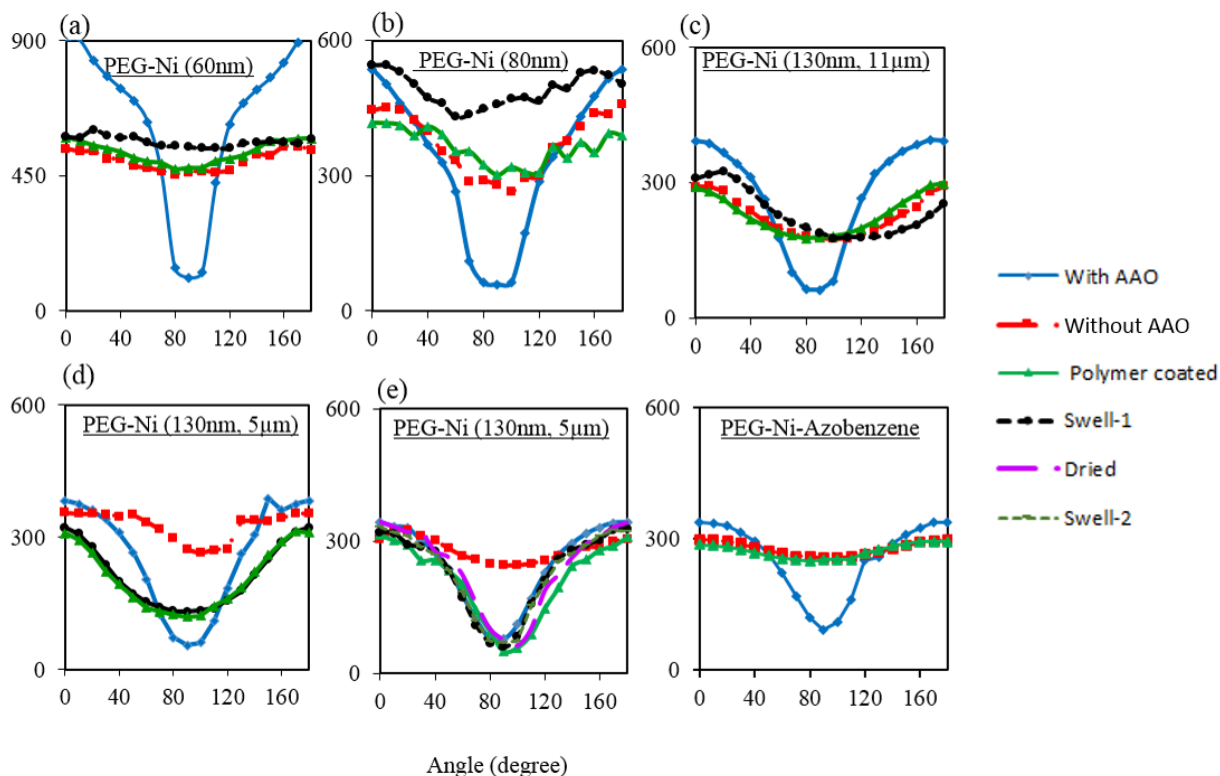
**Figure 4.7.** Angular dependence of coercivity for PEG-Ni nanowires embedded with PEGDA and fabricated using templates with a pore diameter of (a) 60 nm (b) 80 nm to produce 5 µm long nanowires, (c) templates with 130 nm diameter to produce ~11 µm long nanowires, (d) templates with pore diameter 130 nm to produce ~5µm long nanowires, (e) templates with pore diameter 130 nm to produce ~5µm long polymer coated nanowires with very similar magnetic properties as the nanowires with templates. (f) PEG-Ni nanowires with 130 nm diameter nanowires embedded within azobenzene-polyacrylate.

The synthesis that was conducted with PEGDA in the presence of an applied magnetic field produced nanowires with improved magnetic properties (Figures 4.8d and 4.8e) relative to those embedded in polymer without the field (Figure 4.8f). The FESEM images of PEGDA and azobenzene-polyacrylate embedded nanowires are presented in Figures 4.8a and 4.8b,

respectively. Among all these syntheses, Figure 4.8e shows the best case where the polymer embedded nanowires, 130 nm Ni with a length of ~5 μm in PEGDA, showed similar magnetic properties to the wire samples grown directly within the AAO template. In fact, the same magnetic properties were observed even after keeping the sample in water for more than six months.
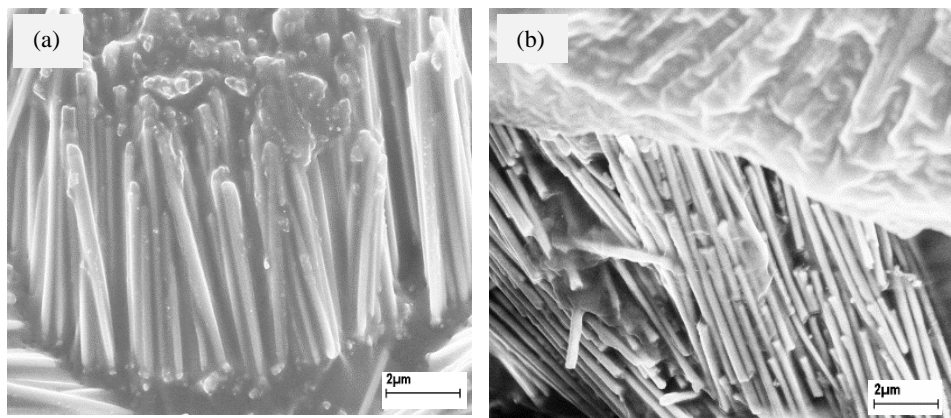


**Figure 4.8.** Cross-section view of (a) PEGDA (b) azobenzene - polyacrylate embedded PEG-Ni nanowires.

## 4.4. Discussion

In this paper, we present a method to successfully synthesize oriented nanowires embedded in the polymer, PEGDA. The PEG coated nickel wires were initially grown in an AAO template, which allows one to set the orientation. The template was dissolved with the wires still attached to a copper tape backing. The wires were then encased in PEGDA where the polymerization was carried out under UV light in the presence of a magnetic field. The magnetic field was effective in helping to maintain the orientation of the nanowires and PEG coating on the nanowires likely helps not only to improve the rigidity of the nanowires but also serves to support polymer growth. One expects that as the polymerization occurs the PEGDA may connect to the PEG on the Ni wires.

Beyond PEGDA, any other polymers that can chemically interact with PEG could also be used to prepare oriented nanowire arrays.

The effectiveness of this processing procedure is better for larger interwire distances and lower aspect ratios of the nanowires. With decrease in interwire distances, two effects can become important, dipole-dipole interactions impacting magnetic interactions and the effect of capillary forces on drying nanowire samples. The dipole-dipole interactions result in wire-wire attraction and can lead to nanowire agglomeration after the removal of template. In terms of capillary forces, according to Robinson et al., agglomeration occurs on drying due to the high surface tension of water and strong interaction with nanowires that collapse wires by capillary force.[18] A further consideration is the aspect ratio of the wires, shorter wires with a larger foot-print had a tendency to be more stable and consequently retain their orientation on drying. Therefore, when the synthesis was conducted using templates with smaller pore diameters (e.g. 60 nm and 80 nm), after dissolving the template the interaction between the nanowires lead to clumping. In contrast, by the use of the template with 130 nm pore diameter, the larger nanowire foot print in combination with the decreased bending tendency lead to more highly oriented polymer embedded nanowire arrays. Further, the presence of PEG on the surface of the nanowires may also help to contribute to stability in that this reduces the surface tension of water between the nanowires and thus helps reduce capillary force between groups of wires.

Evidence of wire clumping can be seen in the comparison of wires with different aspect ratios. The nanowires with higher aspect ratio such as the nanowires with pore diameter 60 nm and 80 nm with 5 μm length (Figure 4.9a) and the nanowires with pore diameter 130 nm with 11 μm length showed clustered structures. On the other hand, the nanowires with lower aspect ratio were more stable and uniform such as the nanowires with 130 nm diameter and 5 μm length given

in Figure 4.9 b without the template. These sets of nanowires were then embedded with polymers in the presence of a magnetic field.

As described in Figure 4.3, when PEGDA containing solution mixture was caste drop-by-drop on the nanowires and then placed under vertical applied electromagnetic field, the coated polymer may have interacted with PEGDA, which possibly improved the orientation of the nanowires with 130 nm pore diameter. These nanowires remained oriented due to polymerization in the presence of UV light.
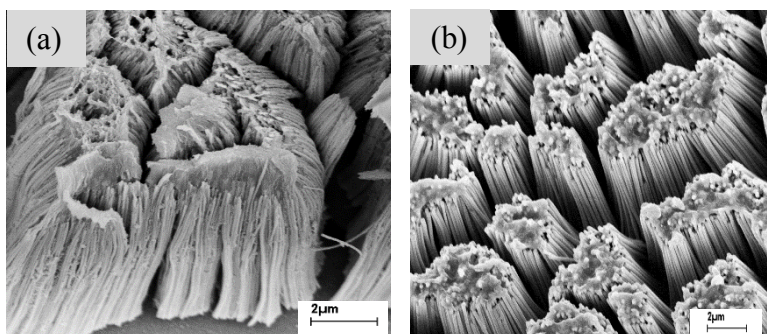


**Figure 4.9.** PEG coated Ni nanowires synthesized using (a) 60 nm and (b) 130 nm templates.

Because of the attached silver layer that was used to grow the wires, swelling of polymer did not move the nanowires as the amount of polymer present in between the nanowires was not sufficient to change the position of the nanowires. Without silver it was difficult to keep the nanowires oriented on any substrate. The higher agglomeration in case of nanowires with smaller pore diameter (e.g. 60 nm and 80 nm) caused disordered orientation (Figure 4.8). This was further confirmed by VSM results that showed angular dependence of magnetization at each step of synthesis. Initially polymer coated nanowires within the template showed the characteristic features of hysteresis loop, higher coercivity at 0º and lower coercivity at 90º and it increases with increase in aspect ratio of wire (Figure 4.7). However, wires with high aspect ratio had a greater tendency to agglomerate after the removal of the template. This behavior significantly affects the

magnetic properties of the assembly as magnetization is a function of the orientation of nanowires. Embedding NWs with polymer in the presence of applied magnetic field could help improve the orientation of nanowires, if the agglomeration is less significant. Therefore, 130 nm diameter and 5 μm length polymer embedded nanowires show better magnetic result compared to any other arrays and this result is retained even after solvent uptake by the polymer (Figure 4.7d). However, when the synthesis was repeated it was often very hard to obtain the polymer embedded nanowires with similar magnetic properties as shown in Figure 4.7e. Further, when azobenzene-polyacrylate was used as the polymer, the magnetic properties were poor compared to PEGDA embedded nanowires. This was likely due to the fact the polymerization was carried out in the absence of an orienting magnetic field; the application of a magnetic field was not possible due to the inert conditions required in the growth of the azobenzene-polyacrylate polymer.

## 4.5. Conclusions

Highly oriented polymer embedded magnetic nanowires could be prepared. Nanowires grown in AAO templates could be released in a controlled fashion and then encased in polymers while retaining the wire orientation. When PEGDA is used as the polymer, UV exposure under an applied magnetic field gives the best results where angular depend variation in coercivity gives the high degree of deflection. This method can also be used to embed nanowires with different polymers those can be polymerized in presence of photons or heat, though it appears the force of the external magnetic field is important to help maintain the alignment of the nanowire arrays.

## 4.6. References

1. (a) Adebajo, M. O., Development of nanostructured materials (metal oxides, zeolites, mesoprorous materials, hydrotalcites and gold/supported gold nanoparticles) for catalytic, photocatalytic and biomedical applications. *Abstracts of Papers of the American Chemical*

*Society* **2006,** *232*, 29-29; (b) Gupta, G.; Staggs, K.; Montano, G. A.; Lopez, G. P., Nanostructured materials for biomedical applications. *Abstracts of Papers of the American Chemical Society* **2009,** *237*; (c) Matyjaszewski, K., Nanostructured materials for potential biomedical applications prepared by controlled radical polymerization. *Abstracts of Papers of the American Chemical Society* **2010,** *240*; (d) Shi, D.; Gu, H., Nanostructured Materials for Biomedical Applications. *Journal of Nanomaterials* **2008**; (e) Xu, T.; Zhang, N.; Nichols, H. L.; Shi, D.; Wen, X., Modification of nanostructured materials for biomedical applications. *Materials Science & Engineering C-Biomimetic and Supramolecular Systems* **2007,** *27* (3), 579-594.

2.  (a) Dong, S.; Chen, X.; Zhang, X.; Cui, G., Nanostructured transition metal nitrides for energy storage and fuel cells. *Coordination Chemistry Reviews* **2013,** *257* (13-14), 1946-1956; (b) Li, L.; Wu, Z.; Yuan, S.; Zhang, X.-B., Advances and challenges for flexible energy storage and conversion devices and systems. *Energy & Environmental Science* **2014,** *7* (7), 2101-2122; (c) Yan, H.; Bai, J.; Wang, J.; Zhang, X.; Wang, B.; Liu, Q.; Liu, L., Graphene homogeneously anchored with Ni(OH)(2) nanoparticles as advanced supercapacitor electrodes. *Crystengcomm* **2013,** *15* (46), 10007-10015; (d) Arico, A. S.; Bruce, P.; Scrosati, B.; Tarascon, J. M.; Van Schalkwijk, W., Nanostructured materials for advanced energy conversion and storage devices. *Nature Materials* **2005,** *4* (5), 366-377.

3.  Soumare, Y.; Garcia, C.; Maurer, T.; Chaboussant, G.; Ott, F.; Fiévet, F.; Piquemal, J.-Y.; Viau, G., Kinetically Controlled Synthesis of Hexagonally Close-Packed Cobalt Nanorods with High Magnetic Coercivity. *Advanced Functional Materials* **2009,** *19* (12), 1971-1977.

4.  (a) Yang, Z.; Huang, Y.; Dong, B.; Li, H.-L., Template induced sol–gel synthesis of highly ordered LaNiO3 nanowires. *Journal of Solid State Chemistry* **2005,** *178* (4), 1157-1164; (b) Gao, F.; Yuan, Y.; Wang, K. F.; Chen, X. Y.; Chen, F.; Liu, J. M., Preparation and photoabsorption characterization of BiFeO3 nanowires. *Applied Physics Letters* **2006,** *89* (10).

5.  (a) Liu, Z.; Li, S.; Yang, Y.; Peng, S.; Hu, Z.; Qian, Y., Complex-Surfactant-Assisted Hydrothermal Route to Ferromagnetic Nickel Nanobelts. *Advanced Materials* **2003,** *15* (22), 1946-1948; (b) Xie, B.-Q.; Qian, Y.; Zhang, S.; Fu, S.; Yu, W., A Hydrothermal Reduction Route to Single-Crystalline Hexagonal Cobalt Nanowires. *European Journal of Inorganic Chemistry* **2006,** *2006* (12), 2454-2459.

6.  (a) Fert, A.; Piraux, L., Magnetic nanowires. *Journal of Magnetism and Magnetic Materials* **1999,** *200* (1–3), 338-358; (b) Encinas-Oropesa, A.; Demand, M.; Piraux, L.; Huynen, I.; Ebels, U., Dipolar interactions in arrays of nickel nanowires studied by ferromagnetic resonance. *Physical Review B* **2001,** *63* (10), 104415; (c) Pan, H.; Liu, B.; Yi, J.; Poh, C.; Lim, S.; Ding, J.; Feng, Y.; Huan, C. H. A.; Lin, J., Growth of Single-Crystalline Ni and Co Nanowires via Electrochemical Deposition and Their Magnetic Properties. *The Journal of Physical Chemistry B* **2005,** *109* (8), 3094-3098.

7.  Li, Y. B.; Zheng, M. J.; Ma, L., High-speed growth and photoluminescence of porous anodic alumina films with controllable interpore distances over a large range. *Applied Physics Letters* **2007,** *91* (7).

8.  Rhen, F. M. F.; Backen, E.; Coey, J. M. D., Thick-film permanent magnets by membrane electrodeposition. *Journal of Applied Physics* **2005,** *97* (11), -.

9.  (a) Kuanr, B. K.; Veerakumar, V.; Marson, R.; Mishra, S. R.; Camley, R. E.; Celinski, Z., Nonreciprocal microwave devices based on magnetic nanowires. *Applied Physics Letters* **2009,** *94* (20), -; (b) Goglio, G.; Pignard, S.; Radulescu, A.; Piraux, L.; Huynen, I.; Vanhoenacker, D.; Vander Vorst, A., Microwave properties of metallic nanowires. *Applied*

*Physics Letters* **1999,** *75* (12), 1769-1771; (c) Law, M.; Sirbuly, D. J.; Johnson, J. C.; Goldberger, J.; Saykally, R. J.; Yang, P. D., Nanoribbon waveguides for subwavelength photonics integration. *Science* **2004,** *305* (5688), 1269-1273.

10. Piraux, L.; Renard, K.; Guillemet, R.; Mátéfi-Tempfli, S.; Mátéfi-Tempfli, M.; Antohe, V. A.; Fusil, S.; Bouzehouane, K.; Cros, V., Template-Grown NiFe/Cu/NiFe Nanowires for Spin Transfer Devices. *Nano Letters* **2007,** *7* (9), 2563-2567.

11. (a) Mock, J. J.; Oldenburg, S. J.; Smith, D. R.; Schultz, D. A.; Schultz, S., Composite plasmon resonant nanowires. *Nano Letters* **2002,** *2* (5), 465-469; (b) Stoermer, R. L.; Cederquist, K. B.; McFarland, S. K.; Sha, M. Y.; Penn, S. G.; Keating, C. D., Coupling Molecular Beacons to Barcoded Metal Nanowires for Multiplexed, Sealed Chamber DNA Bioassays. *Journal of the American Chemical Society* **2006,** *128* (51), 16892-16903.

12. White, S. I.; Mutiso, R. M.; Vora, P. M.; Jahnke, D.; Hsu, S.; Kikkawa, J. M.; Li, J.; Fischer, J. E.; Winey, K. I., Electrical Percolation Behavior in Silver Nanowire-Polystyrene Composites: Simulation and Experiment. *Advanced Functional Materials* **2010,** *20* (16), 2709-2716.

13. Yu, Z.; Li, L.; Zhang, Q.; Hu, W.; Pei, Q., Silver Nanowire-Polymer Composite Electrodes for Efficient Polymer Solar Cells. *Advanced Materials* **2011,** *23* (38), 4453-+.

14. Vernier, N.; Allwood, D. A.; Atkinson, D.; Cooke, M. D.; Cowbu, R. P., Domain wall propagation in magnetic nanowires by spin-polarized current injection. *Europhysics Letters* **2004,** *65* (4), 526-532.

15. Sipics, J.; Libera, M. In *Poly(acrylic acid) modified PEG hydrogels*, Bioengineering Conference, 2005. Proceedings of the IEEE 31st Annual Northeast, 2-3 April 2005; 2005; pp 204-205.

16. (a) Durst, C. A.; Cuchiara, M. P.; Mansfield, E. G.; West, J. L.; Grande-Allen, K. J., Flexural characterization of cell encapsulated PEGDA hydrogels with applications for tissue engineered heart valves. *Acta Biomaterialia* **2011,** *7* (6), 2467-2476; (b) Seo, J.; Jang, W.; Lee, S.; Han, H., The stability of semi-interpenetrating polymer networks based on sulfonated polyimide and poly(ethylene glycol) diacrylate for fuel cell applications. *Polymer Degradation and Stability* **2008,** *93* (1), 298-304; (c) Lee, K. G.; Park, T. J.; Soo, S. Y.; Wang, K. W.; Kim, B. I. I.; Park, J. H.; Lee, C.-S.; Kim, D. H.; Lee, S. J., Synthesis and utilization of E. coli-encapsulated PEG-based microdroplet using a microfluidic chip for biological application. *Biotechnology and Bioengineering* **2010,** *107* (4), 747-751.

17. Zhang, J. Active Response of Polymer Materials from External Stimuli – Solvents and Light; Grafting Reactions on Perovskite Layers.

18. Robinson, A. P.; Burnell, G.; Sahonta, S.-L.; MacManus-Driscoll, J., Perfectly Ordered, Free-Standing Nanowire Arrays With Controllable Geometry. *Advanced Engineering Materials* **2009,** *11* (11), 907-911.

**Chapter 5**

**Structural Variation in Bimetallic Transition Metal Nanowires: Core-shell versus Alloy Structures as a Function of Template Pore Diameter and Applied Potential.**

**5.1. Introduction**

Nanomaterials with their unique properties have wide application in many different fields. One-dimensional nanomaterials, such as nanowires core-shells,[1] composites,[2] and alloys,[3] nanotubes, and nanorods with multifunctional properties, have especially attracted great attention due to their distinctive physical properties and potential applications in nanodevices. These materials can be synthesized using porous templates by numerous methods such as sol-gel,[4] template wetting,[5] atomic layer deposition,[6] and electrodeposition.[7] Though it is possible to control the diameter and thickness of these 1D structures using all of the aforementioned methods, quality crystalline structures can often be synthesized in less time using the template assisted electrochemical deposition method. This method offers an easy approach for controlling the reaction parameters needed to access uniform hexagonally arranged 1D materials in anodized aluminum oxide (AAO) membranes.

Using an electrodeposition method, a number of multi-metallic one-dimensional ferromagnetic nanostructures have been synthesized, such as alloys of CoFe,[8] CoCu,[9] NiFe,[10] CoCrPt,[11] multi-segmented nanowires of Ni-Cu[12] and Co-Cu[13] and core-shell nanowires of Ni-La[14] and $MgO/Fe_3O_4$.[15] These multi-metallic ferromagnetic wires have fundamental and practical applications in a variety of areas including nanoscale devices and catalysis,[16] biomedicine,[17] supercapacitors,[18] where metal-metal interactions are facilitated by the layer thickness and the amount of material present in the nanowires. For example, multi-segmented nanowires containing

magnetic (Ni) and diamagnetic (Cu) segments have been reported by Chen et al.[12] that exhibit tunable magnetic properties due to variation in the thickness of Cu and Ni layers and their shape anisotropy. Presence of higher amounts of Cu reduces the dipole-dipole interaction between Ni segments. As a result, their magnetic properties are improved compared to the single 1D Ni nanowires. However, when magnetic and diamagnetic materials are combined to form alloys, variation in their magnetic properties depends on the resultant phase. Liu et al.[19] reported the fabrication of nanowire arrays containing both Ni-Zn at different potentials showed varying phase structures due to a change in the amount of Ni and Zn. Because of the modified composition and phase, their magnetic properties changed. Core-shell nanowires are also a type of multi-metallic nanowires that can be fabricated either by simultaneous growth of core and shell[1, 14] or by growing the shell first and then the core.[20] In core-shell nanowires, presence of magnetic materials as both cores and shells influences the net magnetic property due to magnetic interaction between the layers. As described by Shi et al.[14] simultaneous deposition of Ni and La resulting Ni-La core-shell structures containing magnetically hard and soft phases, the hard phase completely decoupled the soft phase. Similarly, Lee et al.[21] described the formation of Fe-FeO$_x$ core-shell structures with tunable magnetic properties under different reaction conditions.

Due to their tunable magnetic properties, multi-metallic nanowires are of greater interest. However, in simultaneous deposition of two metals, synthesis of different structures of nanowires is limited to the applied potential by direct deposition or pulsed electrochemical deposition method or by using different types of templates. The study highlighted in this chapter focuses on investigating the influences of pore diameter of anodized alumina template on the synthesis of multi-metallic nanowires with two different structures using the same electrolyte at room temperature.

## 5.2. Experimental

Multi-metallic nanowires were synthesized using a template assisted electrochemical deposition method. AAO templates were used to fabricate the nanowire arrays. For the growth of templates with pore diameter less than 100 nm, a two-step anodization process was used whereas a three-step anodization method was followed for the fabrication of templates with pore diameter more than 100 nm as described in Chapter 3. For the synthesis of nanowires, one side of the template was sputtered closed with a conductive metal for it to act as a working electrode. Electrodeposition was conducted in a three electrode system with the deposition solution containing $NiSO_4 \cdot 7H_2O$ (1.14M) $NiCl_2 \cdot 6H_2O$ (0.18M) $FeSO_4 \cdot 7H_2O$ (0.35M), $H_3BO_3$ (0.72M), ascorbic acid (0.005M) for Ni-Fe nanowires, and $NiSO_4 \cdot 7H_2O$ (1.14M) $NiCl_2 \cdot 6H_2O$ (0.18M) $CoSO_4 \cdot 7H_2O$ (1.06M), $H_3BO_3$ (0.72M), ascorbic acid (0.005M) for Ni-Co nanowires. The synthesis was performed at an applied current of -0.9 mA with less than 100 nm pore diameter templates, and -0.5 mA and -0.9 mA with greater than 100 nm pore diameter templates.
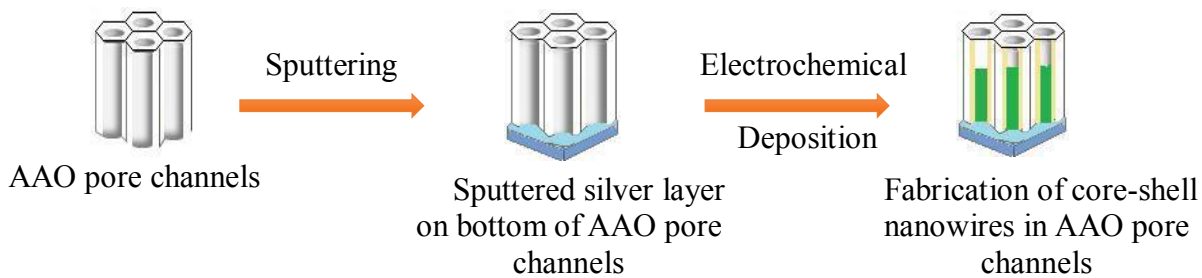


**Figure 5.1.** Schematic diagram of electrodeposition using AAO templates.

## Characterization

After deposition, the surface morphology and structure of these samples were characterized using a LEO 130 VP field emission scanning electron microscope (FESEM). A JEOL EM 2010 transmission electron microscope (TEM) was used for the study of surface topography,

morphology, composition and crystallographic information. The TEM was operated at an acceleration voltage of 200 kV. A Philips X-pert PW 3040 MPD X-ray powder diffractometer was used for X-ray diffraction (XRD) with a CuKα X-ray source. Lakeshore 7300 series vibrating sample magnetometer (VSM) was used for studying the magnetic properties.

## 5.3. Results

A series of nanowires were fabricated separately as given in Figure 5.1 using a deposition solution containing two different transition metal ions. These nanowires were synthesized by modifying the procedure given by Zhang et al.[22] in which synthesis of Ni-Fe alloy nanowires in branched AAO templates was reported. Keeping the composition of electrolytic solution the same at different applied currents and using different pore diameters of templates, core-shell and alloy nanowire structures were obtained (Figure 5.2). In core-shell type nanowires, an average shell thickness is about 10 nm (Figure 5.2a, c). Utilizing this method, Ni-Co core-shell and alloy nanowires were also fabricated by replacing $CoSO_4 \cdot 7H_2O$ with $FeSO_4 \cdot 7H_2O$. Figures 5.2 and 5.3 show the FESEM and TEM images, respectively.

In this study, AAO templates with different pore diameters (130 nm, 100 nm, 80 nm and 60 nm) were used to investigate the influence of confined geometry on deposition. FESEM and TEM microscopy results show morphology differences in core-shell nanowires where clear dark and bright contrast between outer layer and core metal is seen in Figure 5.2a, c (FESEM) and Figure 5.3a, b (TEM). The nanowires synthesized using AAO templates with pore diameter $\geq 100$ nm at -0.9 mA applied current showed core-shell structures. The effect of applied potential on the deposition was investigated in 130 nm pore diameter templates by decreasing the applied current

71
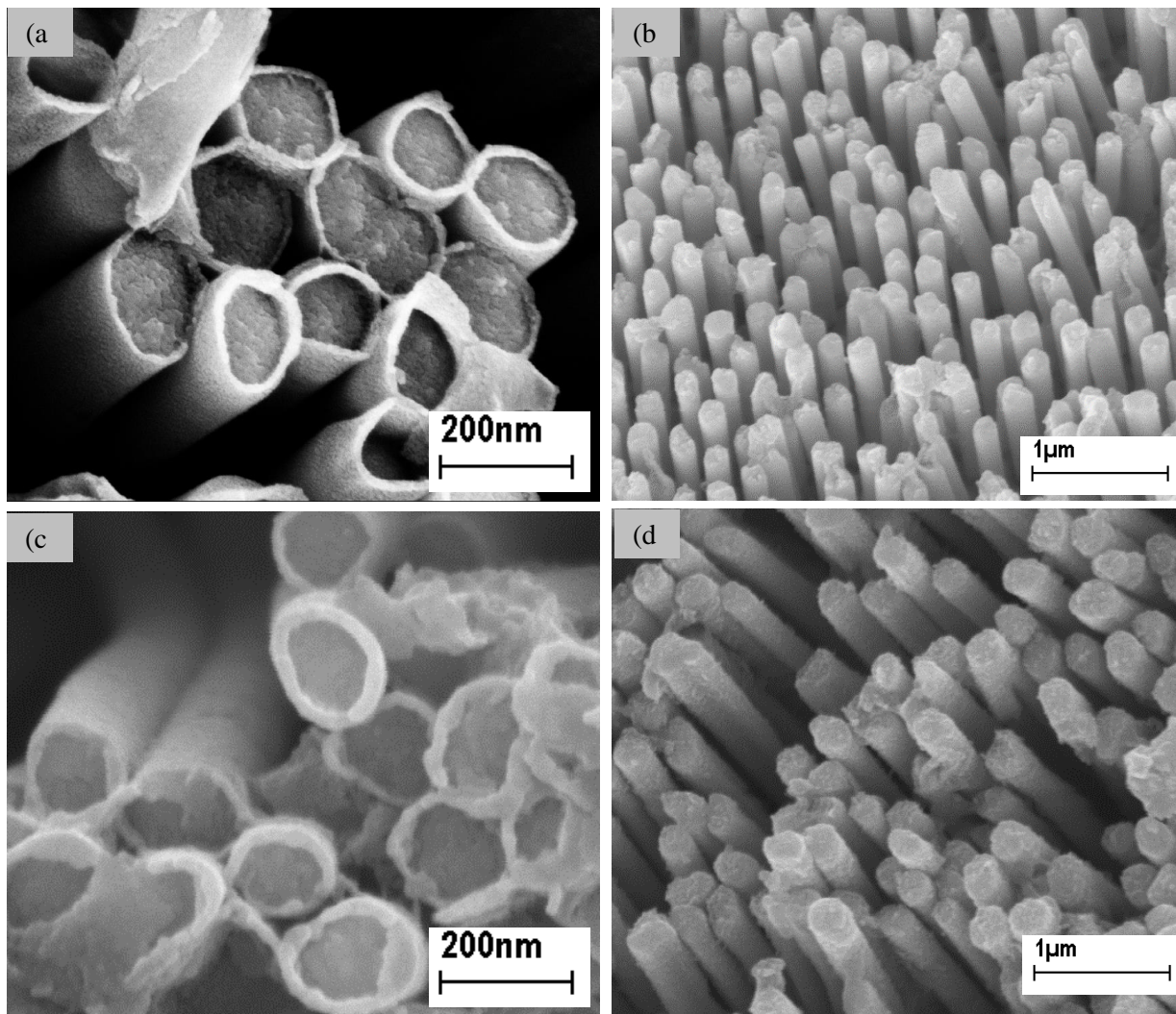
**Figure 5.2.** FESEM images of bi-metallic nanowires fabricated using 130nm AAO templates at (a, c) -0.9 mA containing NiFe and NiCo, respectively and (b, d) -0.5 mA applied current composed of Ni-Fe and Ni-Co, respectively.

to -0.5 mA. Under these reaction conditions, alloy not core-shell, nanowires were formed. The FESEM and TEM images are shown in Figures 5.2b, d and 5.3b, e, respectively. Further, if a

template with pore diameter 60 nm is used for deposition at a constant current of -0.9 mA, alloy nanowires were also formed as shown in Figure 5.3 c, f.
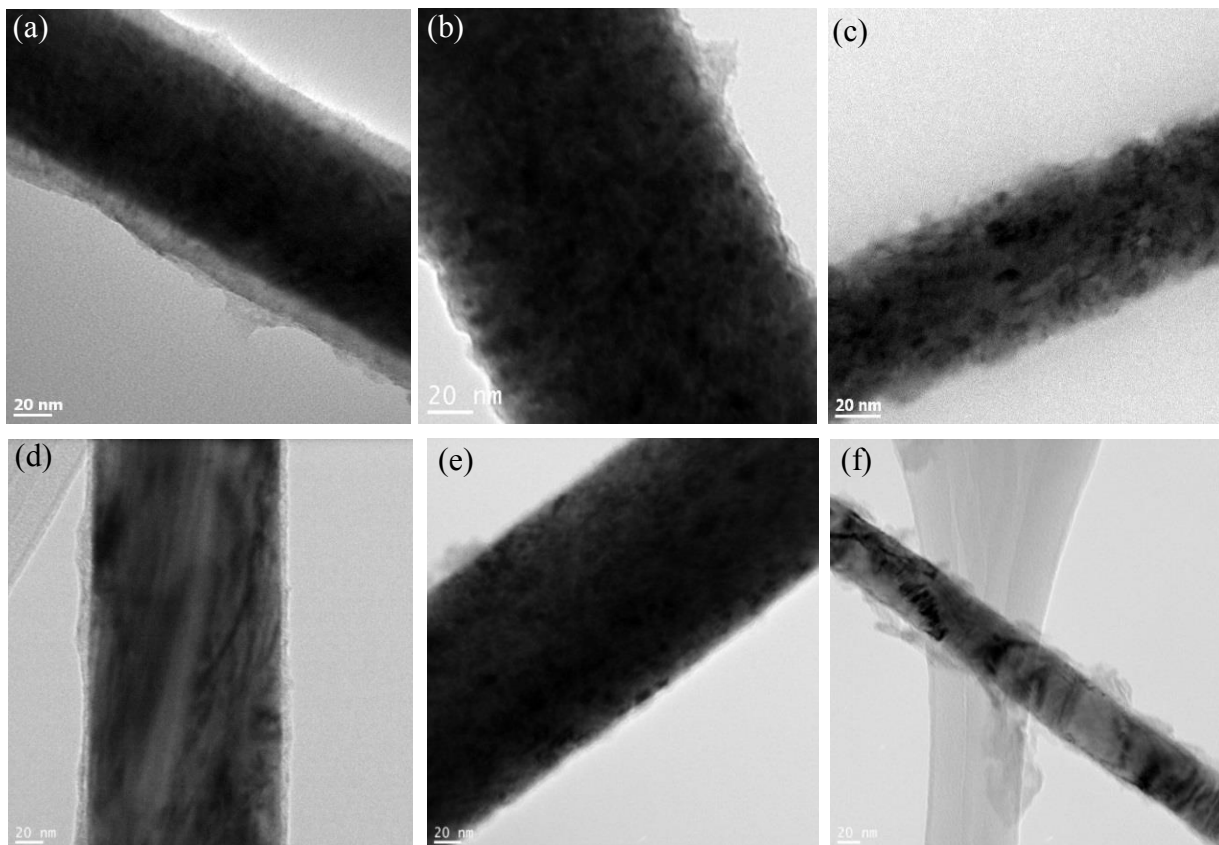


**Figure 5.3.** TEM images of core-shell type (a) NiFe and (d) NiCo bimetallic multilayered nanowires and alloy nanowires of (b) NiFe (e) NiCo using 130 nm AAO template. (c) and (f) NiFe and NiCo alloy nanowires fabricated using 60 nm templates.

Controlled experiments were performed to determine the rate of synthesis of core-shell and alloy nanowire arrays. The relative rate of deposition of NiFe and NiCo depends on the applied potential and concentration of metal ions in the electrolytes. A faster growth of the shell compared to the core was observed when the synthesis was performed with a constant applied current of -0.9 mA.

As result the shell was porous with randomly arranged crystal structure as given in the TEM images in Figure 5.4
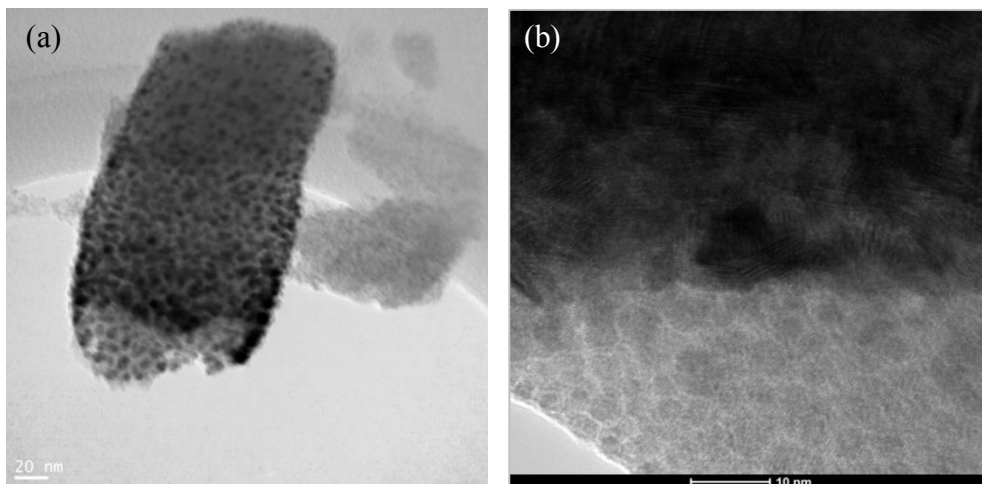


**Figure 5.4.** (a) TEM images of only shell and (b) HRTEM images of core-shell structures.

Growth of alloy wires was much slower when fabricated at -0.5 mA applied current in 130 nm AAO templates. When templates with pore diameter of 60 nm were used, the growth rate of alloy nanowires increased. This shows that nanowire formation depends on the applied current as well as the pore diameter of the template.

XRD patterns were analyzed to examine the resultant phase of materials present in each type of wire. Figures 5.5 and 5.6 shows X-ray diffraction patterns of both FeNi and NiCo nanowires, respectively. The XRD data confirm the presence these transition metals indicating the micro-crystalline structure of bimetallic metal nanowires. As can be seen in Figure 5.5 diffraction peaks are found for cubic NiFe peaks located around 44.6°, 64.9° and 82.3° that correspond to NiFe (111) (110), NiFe (200) and NiFe (211) of an FCC structure. The extra peak at 77.2° is from the sputtered silver labeled with (*). In case of NiCo (Figure 5.6), the presence of hexagonal Co

along with cubic Ni is confirmed by peaks at 41.6° (100), 44.7° (002), 47.5° (101), 51.8° (200) and 76.3° (220) that correspond to NiCo nanowires. In each set the alloy
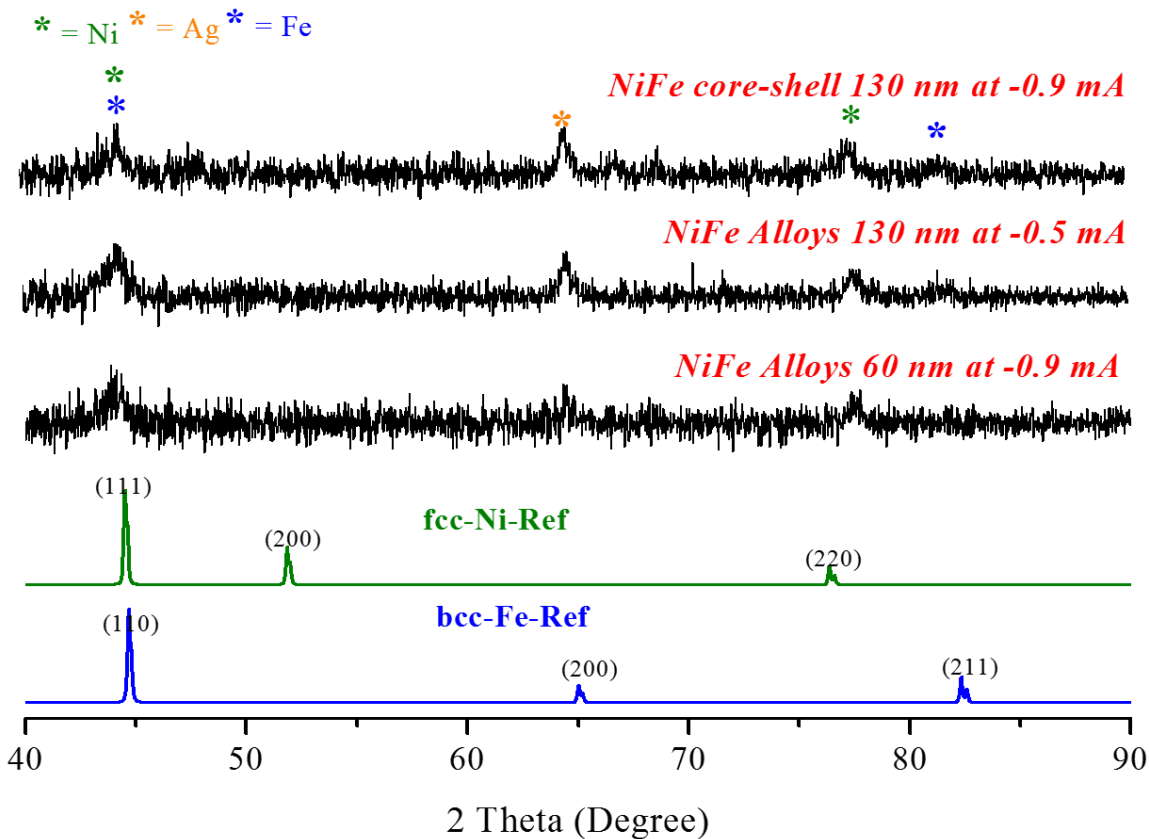


**Figure 5.5.** X-ray diffraction patterns for NiFe nanowires with (a) core-shell nanowires structure fabricated using 130 nm pore diameter template at -0.9 mA applied current, (b) alloy nanowires formed at -0.5 mA using template of pore diameter of 130 nm, (c) alloy nanowires fabricated using 60 nm diameter template. (d) And (e) are the reference patterns for Ni and Fe, respectively.
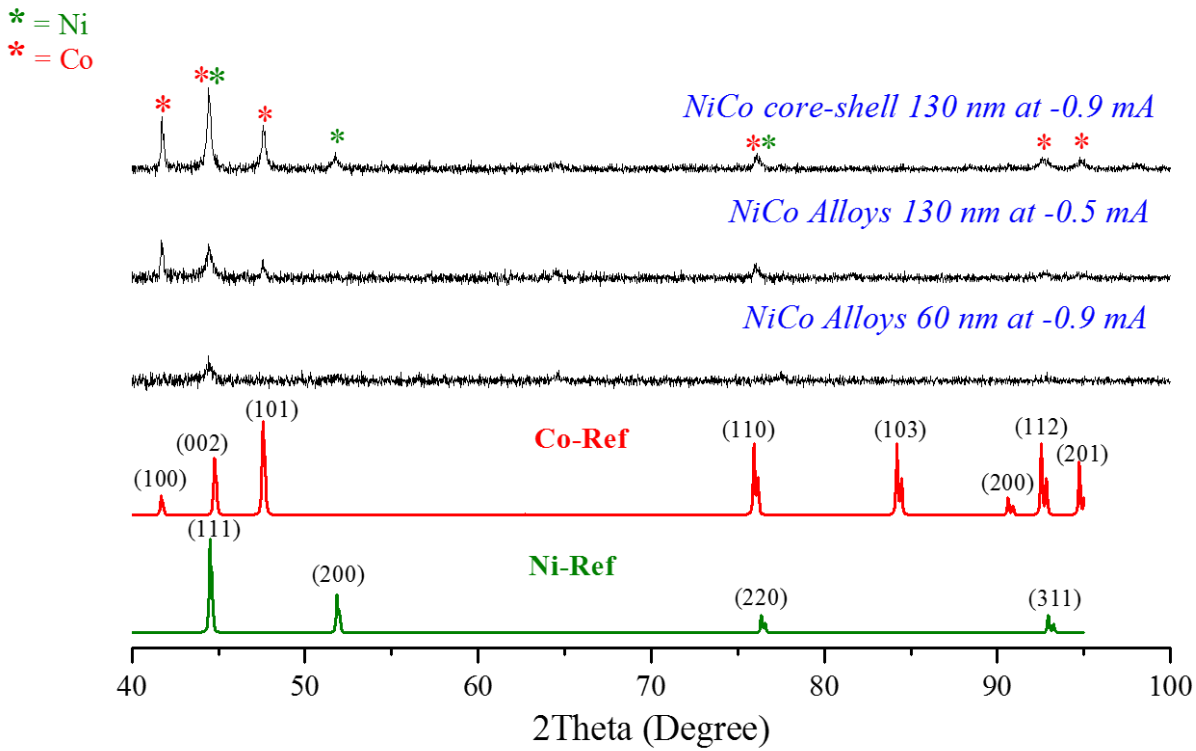
**Figure 5.6.** X-ray diffraction patterns for NiCo nanowires deposited at different applied current and using different pore diameter of AAO templates. (a) NiCo core-shell structure deposited using 130 nm pore diameter AAO template using -0.9 mA applied current, (b) alloy nanowires fabricated at -0.5 mA applied current using 130 nm pore diameter template, (c) alloy nanowire fabricated using 60 nm pore diameter template. (d) And (e) are the reference patterns for Co and Ni, respectively.

nanowires grown using 130 nm and 60 nm template has two different XRD patterns which may be due to dissimilar arrangement of metal ions inside pore diameter of templates. The alloy nanowires formed using 60 nm templates show cubic structure in each study, possibly resulting from the narrow size of the pore compared to 130 nm pore diameter that impacting the nucleation and growth orientation of the magnetic wires.

The EDS data showed the presence of Ni-Fe and Ni-Co in both the core and shell in each set of nanowires as seen in Figures 5.7 and 5.8, respectively. The ratio of Fe and Ni in Ni-Fe nanowire is found to be 1:3 and ratio of Co and Ni in Ni-Co nanowires is 3:1.
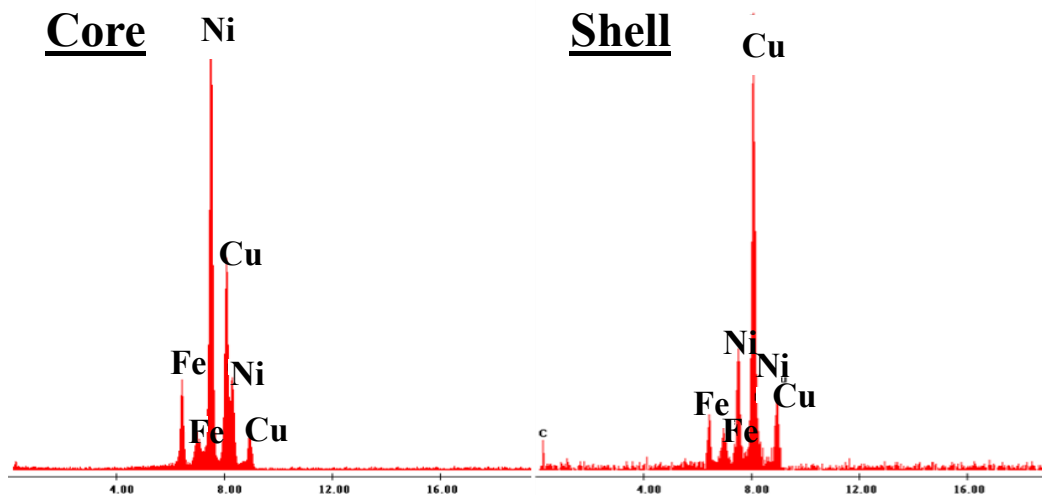


**Figure 5.7.** EDS spectrum of Ni rich NiFe nanowires arrays in the core and the shell layer. The presence of Cu is from the sample grid.
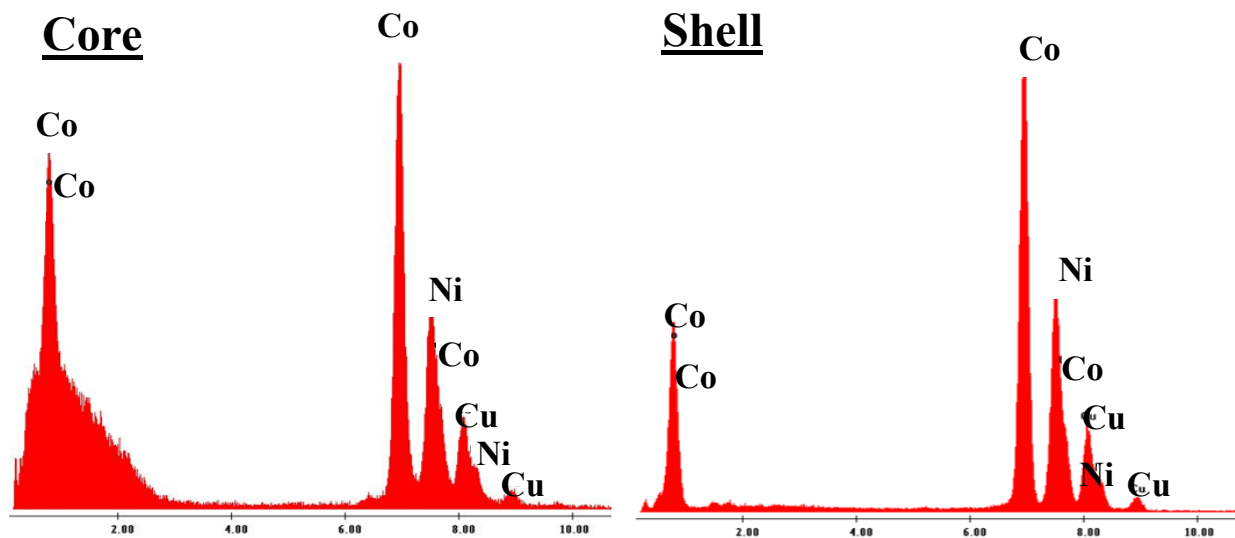


**Figure 5.8.** EDS spectrum of Co rich NiCo nanowires arrays in the inner core layer and outer shell layer, Cu peaks are corresponds to Cu grid use to prepare sample.

The magnetic hysteresis of Ni-Fe and Ni-Co nanowires was measured with both longitudinal and transverse applied magnetic fields relative to the wire axis at room temperature. The corresponding plots are given in Figure 5.9 that show the anisotropic magnetic hysteresis of the nanowires which is exhibited by the higher coercivity value along the wire axis and lower coercivity value perpendicular to the axis.
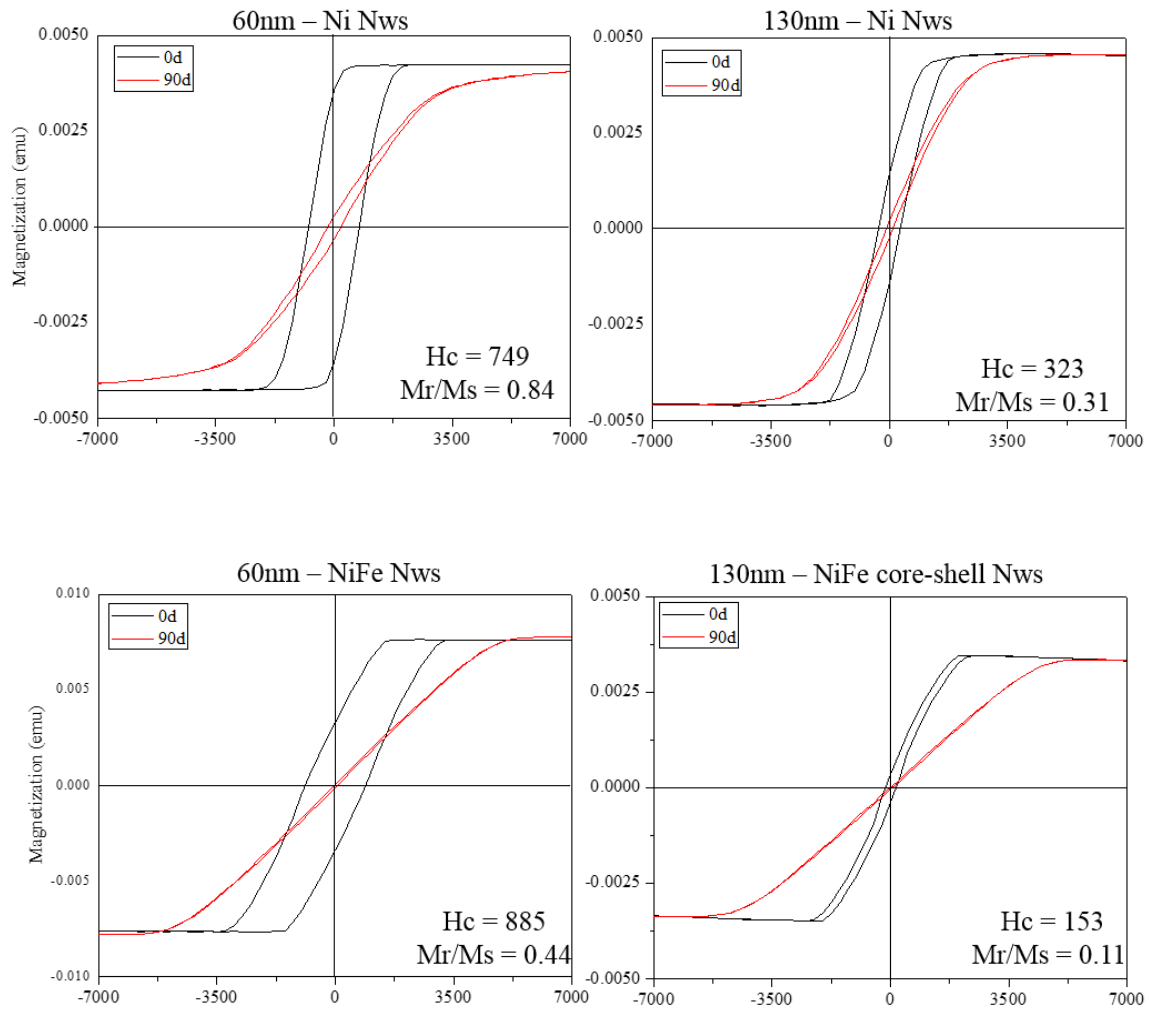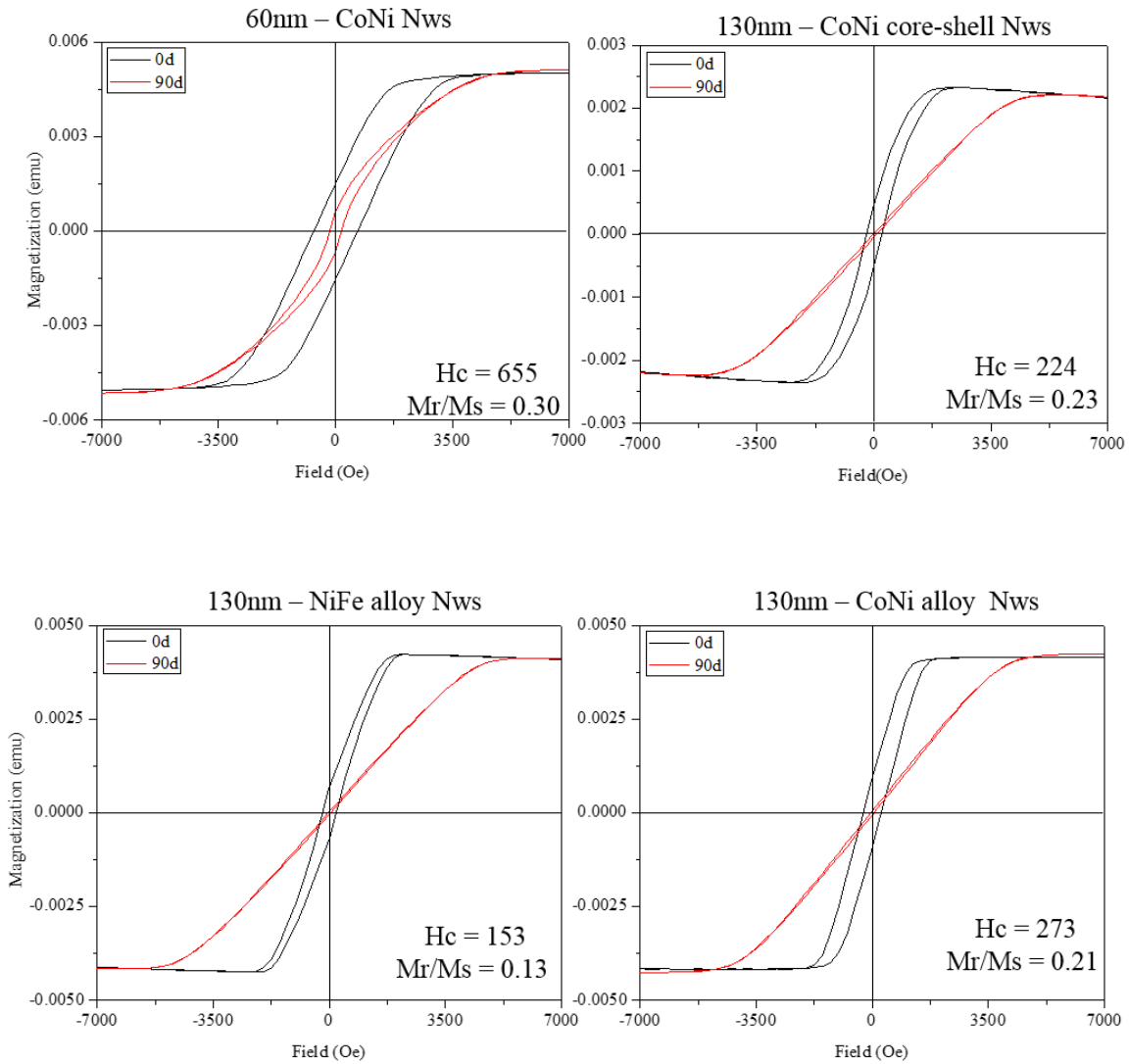
**Figure 5.9.** Room temperature magnetization curves for nanowire arrays collected when the field was applied along the wires (black solid line) and perpendicular to the wires axis (red solid line).

The magnetic properties of these nanowires were compared with the magnetic properties of the Ni nanowires fabricated with the same reaction conditions. The coercivity of multi-metallic nanowire arrays with core-shell structures was found to be less than that of the coercivity of alloys as well as the Ni only nanowires in spite of similar aspect ratios. This may be due to magnetic coupling between the core and the shell containing both magnetic materials. The magnetic

79

properties of the alloy nanowires were also examined, which showed that the magnetization may also depend on formation of different phase of nanowires. The ratio of the magnetic remanence ($M_r$) to the saturation magnetization ($M_s$) gives the squareness of the plot. In this study the nanowires fabricated with same composition using 130 nm templates have comparable squareness values.

## 5.4. Discussion

The electrochemical deposition method is a versatile technique for the production of nanowires at room temperature. In this study, we found that using AAO template with different pore diameters both core-shell and alloy nanowires can be fabricated from the same plating solutions. For core-shell structures, larger pore diameter and higher amount of applied current is favorable, while with lower pore diameter and lower applied current alloy nanowire were obtained.

In the electrochemical deposition method, the growth mechanism, morphology and structural properties of the nanowires depend on the composition of deposition solution and the applied current. Electrodeposition from solutions containing transition metals Ni-Fe or Ni-Co exhibits an anomalous codeposition behavior.[23] During such a codeposition process, the less noble (LN) metal is deposited preferentially relative to the more noble (MN) metal by a two-step reduction mechanism. This is due to competitive adsorption of the intermediates of the two metals which inhibit the deposition of the MN metal (Matlosz et al.).[24] Therefore, when Ni-Fe and Ni-Co nanowires were deposited, growth of nanowires depends upon the deposition mechanism and the kinetics of early stage nucleation of MN metal in presence of LN metal (Fan et al.).[23b] The inhibition of MN metal in the presence of LN was further modeled by Zech et al.[25] According to Zech et al. and Podlaha et al.,[26] when the electrolyte contains two different metals, a mixed metal intermediate containing both metal ions is formed during the first step of reduction. In the next

step, the mixed metal is reduced to form the LN metal and then the MN is reduced, resulting a heterometallic complex at the surface. A variation in ion transport of two different metals helps the deposition of the LN metal near the wall (Shi et al.)[11] forming core-shell nanowires from the same electrolyte that contains the two metal ions. In this study, between Ni and Fe, Fe is less noble than Ni and in the electrolyte containing Ni and Co, Co is less noble than Ni. Therefore, the resulting core-shell structures should have Ni coated with Fe and Ni with an outer Co shell. However, the relative rate of deposition of two metal ions from the electrolyte is also dependent on the applied potential and concentrations. According to Liu et al.[27] Cu-Ni containing large core-shell thin films were deposited when a higher Cu concentration was used with Ni (II) / Cu (II) $\leq$ 8 at higher potential. In this study, when electrodeposition was conducted using higher pore diameter templates, core-shell nanowires were formed at -0.9 mA applied current whereas at -0.5mA alloy nanowires were formed. Furthermore, the growth rate of the shell was higher than the core mainly due to inhibition of MN metal deposition in the presence of LN metal. However, due to higher constant applied current both these metal deposited simultaneously as core and shell.

As the EDS data suggest, the rate of Ni deposition is significantly reduced in the presence of Co (Ni:Co 1:3). As reported by Fan et al.[23b] between Ni and Co the rate of deposition of Co is higher due to high exchange current density of Co even at low concentration and low potential. This suppresses the rate of deposition of Ni metal. As a result the concentration of Ni metal ion decreases in bi-metallic nanowires. However, this mechanism is different for Ni-Fe nanowires as the nickel deposition rate with Fe ions in electrolyte is explained by a hydroxide suppression mechanism. Ni hydroxide dissociation is thousand times more than Fe resulting higher concentration of Ni.[10]  In this case it was found that the ratio of Fe:Ni was (1:3)

The investigation concerning the influence of pore diameter on the deposition revealed that the alloy nanowires were formed due to confinement of nucleation and growth of nanowire as the pore diameter of AAO template was reduced to 60 nm. The x-ray diffraction patterns given in Figure 5.4 and 5.5 showed that , when the nanowires were synthesized at -0.9 mA and -0.5 mA using AAO templates with a pore diameter of 130 nm are very similar whereas the nanowires fabricated using templates with 60 nm pore diameter show only cubic structure which may be due to compositional dependent lattice expansion. This shows that the pore diameters affect the structure of the nanowires significantly where the larger diameters favor core-shell structures and the smaller alloys.

## 5.5. Conclusions

Multi-metal nanowires as core-shell and alloy structures were synthesized with an electrochemical deposition method with the same plating solution. The structure of the nanowires could be modified by simply using AAO templates with different pore diameters or varying the applied potential. Both sets of nanowires exhibit different magnetic properties. Future work could look to study the exact composition of core and shell including the arrangement of atoms in the alloy grown using templates with two different pore diameters at different applied potentials. With controlled size, shape, and composition, these nanostructures could be very useful as building blocks for the design of sensors[28] and microwave filters.[29]

## 5.6. References

1. (a) Zhu, W.; Wang, G.; Hong, X.; Shen, X., One-Step Fabrication of Ni/TiO2 Core/Shell Nanorod Arrays in Anodic Aluminum Oxide Membranes. *Journal of Physical Chemistry C*

**2009,** *113* (14), 5450-5454; (b) Patil, R. M.; Shete, P. B.; Thorat, N. D.; Otari, S. V.; Barick, K. C.; Prasad, A.; Ningthoujam, R. S.; Tiwale, B. M.; Pawar, S. H., Superparamagnetic iron oxide/chitosan core/shells for hyperthermia application: Improved colloidal stability and biocompatibility. *Journal of Magnetism and Magnetic Materials* **2014,** *355*, 22-30.

2. Yang, F.; Cai, F.-G.; Ke, C.; Zhao, Y.; Cheng, C.-H., Effects of Annealing on the Surface Photoelectronic Properties of TiO2 Nanotube/Nanowire Composite Arrays. *Chemical Journal of Chinese Universities-Chinese* **2011,** *32* (11), 2581-2585.

3. Wang, X.; Shang, J.-X.; Wang, F.-H.; Jiang, C.-B.; Xu, H.-B., The structural stability and magnetic properties of the ferromagnetic Heusler alloy Ni-Mn-Sn: A first principle investigation. *Journal of Magnetism and Magnetic Materials* **2014,** *355*, 173-179.

4. Wu, G. S.; Xie, T.; Yuan, X. Y.; Li, Y.; Yang, L.; Xiao, Y. H.; Zhang, L. D., Controlled synthesis of ZnO nanowires or nanotubes via sol-gel template process. *Solid State Communications* **2005,** *134* (7), 485-489.

5. Li, X.; Lim, Y.-F.; Yao, K.; Tay, F. E. H.; Seah, K. H., Ferroelectric Poly(vinylidene fluoride) Homopolymer Nanotubes Derived from Solution in Anodic Alumina Membrane Template. *Chemistry of Materials* **2013,** *25* (4), 524-529.

6. Solanki, R.; Huo, J.; Freeouf, J. L.; Miner, B., Atomic layer deposition of ZnSe/CdSe superlattice nanowires. *Applied Physics Letters* **2002,** *81* (20), 3864-3866.

7. Pan, H.; Liu, B.; Yi, J.; Poh, C.; Lim, S.; Ding, J.; Feng, Y.; Huan, C. H. A.; Lin, J., Growth of Single-Crystalline Ni and Co Nanowires via Electrochemical Deposition and Their Magnetic Properties. *The Journal of Physical Chemistry B* **2005,** *109* (8), 3094-3098.

8. Armyanov, S., Crystallographic structure and magnetic properties of electrodeposited cobalt and cobalt alloys. *Electrochimica Acta* **2000,** *45* (20), 3323-3335.

9. Liu, L.; Zhou, W.; Xie, S.; Song, L.; Luo, S.; Liu, D.; Shen, J.; Zhang, Z.; Xiang, Y.; Ma, W.; Ren, Y.; Wang, C.; Wang, G., Highly efficient direct electrodeposition of Co-Cu alloy nanotubes in an anodic alumina template. *Journal of Physical Chemistry C* **2008,** *112* (7), 2256-2261.

10. Salem, M. S.; Sergelius, P.; Zierold, R.; Moreno, J. M. M.; Goerlitz, D.; Nielsch, K., Magnetic characterization of nickel-rich NiFe nanowires grown by pulsed electrodeposition. *Journal of Materials Chemistry* **2012,** *22* (17), 8549-8557.

11. Shamaila, S.; Liu, D. P.; Sharif, R.; Chen, J. Y.; Liu, H. R.; Han, X. F., Electrochemical fabrication and magnetization properties of CoCrPt nanowires and nanotubes. *Applied Physics Letters* **2009,** *94* (20).

12. Chen, M.; Chien, C. L.; Searson, P. C., Potential modulated multilayer deposition of multisegment Cu/Ni nanowires with tunable magnetic properties. *Chemistry of Materials* **2006,** *18* (6), 1595-1601.

13. Tan, L.; Stadler, B. J. H., Fabrication and magnetic behavior of Co/Cu multilayered nanowires. *Journal of Materials Research* **2006,** *21* (11), 2870-2875.

14. Shi, D.; Chen, J.; Riaz, S.; Zhou, W.; Han, X., Controlled nanostructuring of multiphase core-shell nanowires by a template-assisted electrodeposition approach. *Nanotechnology* **2012,** *23* (30).

15. Zhang, D.; Liu, Z.; Han, S.; Li, C.; Lei, B.; Stewart, M. P.; Tour, J. M.; Zhou, C., Magnetite (Fe3O4) Core−Shell Nanowires: Synthesis and Magnetoresistance. *Nano Letters* **2004,** *4* (11), 2151-2155.

16. (a) Kline, T. R.; Paxton, W. F.; Mallouk, T. E.; Sen, A., Catalytic nanomotors: Remote-controlled autonomous movement of striped metallic nanorods. *Angewandte Chemie-*

*International Edition* **2005,** *44* (5), 744-746; (b) Paxton, W. F.; Kistler, K. C.; Olmeda, C. C.; Sen, A.; St Angelo, S. K.; Cao, Y. Y.; Mallouk, T. E.; Lammert, P. E.; Crespi, V. H., Catalytic nanomotors: Autonomous movement of striped nanorods. *Journal of the American Chemical Society* **2004,** *126* (41), 13424-13431.

17. (a) Pondman, K. M.; Maijenburg, A. W.; Celikkol, F. B.; Pathan, A. A.; Kishore, U.; ten Haken, B.; ten Elshof, J. E., Au coated Ni nanowires with tuneable dimensions for biomedical applications. *Journal of Materials Chemistry B* **2013,** *1* (44), 6129-6136; (b) Jeon, I. T.; Cho, M. K.; Cho, J. W.; An, B. H.; Wu, J. H.; Kringel, R.; Choi, D. S.; Kim, Y. K., Ni-Au core-shell nanowires: synthesis, microstructures, biofunctionalization, and the toxicological effects on pancreatic cancer cells. *Journal of Materials Chemistry* **2011,** *21* (32), 12089-12095; (c) Guo, C.; Huo, H.; Han, X.; Xu, C.; Li, H., Ni/CdS Bifunctional Ti@TiO2 Core-Shell Nanowire Electrode for High-Performance Nonenzymatic Glucose Sensing. *Analytical Chemistry* **2014,** *86* (1), 876-883.

18. Zheng, H.; Zhai, T.; Yu, M.; Xie, S.; Liang, C.; Zhao, W.; Wang, S. C. I.; Zhang, Z.; Lu, X., TiO2@C core-shell nanowires for high-performance and flexible solid-state supercapacitors. *Journal of Materials Chemistry C* **2013,** *1* (2), 225-229.

19. Liu, L.; Li, H.; Fan, S.; Gu, J.; Li, Y.; Sun, H., Fabrication and magnetic properties of Ni-Zn nanowire arrays. *Journal of Magnetism and Magnetic Materials* **2009,** *321* (20), 3511-3514.

20. Lahav, M.; Weiss, E. A.; Xu, Q.; Whitesides, G. M., Core-shell and segmented polymer-metal composite nanostructures. *Nano Letters* **2006,** *6* (9), 2166-2171.

21. Lee, J. H.; Wu, J. H.; Lee, J. S.; Jeon, K. S.; Kim, H. R.; Lee, J. H.; Suh, Y. D.; Kim, Y. K., Synthesis and Characterization of Fe-FeOx Core-Shell Nanowires. *Ieee Transactions on Magnetics* **2008,** *44* (11), 3950-3953.

22. Zhang, Z.; Lai, C.; Xu, N.; Ren, S.; Ma, B.; Zhang, Z.; Jin, Q., Novel nanostructured metallic nanorod arrays with multibranched root tails. *Nanotechnology* **2007,** *18* (9).

23. (a) Nakano, H.; Matsuno, M.; Oue, S.; Yano, M.; Kobayashi, S.; Fukushima, H., Mechanism of anomalous type electrodeposition of Fe-Ni alloys from sulfate solutions. *Materials Transactions* **2004,** *45* (11), 3130-3135; (b) Fan, C. L.; Piron, D. L., Study of anomalous nickel-cobalt electrodeposition with different electrolytes and current densities. *Electrochimica Acta* **1996,** *41* (10), 1713-1719.

24. Matlosz, M., competitive adsorption effects in the electrodeposition of iron-nickel alloys. *Journal of the Electrochemical Society* **1993,** *140* (8), 2272-2279.

25. Zech, N.; Podlaha, E. J.; Landolt, D., Anomalous codeposition of iron group metals - II. Mathematical model. *Journal of the Electrochemical Society* **1999,** *146* (8), 2892-2900.

26. Podlaha, E. J.; Landolt, D., Induced codeposition .3. Molybdenum alloys with nickel, cobalt, and iron. *Journal of the Electrochemical Society* **1997,** *144* (5), 1672-1680.

27. Liu, Z.; Xia, G.; Zhu, F. Q.; Kim, S.; Markovic, N.; Chien, C.-L.; Searson, P. C., Exploiting finite size effects in a novel core/shell microstructure. *Journal of Applied Physics* **2008,** *103* (6).

28. McGary, P. D.; Tan, L.; Zou, J.; Stadler, B. J. H.; Downey, P. R.; Flatau, A. B., Magnetic nanowires for acoustic sensors (invited). *Journal of Applied Physics* **2006,** *99* (8).

29. Darques, M.; Spiegel, J.; De la Torre Medina, J.; Huynen, I.; Piraux, L., Ferromagnetic nanowire-loaded membranes for microwave electronics. *Journal of Magnetism and Magnetic Materials* **2009,** *321* (14), 2055-2065.

**Chapter 6**

**Synthesis and characterization of Piezoelectric Polyvinylidene Fluoride (PVDF) Films and Nanotubes**

**6.1. Introduction**

Piezoelectric polymers are better in some applications than piezoelectric ceramics because of their high flexibility and stretching ability. Therefore, piezoelectric polymers such as polyvinylidene fluoride (PVDF) and co-polymers of trifluoroethylene have had great use in manufacturing of electromechanical and electrothermal transducers such as those have promising medical and industrial applications or in solid electronic memories.[1] PVDF is a semi-crystalline polymer known for its polymorphism; it exhibits four different crystalline phases α, β, γ, and δ.[2] Each of these phases have their specific conformation as shown in Figure 6.1. The structures of the various polymorphs vary depending on the relative orientation, trans (T) or gauche (G), of the fluorides along the length of the polymer backbone (note that gauche is the standard terminology in these systems and is the same as cis).

In the β phase, all the carbon atoms are in the planar trans TTTT zigzag chain conformation with Cm2m (orthorhombic) space group. In contrast, the α phase carbon chains have a TGTG' (trans-gauche-trans-gauche) conformation with P21/c (monoclinic) space group. γ–phase has $T_3GT_3G'$ conformation with C2m space group (orthorhombic). When high electric field is applied to α phase carbon chains, alternate chains may rotate 180° leading to a change in orientation to a polar monoclinic δ-phase.[3]
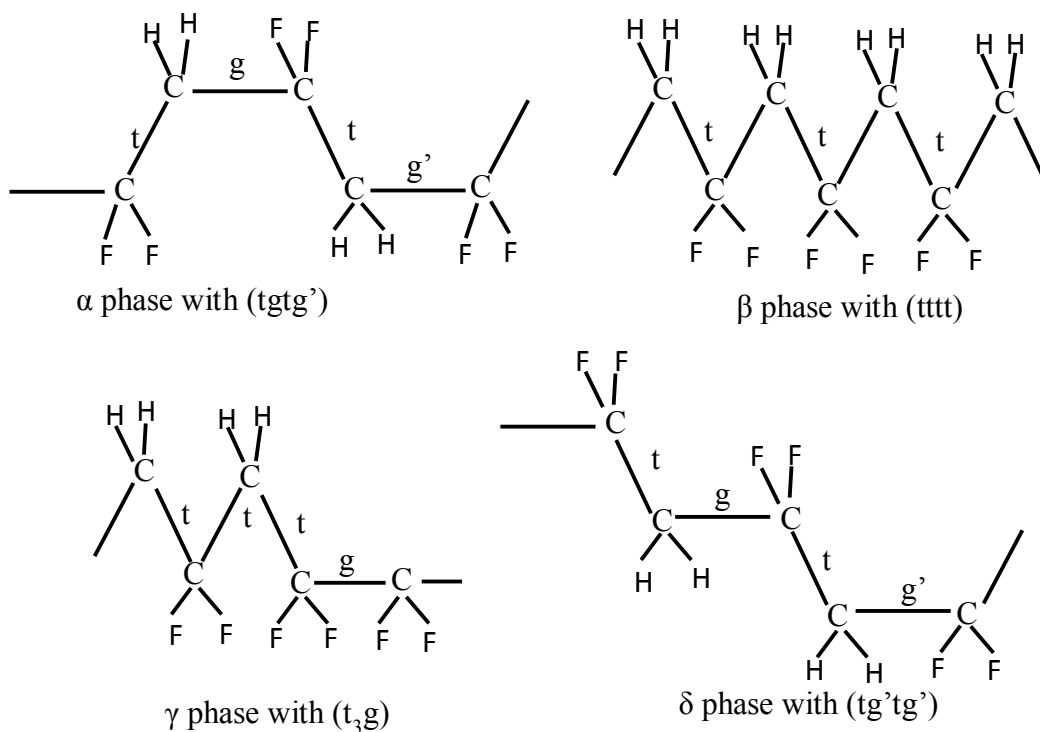
**Figure 6.1.** Orientation of atoms in each phase of polyvinylidene difluoride.

The presence of fluorine atoms in $CH_2CF_2$ repeat units of polymer chains can produce a strong electric moment. Thus the chains have their net dipole moment perpendicular to the polymer chain in the crystalline β, γ and δ phases whereas in α phase, the net dipole moment vanishes.[4] Out of all these phases, the β-phase has largest polarization due to the orientation and arrangement of the polymer chains. Hence, it shows strong pyro- and piezoelectricity.

To fabricate β-phase PVDF, a variety of experimental techniques have been utilized. These most commonly involve mechanical drawing of α phase films[5] and solution recrystallization.[6] Among these two methods, the solution recrystallization method is more frequently used in that it is more easily executed, cheaper, and it takes less time to convert the α and δ phases to β. The method involves the casting of a polymer solution on a substrate and drying. The amount of

86

different phases in a PVDF film depends on the conditions under which the processing was carried out. Bottino et al. prepared films by casting PVDF solution mixtures from eight different types of solvents and found that the final membrane structure is significantly affected by solvent types.[7] The effect of annealing temperature on the morphology and crystal structure of PVDF has been studied by Cheng et al.; they found that the membranes formed at lower temperatures (e.g. 25 °C) in a wet phase inversion method have uniform morphologies with higher amounts of β-phase polymer as compared to membranes prepared at higher temperatures (e.g. 65 °C).[8] Thus the fabrication should be carried out at an appropriate temperature for a particular solution mixture. Satpathy et al. observed the recrystallization of β-phase PVDF films synthesized using dimethyl sulfoxide (DMSO) solvent under several different annealing conditions.[3] They reported a change in recrystallization to other phases as a response to variation in temperature (from 90 °C to 250 °C) and duration of annealing. Therefore, for the fabrication of a piezoelectric PVDF, not only is the casting method and annealing duration important, but the temperature and the types of solvents are also critical.

In this study, we prepared β-phase PVDF films and nanotubes from α phase using two different polar solvents and investigated the corresponding optimal annealing temperatures. One of the annealing temperatures was below and another was above the α phase relaxation temperature (90 °C). In addition to growing films and tubes, $Fe_3O_4$ nanoparticles were used to grow polymer composite films that showed no interference with β-phase of polymers.

## 6.2. Experimental

The reagents PVDF, dimetlylformamide (DMF, 99%) and acetone were purchased from Alfa Aesar and Magnesium Nitrate hexahydrate from Baker Analyzed Reagent (99.2% purity).

*Synthesis of PVDF thin films:* A wet phase inversion method was used to synthesize β phase polymers. PVDF powder was dissolved at room temperature in DMF at three different concentrations (12%, 30% and saturated PVDF).[6a] The solutions were magnetically stirred for at least one day for complete dissolution of the polymer. Subsequently, the solutions were spread uniformly on glass slides with a spatula. The films were covered with another set of glass slides and dried overnight inside a fume hood. Identification of the crystalline phase of PVDF films was performed after two days by X-ray diffraction (XRD) and the crystalline phases of PVDF films were compared with the results from the literature.[8] Out of the three samples of PVDF, the 30% PVDF in DMF showed the highest percentage of the desired β-phase. Therefore, the reaction conditions of 30% PVDF was refined to maximize the fraction of β-phase in the thin film. In this procedure, granular PVDF was dissolved in DMF at room temperature. After complete dissolution, the mixture was spread uniformly on separate glass slides with a spatula. Next, the gelatinous mixtures were heated at two different temperatures. A drop of solution mixture gel was caste on a glass slide and heated at 60 °C for 2-3 min and then the melted solution was covered by another glass slide. Next, a heavy load was placed on the top of it and kept inside a hood at room temperature overnight. The second sample was prepared in the same way but at a different temperature (45°C).

*Synthesis of PVDF-$Fe_3O_4$ films and nanotubes:* The above polymer solution used in the fabrication of PVDF films had a higher viscosity than that which is optimal for the synthesis of PVDF containing nanoparticles and PVDF tubes. Therefore 5 wt% of PVDF was prepared using a mixture solution of DMF, acetone (1:1) and 0.4 wt% $MgNO_3 \cdot 6H_2O$. Adding this salt solution to the PVDF and DMF mixture helped to decrease the viscosity of the solution mixture. Using this solution, thin films were grown by casting the solvent mixture on a glass slide and drying it at 45

°C followed by annealing at 145 °C for overnight and then at 90 °C for 5 h. After verifying that adequate β phase polymers were generated by XRD and FTIR spectroscopy, the same synthesis conditions were used to grow PVDF tubes. After characterization when sufficient β phase was found, PVDF film containing $Fe_3O_4$ nanoparticles were prepared using the same solution mixture (NPs grown by Clare Davis-Wheeler). $Fe_3O_4$ nanoparticles were grown in a solution of 1 mmol Fe(III) acetylacetonate, 4 ml benzylether and 6 ml oleylamine dispersed in toluene.[9] The mixed solution was heated in a four-neck distillation flask and the temperature was increased slowly from room temperature to 300 °C. At 300 °C the solution was heated for 1 h in nitrogen atmosphere. The resulting particles were washed with ethanol and then with acetone. Subsequently, the dry nanoparticles were then mixed with the low viscosity PVDF solution. A drop of this mixture was caste on a glass slide and nanoparticle containing thin films were prepared as described above.

PVDF nanotubes were fabricated from anodized aluminum oxide (AAO) templates by dipping the template inside the PVDF solution mixture, vacuum drying and annealing using the same method used above to grow the thin films. After removal of AAO template using 1M NaOH solution, crystalline phases of PVDF nanotubes were further confirmed by XRD.

*Characterization*

Field emission Scanning Electron Microscopy (FESEM, LEO 130 VP ) was used to examine the surface morphology of the fabricated structures. Crystallinity was measured by X-ray powder diffraction (XRD) using a Philips X-pert PW 3040 MPD diffractometer with CuKα X-ray source in the range $10 < 2\theta < 60$. A JEOL EM 2010 transmission electron microscope (TEM) was used to analyze the size of the nanoparticles. Fourier Transform Infrared (FT-IR) Spectroscopy (Spectrum 2000, PerkinElmer) was used to analyze the crystalline phases. A vibrating sample

magnetometer (VSM, Lake Shore 7300 series) was used to study the magnetization of $Fe_3O_4$ nanoparticles and polymer composites.

## 6.3. Results

***Surface morphology and crystal structure of PVDF thin films formed from DMF:*** A series of PVDF films were prepared separately to check the effect of temperature on film formation while maintaining the same concentration of solution mixture. Figure 6.2a shows FESEM images of the raw PVDF powder before mixing with DMF. The surface morphology of PVDF films formed by casting and heating the solution at 45 °C and 60 °C are shown in Figure 6.2b and 6.2c, respectively. These figures exhibit the difference in grain size between the thin films and the powder. The diameter of the raw powder grains was approximately 200 nm. After adding DMF to the PVDF, the polymer nucleated and recrystallized. At 45 °C larger grains nucleated partially and recrystallized, while the films formed at 60 °C had uniformly distributed small grains. The morphology changed due to complete nucleation and recrystallization. However, the films are too porous for electrical applications.
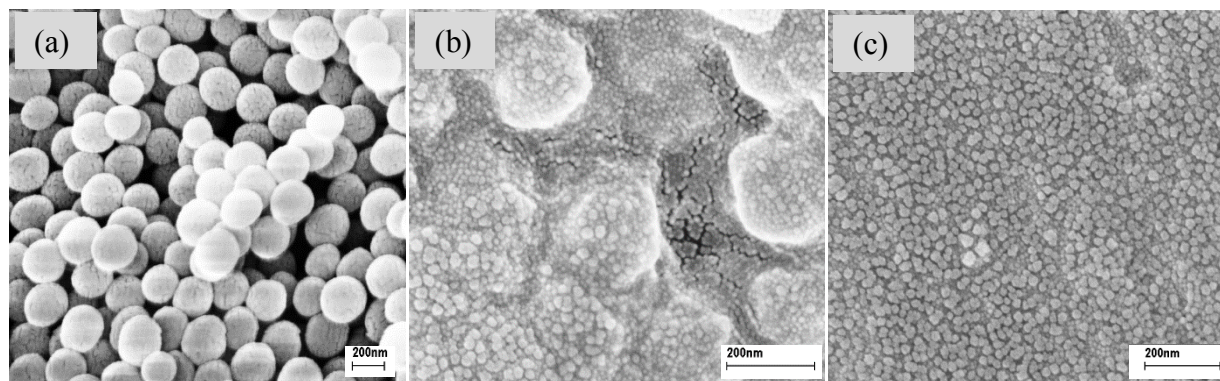


**Figure 6.2.** FESEM surface images of PVDF films formed from the solvent mixture of DMF and PVDF (a) PVDF powder used in the solvent mixture (b) Film formed by heating the casted solvent at 45 °C (c) PVDF film formed by heating the mixture solution at 60 °C.

It is known that the XRD of the semicrystalline polymer films show diffraction peaks at 17.6, 18.4, 19.9 and 26.6 degrees two-theta for α phase and only 20.7 degrees two-theta refers to β phase.[6a]  For this study, XRD analyses were performed to examine the resulting crystalline phases of the polymer films relative to the diffraction patterns of the raw PVDF power. The effect of variation in temperature on recrystallization is shown in Figure 6.3. Figure 6.3a shows that the PVDF powder had maximum intensity at degrees $2\theta = 17.6$ (*hkl = 100*), 18.4 (*020*), 19.9 (*110*), and 26.6 (*021*), which indicates the presence of only α-phase. The XRD patterns of the PVDF thin film formed at 45 °C (Figure 6.3b) showed higher intensity at 20.7 (*200*), however, it has a 26.6 (*021*) peak, which confirms the presence of both α and β phases.  The XRD peak positions of the PVDF film synthesized at 60 °C shows β phase peak at 20.5 (Figure 6.3c). In this film, the β phase is more abundant compared to the other film synthesized at 45 °C using the same solvent mixture. The more abundant β phase in the PVDF film synthesized at 60 °C can be inferred from the high intensity sharp peak at 20.7 in Figure 6.3c.
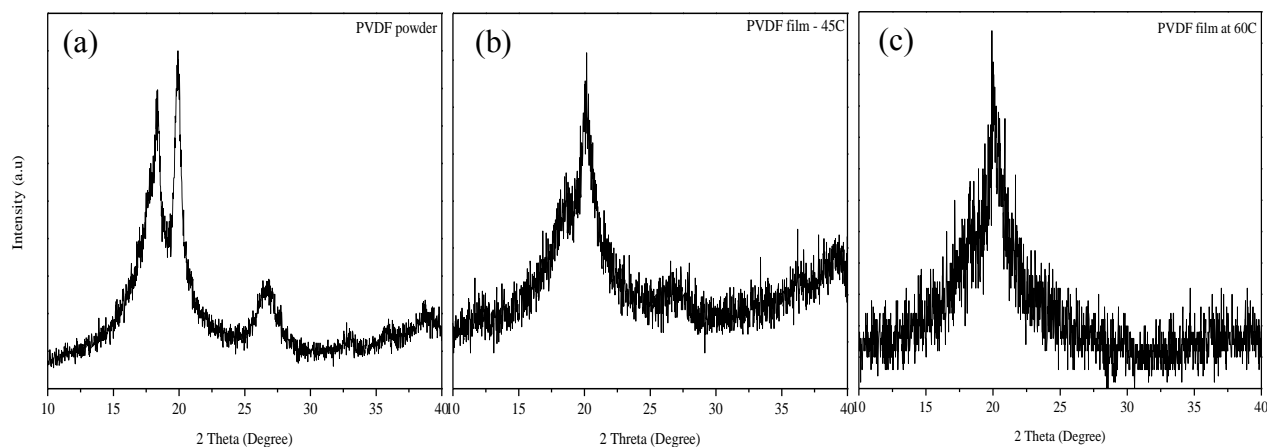


**Figure 6.3.** XRD data of (a) PVDF powder (b) PVDF film formed at 45 °C and (c) PVDF film formed at 60 °C.

Identification of the crystalline phases of the polymer was also carried out by FTIR spectroscopy. Buonomenna et al. reported 531, 612, 766, 795, 855 and 976 cm$^{-1}$ bands are observed for α form of the polymer whereas presence of 470, 511 and 840 cm$^{-1}$ indicate the presence of β phase polymer.[6a] According to Salimi et al. bands at 531cm$^{-1}$ is due to CF$_2$ vibrational bending, 615cm$^{-1}$, 765cm$^{-1}$ and 795 cm$^{-1}$ are the result of CF$_2$ bending, skeletal bending and CH$_2$ rocking respectively represent α phase. However bands at 510 cm$^{-1}$ and 840 cm$^{-1}$ refers to CF$_2$ bending and CH$_2$ rocking supports the β form of the polymer.[4]

Based on FT-IR data of the films, the characteristic peaks at 976, 762 and 614 cm$^{-1}$ in the films that were caste at 45 °C showed a mixture of α and β forms with peaks at 976, 762, 614 cm$^{-1}$ and 510, 600, 840 cm$^{-1}$, respectively (Figure 6.4a). On the other hand, the PVDF film prepared by casting the solution at 60 °C contained dominant peaks of β form at 510, 600 and 840 cm$^{-1}$ (Figure 6.4b). The sample did contain a small amount of α phase, which is similar to the findings of Buonomenna et al.[6a]
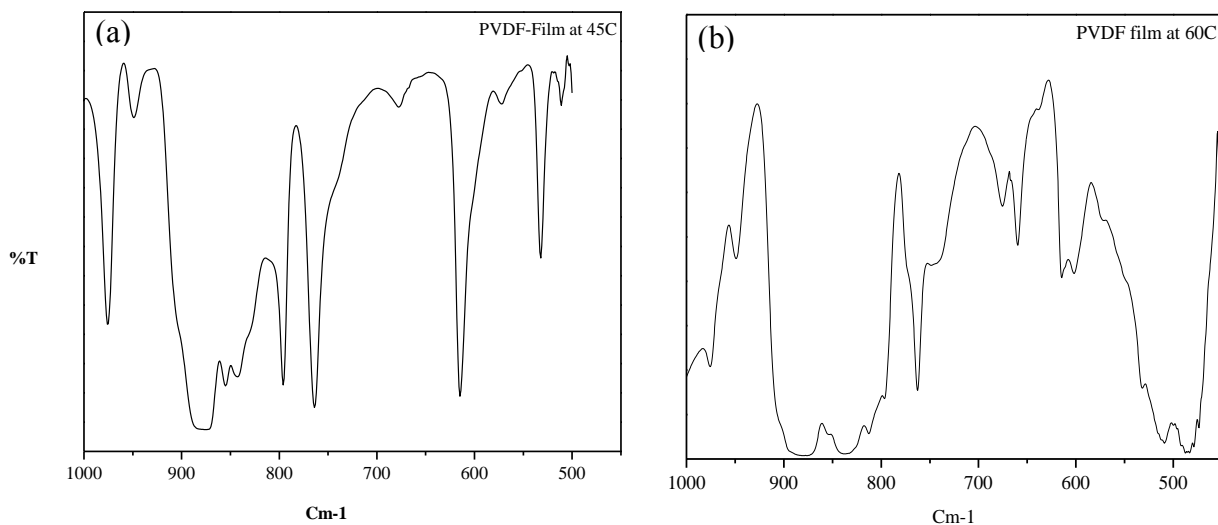


**Figure 6.4.** FTIR spectra of film formed by casting solution at (a) 45 °C and (b) at 60 °C.

*Morphology of PVDF-Fe₃O₄ Films and Nanotubes*

After PVDF-Fe$_3$O$_4$ films and PVDF nanotubes were fabricated, FESEM was used to examine the surface morphologies. FESEM data are given in Figures 6.5a, b and c. The PVDF films showed small polymer grain in the films in Figures 6.5a. Figure 6.5b shows the surface and Figure 6.5c shows the cross-sectional hollow tube structures, after the removal of the AAO template. However, after the removal of AAO templates these tubes were not free-standing. In Figure 6.6, an optical image of PVDF-Fe$_3$O$_4$ film shows that the nanoparticles are arranged together as rows of wire-like arrays.
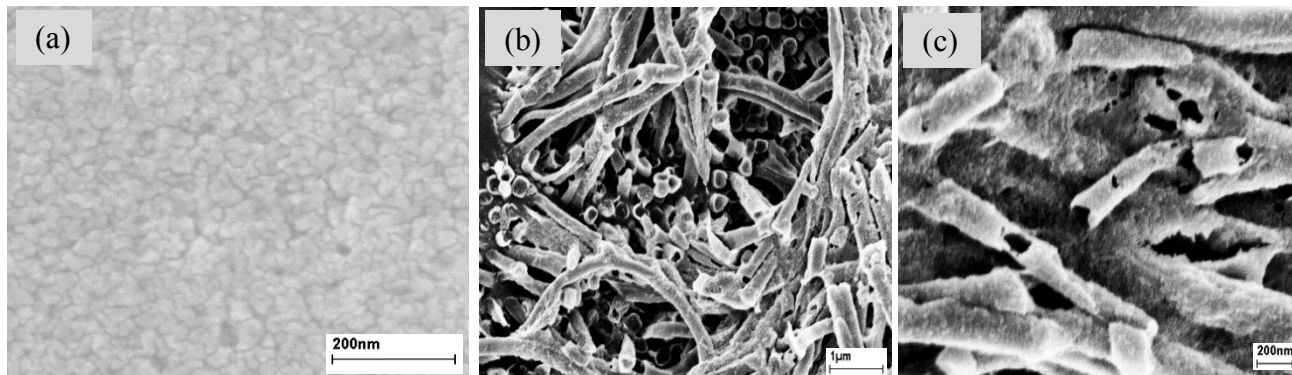


**Figure 6.5.** FESEM Images of (a) PVDF film and (b) PVDF tubes magnified top surface image (c) PVDF tubes cross-sectional image fabricated using commercial AAO templates and after dissolving the template.

The crystalline phases of PVDF-Fe$_3$O$_4$ films and nanotubes were also characterized using XRD and FTIR. As compared to the previous PVDF film prepared from DMF, this film shows better crystallinity of β form peaks indicating dominance of ferroelectric phase in films and tubes as given in Figure 6.7 a, b, and c. Figure 6.7b shows XRD patterns for PVDF-Fe$_3$O$_4$ films with dominated β phase peaks at 20.5˚ and at 31.2° (*220*), 36.8° (*311*) showed the presence of nanoparticles. These results concur with FT-IR spectra as given in Figure 6.8
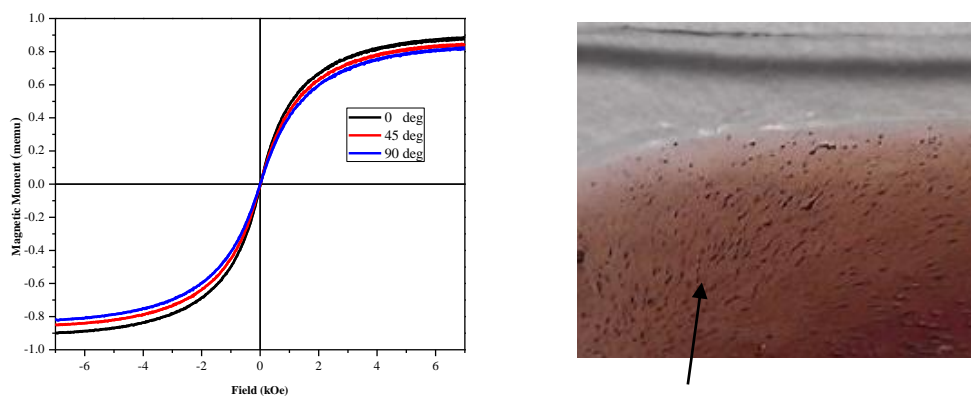
**Figure 6.6.** Image of PVDF containing $Fe_3O_4$ nanoparticles and VSM data showing the Magnetic properties of the composite thin film.
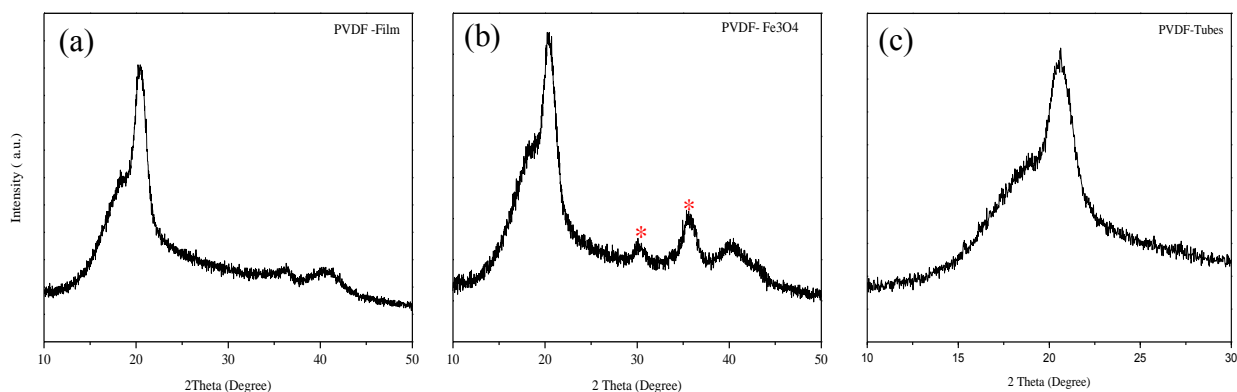


**Figure 6.7.** XRD data of (a) only PVDF film (b) PVDF film containing $Fe_3O_4$ nanoparticles (*) (c) PVDF nanotubes.

As observed in Figures 6.8a and 6.8c, a broad peak between 2923 and 3702 $cm^{-1}$ is present due to the O-H stretching that was absent in the thin film made using only PVDF and DMF. In addition, in Figure 6.8b and 6.8d, the two films synthesized using the same solution mixture had dominant β form peaks at 510, 600 and 840 and 1276 $cm^{-1}$. This demonstrates that Mg $(NO_3)_2.6H_2O$ can help promote β phase in PVDF films.

94
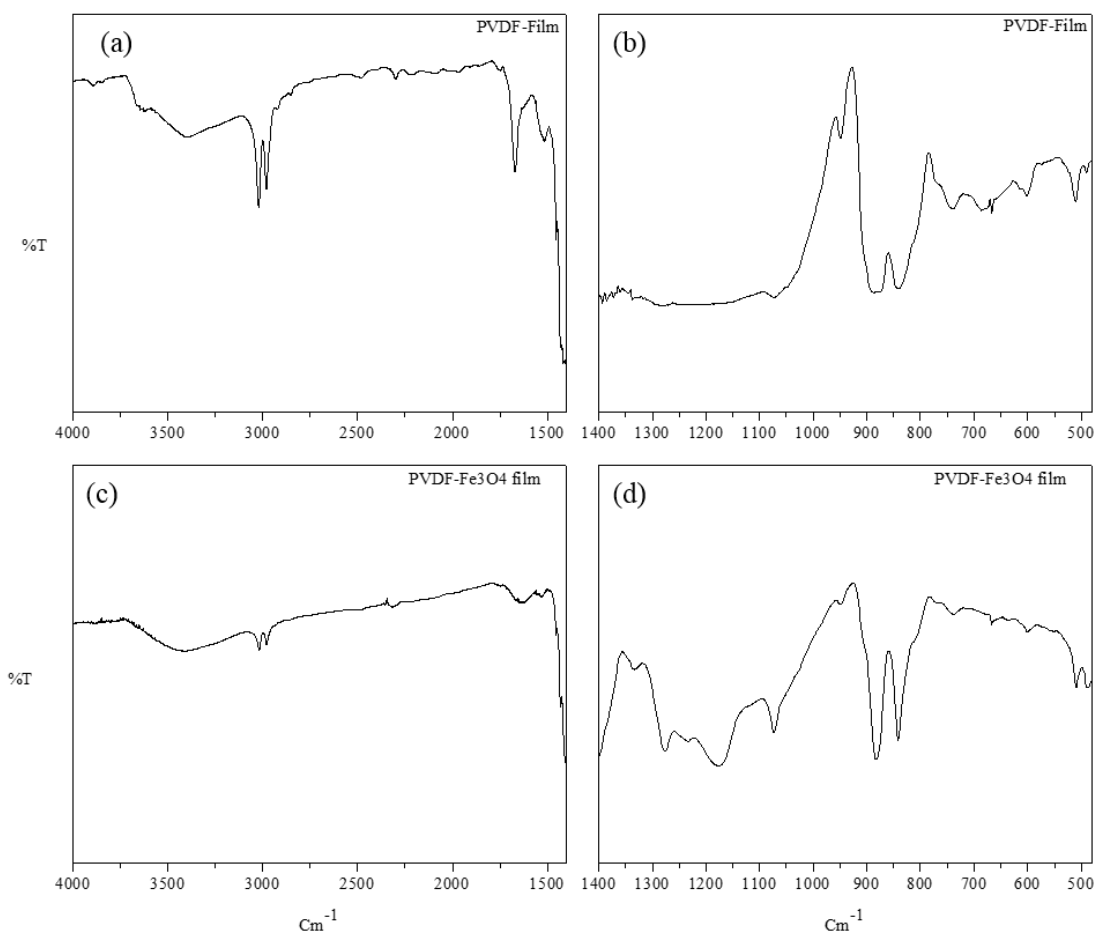
**Figure 6.8.** FT-IR spectra of (a,b) only PVDF film (c,d) PVDF film containing $Fe_3O_4$ nanoparticles.


**Discussion**

The approach described here presents an effective solution recrystallization method for the formation of β phase thin films. While transformation of α phase into β is difficult by mechanically deforming the PVDF film, using solution recrystallization through solvent casting on substrate, β form can be readily obtained and this approach is much more flexible. Further, solution recrystallization, unlike stretching method, is not limited to the synthesis of thin films only. It also

95

allows synthesis of different types of structures such as PVDF composites, nanorods and nanocrystals with tunable morphologies.[10]

Several factors are important for the success of this method. Polar solvents such as DMF can be used to aid in recrystallization of PVDF, which are critical for the growth of ferroelectric phase. Li et al. used inorganic salts in the solution mixture to increase the polarity.[11] Additionally, annealing temperature also plays a key role. Synthesis at > 90 ℃ showed a higher level of phase change due to the rotation of conjugated atoms around the carbon chain to form different conformations.[3] In this study, we have used acetone and the inorganic salt, $MgNO_3. 6H_2O$, at 145 and 90°C to fabricate several different PVDF films and tubes after changing the viscosity of the solution mixture.

From the observations of thin film formation under several different temperatures in this study, it was concluded that the rate of nucleation and recrystallization of PVDF thin film and consequently the grain size is dependent on annealing temperature (Figure 6.1). According to the characterizations, the PVDF thin films fabricated by solution mixtures containing DMF, acetone and hydrated inorganic salts were dominated by β-phase, while the thin films formed by DMF solution contained less β phase polymers. Surface morphologies of the thin films formed using these two different set of solution mixtures were also different (Figures 6.2a and 6.5a).

It has been reported in the literature that PVDF molecules can form intermolecular bonds with polar solvents such as DMF which helps in promoting the β phase.[6a] During recrystallization, the interaction of PVDF with solvent plays an important role on the resulting structure of the PVDF. When DMF was added to PVDF, the dipolar interaction between -C=O- of DMF and -$CH_2$-$CF_2$- of the PVDF chain disrupted the inter-chain interaction of solid PVDF and dissolved the powder resulting in a precipitate.[12] Thus an incipient precipitated gelatinous solution mixture

was formed at room temperature.[8] This precipitate was highly populated with pre-nucleation aggregates. Upon casting the precipitate on a glass slide and heating, initially it went to liquid state as a result of the solvation of many short polymer chains. With continued heating, this supported nucleation and recrystallization of the PVDF. The hydrogen bonding and dipolar interaction between the polymer and the polar solvent supported rotation of C-F bonds and reduced the energy barrier by forming more expanded β conformation chain structure.

The strong effect of temperature on the gelatinous mixture and the resulting film morphology is illustrated in Figures 6.1b and 6.1c. Films formed at 45 °C have partially nucleated PVDF, hence we can see the presence of both α and β phase peaks in XRD patterns and FTIR spectra. Increase in temperature supports further nucleation, therefore the resulting thin film had uniform grain structure with dominant ferroelectric phase. The resulting thin films have different surface morphologies due to a variation in applied thermal energy.

Solution mixture containing PVDF and DMF could not support fabrication of nanotubes due to its high viscosity. Hence the second set of solution was prepared with 5 wt% of PVDF in mixture solution of DMF, acetone and $MgNO_3 \cdot 6H_2O$. This solution mixture was more dilute compared to the previous gelatinous solution. As reported by Kobayshi et al. in a polymer chain, intermolecular force between H atoms and adjacent F atoms is mainly responsible for holding the long chain polymer together.[13] Because of weak hydrogen bonds, when the prepared thin film from this solution was annealed at elevated temperature (145 °C), the increased thermal energy rotated $CF_2$ dipoles. Therefore, trans–gauche conformation of α-phase changed to TTTGTTTG' form resulting in large percentage γ phase. At this temperature, though most of the solvent evaporated, the inorganic salts still remained in the system because of high boiling point of the salt. High mobility of the inorganic salt compared to the PVDF further helped formation of nucleation sites

for recrystallization. In addition, the presence of hydroxyl groups in solvent increased the polarity of solution and hence strong hydrogen bond formed between O—H ···· F—C. The amount of salt added was just appropriate as it was sufficient enough for hydrogen bonding but was not as excessive as to buildup water which could cause dielectric loss. Annealing at a decreased temperature of 90 °C for 5 h modified the chain mobility that supported reorganization of the structure of the conformers. At this temperature the modified C-C chain rotation initiated the formation of β phase more than any other phase.[5b] Therefore, annealing the PVDF film at 90 °C resulted most dominant ferroelectric β phase.

Further, in the PVDF thin films containing nanoparticles with oleylamine capping groups, the β form was dominant. The FTIR spectra further confirms, there is no evidence of formation of secondary amine or -C-N- bond stretching in the FTIR spectra. Hence presence of oleylamine doesn't show any interference in the formation of the β form. However, these interactions between oleylamine and PVDF need to be studied further.

## 6.5. Conclusions

This solution recrystallized thin film fabrication approach was effective in the fabrication of ferroelectric PVDF. From XRD and FTIR characterizations, it was clear that there was a phase transformation during annealing at specific temperatures. Additionally, the experimental results showed that the use of hydrated salt with higher dehydration temperature than the crystallization temperature helped promote the ferroelectric phase because of formation of hydrogen bonds. Therefore, synthesis of thin film depends on the composition of solution mixture and annealing temperature. In this study we have obtained β phase from γ phase by annealing the thin film at 90 ℃ for 5 h.

## 6.6. References

1. (a) Chen, Q. X.; Payne, P. A., INDUSTRIAL APPLICATIONS OF PIEZOELECTRIC POLYMER TRANSDUCERS. *Measurement Science & Technology* **1995,** *6* (3), 249-267; (b) Ang, C.; Yu, Z.; Cross, L. E., Electrostrictive and dielectric properties of stretched poly(vinylidene fluoride-trifluoroethylene) copolymers at cryogenic temperatures. *Applied Physics Letters* **2003,** *83* (9), 1821-1823; (c) Naber, R. C. G.; Tanase, C.; Blom, P. W. M.; Gelinck, G. H.; Marsman, A. W.; Touwslager, F. J.; Setayesh, S.; De Leeuw, D. M., High-performance solution-processed polymer ferroelectric field-effect transistors. *Nature Materials* **2005,** *4* (3), 243-248.
2. Dillon, D. R.; Tenneti, K. K.; Li, C. Y.; Ko, F. K.; Sics, I.; Hsiao, B. S., On the structure and morphology of polyvinylidene fluoride-nanoclay nanocomposites. *Polymer* **2006,** *47* (5), 1678-1688.
3. Satapathy, S.; Pawar, S.; Gupta, P. K.; Varma, K. B. R., Effect of annealing on phase transition in poly(vinylidene fluoride) films prepared using polar solvent. *Bulletin of Materials Science* **2011,** *34* (4), 727-733.
4. Salimi, A.; Yousefi, A. A., Analysis Method: FTIR studies of β-phase crystal formation in stretched PVDF films. *Polymer Testing* **2003,** *22* (6), 699-704.
5. (a) Sajkiewicz, P.; Wasiak, A.; Gocłowski, Z., Phase transitions during stretching of poly(vinylidene fluoride). *European Polymer Journal* **1999,** *35* (3), 423-429; (b) R. P, V.; Khakhar, D. V.; Misra, A., Studies on α to β phase transformations in mechanically deformed PVDF films. *Journal of Applied Polymer Science* **2010,** *117* (6), 3491-3497.
6. (a) Buonomenna, M. G.; Macchi, P.; Davoli, M.; Drioli, E., Poly(vinylidene fluoride) membranes by phase inversion: the role the casting and coagulation conditions play in their morphology, crystalline structure and properties. *European Polymer Journal* **2007,** *43* (4), 1557-1572; (b) Young, T.-H.; Cheng, L.-P.; Lin, D.-J.; Fane, L.; Chuang, W.-Y., Mechanisms of PVDF membrane formation by immersion-precipitation in soft (1-octanol) and harsh (water) nonsolvents. *Polymer* **1999,** *40* (19), 5315-5323; (c) Lin, D.-J.; Chang, C.-L.; Chen, T.-C.; Cheng, L.-P., Microporous PVDF membrane formation by immersion precipitation from water/TEP/PVDF system. *Desalination* **2002,** *145* (1–3), 25-29.
7. Bottino, A.; Camera-Roda, G.; Capannelli, G.; Munari, S., The formation of microporous polyvinylidene difluoride membranes by phase separation. *Journal of Membrane Science* **1991,** *57* (1), 1-20.
8. Cheng, L.-P., Effect of Temperature on the Formation of Microporous PVDF Membranes by Precipitation from 1-Octanol/DMF/PVDF and Water/DMF/PVDF Systems. *Macromolecules* **1999,** *32* (20), 6668-6674.
9. Adireddy, S.; Carbo, C. E.; Yao, Y.; Vargas, J. M.; Spinu, L.; Wiley, J. B., High-Yield Solvothermal Synthesis of Magnetic Peapod Nanocomposites via the Capture of Preformed Nanoparticles in Scrolled Nanosheets. *Chemistry of Materials* **2013,** *25* (19), 3902-3909.
10. (a) Lee, M. K.; Lee, J., Fabrication of Ferroelectric Polymer Nanocrystals with Tunable Morphologies. *Crystal Growth & Design* **2013,** *13* (2), 671-678; (b) Kim, D.; Hong, S.; Hong, J.; Choi, Y.-Y.; Kim, J.; Park, M.; Sung, T.-h.; No, K., Fabrication of vertically aligned ferroelectric polyvinylidene fluoride mesoscale rod arrays. *Journal of Applied Polymer Science* **2013,** *130* (6), 3842-3848; (c) Dillon, D. R.; Tenneti, K. K.; Li, C. Y.; Ko, F. K.; Sics, I.; Hsiao, B. S., On the structure and morphology of polyvinylidene fluoride–nanoclay nanocomposites. *Polymer* **2006,** *47* (5), 1678-1688.

11. Li, X.; Chen, S.; Yao, K.; Tay, F. E. H., Ferroelectric poly(vinylidene fluoride) PVDF films derived from the solutions with retainable water and controlled water loss. *Journal of Polymer Science Part B: Polymer Physics* **2009,** *47* (23), 2410-2418.

12. Bilton, C.; Howard, J. A. K.; Madhavi, N. N. L.; Nangia, A.; Desiraju, G. R.; Allen, F. H.; Wilson, C. C., When is a polymorph not a polymorph? Helical trimeric O-H center dot center dot center dot O synthons in trans-1,4-diethynylcyclohexane-1,4-diol. *Chemical Communications* **1999,** (17), 1675-1676.

13. Tashiro, K.; Takano, K.; Kobayashi, M.; Chatani, Y.; Tadokoro, H., Structure and ferroelectric phase transition of vinylidene fluoride-trifluoroethylene copolymers: 2. VDF 55% copolymer. *Polymer* **1984,** *25* (2), 195-208.

**Chapter 7**

**Conclusions**

Methods have been developed to synthesize 1D materials with different structures using anodized alumina oxide template (AAO) template assisted deposition method. Nanowires, core-shells, alloys and composite nanowires of ferromagnetic materials have been fabricated using a series of AAO templates with different pore diameters. The variation in the structures by controlling the aspect ratio of the nanowires or by embedding the nanowires with stimuli-active polymer led to changes in magnetic properties of the 1D materials.

To grow thick porous AAO templates, a two-step mild anodization process was developed. 0.5 mm thick Al films were used to grow oxide layer with continuous porous channels. The thickness of the oxide layers formed in a certain time interval depends on the pH of the electrolytic solution used, the applied voltage, and the temperature.

Polyethylene glycol (PEG) coated ferromagnetic nanowires were also fabricated using template assisted electrodeposition method by simultaneous deposition of PEG and ferromagnetic materials. These nanowires were grown along their energetically favorable direction of spontaneous magnetization. Due to the outer polymer coating support, these nanowires exhibit a greater tendency to bend before breaking. Further, embedding these polymer coated nanowires with polyethyleglycol diacrylaye (PEGDA) (a solvent-active polymer containing the same functional group) by simultaneous polymerization under an applied magnetic field resulted similar orientation of nanowires as the nanowires within a template.

Using a template assisted electrochemical deposition method 1D nanowires with different structures were fabricated from the same electrolytic solution at constant applied current. Use of

template with different pore diameters at same and/or different applied constant current resulted core-shell and alloy nanowires of NiFe and NiCo. The resultant nanowires with different phases exhibited different magnetic properties.

In a different study, polyvinylidene fluoride (PVDF) containing ferroelectric phase was synthesized using dimethylformamide (DMF). For the synthesis of several different structures such as thin films and nanotubes, the composition mixture of PVDF and DMF was changed and balanced by adding acetone and $MgNO_3.6H_2O$. These methods showed the presence of ferroelectric phase which can be easily grown easily in less time.

## Vita

Jagnyaseni Tripathy was born in Joda, a city in the state of Orissa, India. She obtained Bachelor of Science in Chemistry from Utkal University. To explore the subject from both theoretical and applied aspects, she joined the master's program at the Regional Engineering College (REC), Rourkela. After obtaining her MS degree in the year 2002, she joined Regional Institute of Education at Bhubaneswar, India as an instructor. In August 2003, she joined Swastik Agro India Limited (SAIL), Bhubaneswar as a Chemist. Since September 2004, she was teaching general chemistry to undergraduate students until she came to the USA. She joined Prof. John B. Wiley's research group at the University of New Orleans in spring 2010 to pursue her Doctoral degree in chemistry. Her research was focused on studying the ferromagnetic nanowires, core-shells, simulative polymers and polymer composites.